77-11,235

VAN WIE, William Arthur, 1945-
SEDIMENTOLOGY OF ALLUVIAL
FANS IN SOUTHERN NEVADA.

University of Cincinnati, Ph.D., 1976
Geology

Xerox University Microfilms, Ann Arbor, Michigan 48106

CONTENTS

Page

LIST OF FIGURES

Figure Page

Figure Page

LIST OF TABLES

ABSTRACT

Plane table maps of several segments of braided stream channels, shape and textural analyses of sediments, and bedding studies of available outcrops were used to construct sedimentologic models of alluvial fans in southern Nevada.

Measurements of pebble long-axis orientations indicate an overall tendency toward flow-transverse alignment. Dip azimuths of imbricated pebbles are also good indicators of current direction, but the abundance of imbricated pebbles decreases toward the toe of the fan. Pebble shape analysis revealed no significant shape-sorting along major channels.

Mean and maximum particle size decrease in a down-fan direction, but in an erratic manner. Cumulative curves drawn from ¼ phi sieve analyses of alluvial-fan sediments yield polymodal distributions with a wide range in particle size, from coarse gravel to silt. Particles less than medium sand size occur in low percentages in the mid- and upper-fan reaches and increase in the distal fan areas.

Bed thicknesses and bed lengths decrease down fan because of a loss of channel confinement and an increase in anastomosis of braided channels. Measured bed length/bed thickness ratios average 15/1. Cross channel profiles also exhibit a decrease in channel width and channel depth in a down-fan direction.

Stratification is mostly massive or horizontal with

gravel-sized material comprising over 85 percent of the sediment. Individual beds are laterally discontinuous, have curved erosional bases, and exhibit very abrupt lateral variations in texture. Cross-stratification arising from migration of gravel bars with channel-ward dipping slopes are common. Most of the gravels are grain supported and voids have been infilled with matrices of coarse sand to silt. In exposed outcrops, openwork gravel fabrics are rare.

Minor bedded units consist of cross-stratified sand, rippled fine sand, and horizontally laminated silts which were deposited as surface veneers in low areas during reduced discharge. Their abundance increases in a down-fan direction.

Debris flow phenomena were observed as minor contributors of sediment to the surfaces of the Kyle Canyon and Lida Wash fans. The deposits are entirely reworked by flowing water. Alluvial-fan sediments of the Muddy Creek Formation (Pliocene) however, were deposited primarily by debris flows. The sediments are characterized by an absence of erosional surfaces, very poor sorting, good lateral bed continuity, matrix supported boulders and the near absence of internal bedding. Some debris-flow units exhibit graded bedding and particles often have their long axes parallel to bedding. The debris flow character changes laterally to braided stream deposition.

Vertical exposures of the Muddy Creek Formation exhibit a definite coarsening upward sequence and several angular unconformities are present in the section. During the late Tertiary the area was tectonically active and alluvial fans, forming at the bases of uplifted blocks, encroached upon playa deposits as they infilled the basin.

Lateral variations in alluvial-fan sediments can be explained by the fact that there is a decrease in the frequency and intensity of transporting and depositional events from the fan apex to the fan toe. Clast size, bedding thickness, and sedimentary structures reflect a dispersion of flow across the surface of the alluvial fan, with the highest energy conditions existing near the fan apex.

INTRODUCTION

Purpose and Scope

Alluvial fans, the dominant depositional features in the arid and semi-arid regions of the southwestern United States, are stream deposits built up at the base of mountain fronts. Great thicknesses of these clastic deposits have a good chance for preservation in the stratigraphic record because of their tectonic setting. Yet, very few detailed sedimentologic studies have been made on alluvial fans. Geomorphologists have produced some excellent studies on alluvial fan formation and morphology but no detailed studies of the sediments of Recent alluvial fans exist. The purpose of this paper is to provide documentation of the nature of alluvial-fan sediments to facilitate their recognition in the stratigraphic record.

Blissenbach (1954) states that mudflow deposits constitute about 5-10 percent of fan deposits and that moderate stream floods or streams are responsible for the deposition of the other 90-95 percent of the sediment. This estimate is born out by this study. Hence, this investigation deals mainly with the deposits of braided streams on alluvial fans.

Previous Work

Recent alluvial fans

The history and morphology of alluvial fans in the arid and semi-arid regions of the southwestern United States have been the subjects of several studies made by geomorphologists. These researchers have incorporated discussions of the sedimentology of alluvial fans, but alluvial-fan sediments have been almost ignored by sedimentologists. Studies have been conducted in Recent braided-stream depositional environments that have some direct applications to alluvial fan sedimentology. Basic alluvial-fan terminology used in this report is illustrated in Figure 1.

Geomorphological studies have contributed greatly to our understanding of alluvial-fan morphology. Bull (1972, p. 63) summarizes the following definitive characteristics of modern alluvial fans. "Each fan is derived from a source area with a drainage network that transports the erosional products of the source area to the fan in a single trunk stream." The result of fluvial deposition by the stream is a cone-shaped deposit that is commonly fan shaped and yields contours which bow downslope from the fan apex. Overall radial profiles are concave and cross-fan profiles are convex. Bedrock knobs which are commonly associated with pediments, rarely protrude through the thick alluvium. If present, they are most common near the fan apex, as found in the Kyle Canyon area described in this report. Most fan deposits occur as a series of coalescing cones that form a piedmont slope that is sometimes called a bajada.

Denny (1965) emphasizes the important point that many different combinations of geomorphic factors can be

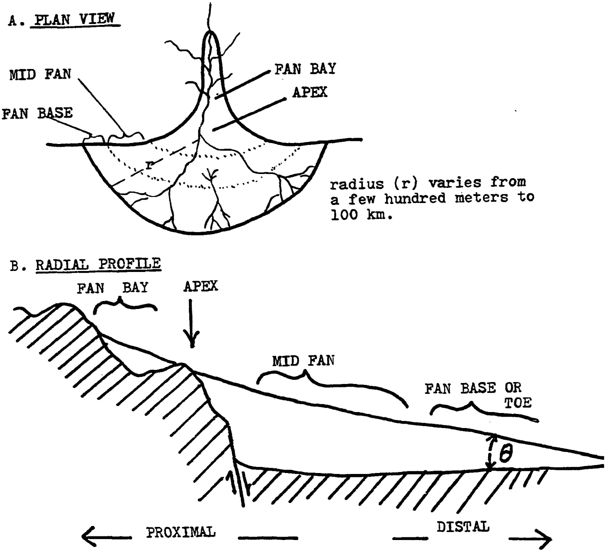

Figure 1. Alluvial-fan terminology modified after Blissenbach (1964) and Bull (1964a). Slope angle (θ) averages 3-6 degrees and rarely exceeds 10 degrees.

postulated to account for the formation of alluvial fans. His theory of alluvial fan formation postulates that a steady state of balance, once reached, will be maintained as long as the geologic processes remain constant. As an example, Denny assumes that if detritus is supplied to a stream at a constant rate by a recently elevated highland, a fan at the base of the highland will grow in surface area year by year. When drainage diversions take place, the area of deposition may be placed down-fan causing erosion of the fan segments near the apex. Once deposited, the debris is not easily moved by local runoff on the piedmont until it has weathered to smaller-sized particles. The area of the fan being eroded will increase until it equals the sediment supply. However, as the source area is reduced in relief, it will supply less and less detritus to the main washes and erosion will become the dominant process causing the area of the fan to increase. Denny's theory relies heavily on tectonic activity or inactivity and does not include climatic factors which may influence the amount of material supplied to the washes.

Other conclusions reached by Denny during his study of 60 alluvial fans in the Death Valley region are as follows:

1. The area of deposition on a fan is equal to one-third to one-half the size of the source area.

2. The available grain size generated in the source area controls the steepness of the fan's longitudinal profile. The easily eroded source rocks produce more gently sloping, longer fans.
3. Changes in grain size down washes vary from fan to fan.
4. Braided channels and gravel bars have a microrelief of 1 foot to three feet
5. The samples from the floors of the desert washes are not well sorted. The standard deviation ranges from 0.45 to 2.85 phi units. Sorting is independent of mean grain size.
6. Changes in the size of bed material from one sample to the next are considerably greater than any overall decrease in size from the apex to the toe of the fan.
7. Most grain size curves exhibit a unimodal distribution with the most abundant class being 4 phi. The remainder are bimodal with 6 phi being the primary mode and 1 phi the secondary mode. Lithologic diversity in the source area seems to control the grain size distribution.

Alluvial fans are most widespread in the drier parts of the world, but they also occur in humid regions such as Japan (Murata, 1966), the Himalayan Mountains (Drew, 1873), Canada (Winder, 1965; Ryder, 1971), and in the artic regions of Scandinavia (Hoppe and Ekman, 1964). Erich Blissenbach (1954) made the first comprehensive study of alluvial fans in the southwestern United States. He defines an alluvial fan as ". . . a body of detrital sediments built up by a mountain stream at the base of a mountain front." The paper gets somewhat bogged down with definitions, but Blissenbach made a significant contribution by pointing out that many ancient alluvial-fan deposits may have escaped recognition because of the common misconception that fan sediments are unstratified, angular, poorly sorted, and are without distinctive sedimentary structures.

Blissenbach describes three general sediment types present on alluvial fans: fan gravel, fan sand and fan mud. The lithified equivalents are fanglomerate (a term first used by Lawson in 1913), fan sandstone and fan mudstone. He found that the particles in alluvial-fan sediments display a rapid decrease in maximum particle size away from the fan apex and that they range in size from boulders to clay. In general, coarse gravels predominate near the apex; material of intermediate particle size may occupy a central zone, and slits and clays are found in the area close to the base of the fan. This gradation is also discussed by Lawson (1913), Vaughn (1922), Troxell et al (1942), Sharp (1948), Beaty (1963), Drewes (1963), Bull (1964a), Ruhe (1964), Bluck (1964), and Hooke (1967).

Blissenbach also observed that the relationship between particle roundness and the distance from the fan apex may be linear. Poorly rounded fragments occur at the apex and roundness increases as the distance from the apex of the fan increases. Particle sphericity on the other hand, exhibits no major change across the fan surface.

Stratification in most of the fans studied by Blissenbach (1954) is fair and he relates it to the processes active on particular fans. Where mudflows predominate, stratification is poor, while stream deposits exhibit good stratification where the mean particle size allows such development. Cross-stratification is also well developed in deposits formed by streams on alluvial fans. Current ripple marks may be present, but by far the most common and conspicuous type of sedimentary structure is cut-and-fill.

The thickness of individual strata as observed by Blissenbach ranges from a fraction of an inch to 15 or 20 feet with most stream deposits on the order of one inch to one foot. Mudflow units range from one foot to 15 or 20 feet in thickness. Individual stream-laid deposits are crudely lenticular, whereas sheetflood deposits occur as definite continuous layers that terminate sharply.

Particles in mudflow sediments frequently stand on edge and rarely exhibit a preferred orientation. Imbrication is pronounced in gravels deposited by stream action where particle shape favors such development.

Blissenbach believes that the abrupt decrease in stream gradient from the mountain stream to the fan surface is responsible for the deposition of sediment on alluvial fans. However, Bull (1964a), through study of topographic maps of Fresno County, California, shows that the gradient of the valley above the fan apex is about the same as the gradient of the upper segment of the fan. Bull (1964a) also found that the overall radial profiles of alluvial fans are gently concave upward, but that the slopes do not decrease at uniform rates downslope from the apexes, and interprets the radial profile of most fans to consist of three well-defined straight line segments. The surface represented by each segment makes a band of uniform slope and runs concentrically about the apex. Lattman (1973) working with alluvial fans in southern Nevada, states that the radial profiles of fan surfaces can be fitted to an exponential curve of the form $y = ae^{-bx}$ with very small residuals. Again, no abrupt change in slope is noted. Bull (1964a) concludes that deposition on alluvial fans is caused by a combination of an increase in width of flow accompanied by a decrease in both velocity and depth. Water infiltration into the fan surface may also accelerate sediment deposition by decreasing discharge (Hooke, 1967; Blissenbach, 1954). Lattman (1973, personal communication) believes that the rate of deposition on the fan-proper is climatically controlled; periods of higher rainfall cause increased deposition in the mountain valleys which is removed and deposited on the fan during periods of decreased rainfall. However, an experimental study of alluvial fan growth by Weaver and Schumm (1974) reveals that fan-head trenching is inherent in the growth of an alluvial fan and need not be the result of a change in external conditions such as climate. They found that sediment buildup at the fan apex was flushed by trenching after its slope exceeded a threshold of stability, which dispersed the sediment to the lower extremities of the fan and reduced the slope near the head of the fan.

William Bull has published several excellent papers (1964z, 1964b, 1972) that describe in part the sediments present on alluvial fans in southern California. Based on textural parameters, he classifies the sediments into three basic groups: water laid sediments, mudflow deposits, and deposits that are intermediate between the two (Figure 2). He also describes the textural characteristics of the sediments and concludes that:

1. Alluvial fan deposits range from very well sorted sands to very poorly sorted mixtures of clays and sand.
2. Logarithmic plots of the coarsest one percentile particle size (C) and the median particle size (M) provide two distinctive patterns (Figure 2). A sinuous pattern representing a tractive-current

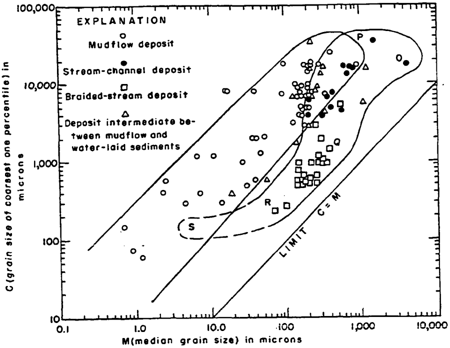

Figure 2. CM patterns of surficial alluvial-fan deposits, western Fresno County, California. (After Bull, 1972.)

type of ephemeral stream deposition is common, and a rectilinear pattern that roughly parallels the limit C = M is typical of debris-flow or mudflow deposition.

3. Textural parameters of the three basic sediment types are:

Mudflow	S	Sd P	QD P
Range	5-25	4-6	2.3-4.7
Mean	9.7	4.7	3.1
Median	8.6	4.3	3.1
Water Laid Sediments			
Range	1.1-4.8	0.48-3.4	0.15-2.3
Mean	1.8	1.4	0.79
Median	1.65	1.15	0.66
Intermediate Sediments			
Range	2.6-5.0	3.1-4.7	1.4-2.3
Mean	4.0	3.9	2.0
Median	4.2	3.96	2.05

Where S = Trask sorting coefficient
Sd P = phi standard deviation
QD P = quartile deviation

A significant paper by Bluck (1964) describes the nature of an alluvial fan sequence in southern Nevada not far from the area studied in this investigation. Bluck considered stratification, particle size, particle sphericity and particle shape and concluded that:

1. An exponential rate of particle size decline in both stream and mudflow phases is brought about by selective sorting and abrasion.

2. The rate of decline of the maximum particle size with distance is more rapid in the mudflow than in the stream deposit.
3. Particle size also diminishes through time, caused by the breakdown of particles by weathering.
4. Changes in sphericity are irregular.
5. There is a uniform increase in rod-shaped particles downstream, as a result of selective transportation by traction.
6. An increase in disc-shaped particles is greatest where there is also a break in the rate of decline of maximum particle size, probably due to a change from an area where deposition comes predominantly from the tractive load to one where it is predominantly from the suspended load.

Bluck's study was followed by an examination of the processes active on arid-region fans by Hooke (1967), who studied several Recent fans and followed up the field study with laboratory model experiments. Hooke concluded that material is transported to fans by debris flows or water flows that follow a main channel. The main channel is incised into the fan head and emerges onto the surface near a midfan point, which Hooke defines as the "intersection point". On his laboratory fans, most deposition above the intersection point is by debris flows that exceed the depth of the incised channel. Fluvial deposition dominates below the intersection point. On fans deficient in fine sediment, Hooke found that large discharges may infiltrate completely before reaching the toe of the fan. Coarse debris is then deposited as lobate masses which he calls "sieve deposits". In many respects sieve deposits resemble debris-flow deposits but they lack primary fine material and fresh lobes are permeable.

Finally, published direct observations of fluvial processes in areas of very low annual precipitation are rare. Due to the infrequent occurrence of storm conditions and the low population density, very few people have observed flow conditions in the channels of alluvial fans. P. Beaumont and T. M. Oberlander (1971) present rare data of this type. They were fortunate to be in the Death Valley area during the time when .81 inches of rain fell in a 24 hour period (mean annual precipitation in the area is 1.78 inches), and they made the following observations on the Mosaic Canyon alluvial fan.

1. Water discharge at the apex of the fan took place along the stream channel and water flow was concentrated in a series of rapidly changing braided channels up to 10 feet (3 meters) in width.
2. Average channel depths were less than one foot.
3. Observed velocities were surprisingly constant at 6.65 ft/sec and 3.5 ft/sec.

4. Discharge was calculated to be 26.6 cubic feet per second.
5. The initial depth of flow was calculated as 0.54 feet and indicated that the flow was supercritical.
6. A Manning's roughness coefficient of n = 0.029 fell within the range of n values for gravel-bottomed channels.
7. Standing waves, often 6 inches above the general water level, were observed.
8. Maximum particle size being moved was 21.3 cm and the smallest retrieved was 10 cm. Their weight varied from 1.34 pounds to a maximum of 5.06 pounds, while their volumes varied from 200 cubic cm to 51.3 cubic cm.
9. The intermediate axis of most of the particles was greater than the maximum depth of water observed in the stream channel.

Ancient Alluvial Fans

Alluvial-fan deposits have been recognized in the stratigraphic record, and there is much data on ancient alluvial fans in the literature. Of the papers referenced in Table 1, several present excellent geologic and sedimentologic analyses of ancient alluvial-fan deposits and deserve a thorough examination. Ancient conglomerates have been identified as being deposited in an alluvial-fan environment primarily through their geologic and structural

Table 1. Published examples of ancient alluvial fans.

Age	Area	Author
Pleistocene	Arizona	Melton, 1965
Tertiary	California	Crowell, 1954
		Flemal, 1967
	Wyoming	Spearing, 1969
U. Cretaceous/ L. Tertiary	Wyoming	Lindsey, 1972
	Montana	Wilson, 1970
Cretaceous	Montana	Gwinn and Mutch 1965
Triassic	Connecticut	Klein, 1968
	Massachusetts	Wessel, 1969
	Wales and Scotland	Bluck 1965, 1970
	N. E. Canada	Klein, 1962
Permian	England	Laming, 1966
Pennsylvanian	Colorado	Boggs, 1966
		Hubert, 1960
		Howard, 1966
	Appalachian (central)	Meckel, 1967
Devonian	Norway	Nilsen, 1969
	Northwest Territories Canada	Miall, 1970a, 1970b
Precambrian to Cambrian	Texas	McGowen and Groat, 1971

setting and their unusual thicknesses. Their continental affinity has also been a key to interpreting an alluvial-fan environment. Analysis of trends in clast size, sedimentary structures, fabrics, clast roundness and clast sphericity has enabled students of ancient alluvial-fan sequences to make detailed paleogeographic interpretations. The following discussion encompasses four papers in which the authors present sound sedimentologic data as a basis for interpreting ancient conglomerates as alluvial fan sequences.

Lindsey (1972) presents a very thorough discussion of the quartzite roundstone conglomerates of the Harebell Formation and the Pinyon Conglomerate in Jackson Hole, Wyoming which are Upper Cretaceous and lower Tertiary in age. Lindsey studied lithologic composition, paleocurrent directions, maximum and mean particle sizes and was able to define the major paleostreams responsible for the deposition of the conglomerates.

After first establishing paleocurrent directions by measuring cross-bedding and pebble imbrication he noted that clast size decreases in a downstream direction. He used regions of maximum clast size to supplement paleocurrent measurements to interpret major paleostreams. By establishing a relationship between paleocurrents and possible source rocks for the conglomerates, Lindsey inferred a rather long transport distance (100-200 miles) and successive uplift and reworking of the conglomerates. Lindsey also presents calculations to illustrate the range of physical conditions required to transport the clasts found in the conglomerates using the Sixth-power Law and the Manning equation. Slopes of 5 percent or less yield reasonable estimates of velocity, depth, and projected relief in the source area.

Lindsey concluded that the Harebell Formation and the Pinyon Conglomerate were deposited in a continental environment by observing that:

1. Continental fossils are common.
2. Imbrication inclinations of 28-29° and abundant percussion marks on quartzite clasts correspond with modern fluvial environments.
3. The paleocurrent systems are strongly unidirectional.
4. The geometry of the conglomerates (32 miles long, 17 miles wide, and from 1,000 to 1,500 feet thick upstream to 200 feet thick downstream) does not have many known analogs in the marine geologic record.

The sedimentary structures and fabrics observed in the conglomerates are consistent with either deposition on an alluvial plain or on an alluvial fan. No poorly sorted deposits of mudflow origin were noted. Lindsey concluded that a subsiding alluvial-fan model best explains the geometry of the deposits, the lobate features outlined by analysis of maximum particle size, the large clasts (commonly 3 feet in diameter), and the decrease in particle size downstream.

In contrast, the Lower to Middle Devonian conglomerates studied by Miall (1970b) are poorly sorted and have mean grain sizes in the pebble range. The succession of conglomerates reaches 1,000 feet in thickness, is up to 150 miles long and is 10 miles wide. Miall studied directional sedimentary structures, clast lithotypes, maximum particle size, grain size distribution, roundness and sphericity of the conglomerates to construct the depositional model shown in Figure 3.

Paleocurrent directions were derived from clast imbrication in the conglomerates and cross-bedding in the associated sandstone lenses. Sedimentary structures are rare but Miall was able to establish a consistent westerly paleocurrent direction.

Average grain size was found to be 5.0 cm (-5.7 ϕ) which is in the coarse pebble range with an average standard deviation of 2.64 phi units (very poorly sorted).

Variations in clast lithology were studied both laterally and vertically. Vertical variations were explained as the result of rejuvenation of the source area. Areal variations in the clast lithotypes revealed dispersal patterns of the conglomerates. The presence of soft, less resistant lithologies in the conglomerates enabled Miall to deduce the transport direction because these clasts decrease in numbers rapidly with distance of transport.

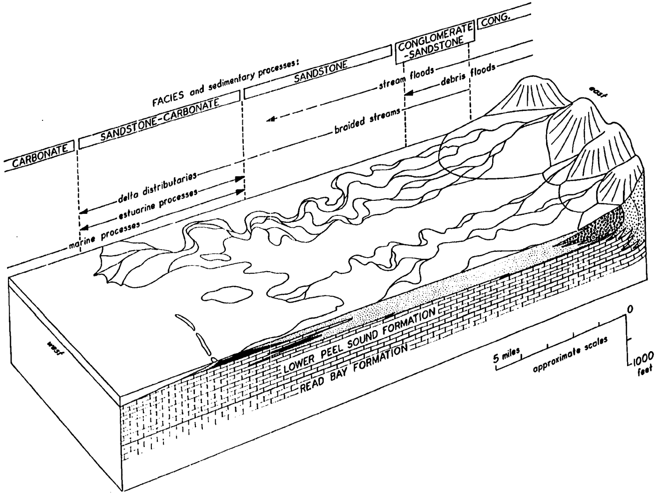

Figure 3. Depositional model for the Devonian Peel Sound Formation. (After Miall, 1970 a.)

Maximum clast size values yielded a concentric pattern of isopleth lines and Miall interpreted the direction of transport to be more or less perpendicular to these lines.

Miall attributed a vertical increase in particle roundness to a reduction of relief in the source area which had the effect of reducing stream slope and increasing stream length by headward erosion, thus allowing more time for abrasion to take place. Lateral variations in roundness showed a decrease in the downstream direction which led Miall to postulate the convergence of two alluvial fans. Mechanical weathering on the alluvial-fan surfaces could also account for this phenomenon.

Grain size distributions and textural characteristics (poor sorting, coarseness, lack of well developed clast framework) of the conglomerates led Miall to conclude that the predominant mode of deposition was debris flow. Miall's study indicates several methods of investigation that can be used successfully in studies of ancient conglomerates. In general terms, vertical variations in conglomerate character may be related to evolutionary processes on single alluvial fans and their source areas, whereas lateral variations, if measured over a sufficiently wide area, will reflect differences between adjacent alluvial fans. Downfan and across fan changes are likely to be small in comparison to the variability displayed between fans of markedly different size and sediment source.

Nilsen (1969) studied sedimentary structures, textures, fabric, and paleocurrent directions of the Devonian Buelandet-Vaerlandet Formation in Norway. The sequence which has a maximum thickness of 3,400 meters consists of breccia, conglomerate and sandstone. The breccias, which lack stratification and have a dispersed framework with an abundance of clay-sized matrix, are interpreted to have been deposited by mudflow processes. The conglomerates have widely spaced, rare bedding surfaces which are discontinuous laterally, and are interbedded with sandstone units averaging 1-3 cm in thickness. Nilsen suggests that the conglomerates were deposited by running water in the upper flow regime and that the sands represent fill deposits behind gravel bars in areas of braided stream deposition. The interstratified sandstone and conglomerates contain irregularly bedded layers of conglomerate up to 1 meter in thickness, alternating with horizontally bedded or trough stratified sandstones that increase in thickness toward the south. These deposits are thought to have been deposited by braided streams with the gravel lenses representing preserved gravel bars formed by stream currents segregating the coarser debris into elongate deposits parallel to flow.

The largest particles range from 2 meters close to the source area to 30-40 cm in the distal deposits. A progressive decrease in roundness toward the south, away from the source area, was observed and Nilsen suggests that roundness is purely a function of grain size. However, the roundness contours established a trend perpendicular to the inferred transport direction. Sphericity data indicate an inverse relationship between mean clast roundness and mean clast sphericity. The mean sphericity increases steadily in the inferred transport direction.

Rose diagrams of the orientation of elongate clasts indicate strong preferred orientation of their long axes. Measurements of paleocurrent directions from cross-strata show a considerable scatter but the net vectors also exhibit a north to south transport direction.

Nilsen concluded that the Buelandet-Vaerlandet Formation is the result of rapid uplift and erosion that resulted in deposition of a broad coalesced alluvial-fan piedmont. His depositional model is shown in Figure 4 which illustrates proximal deposition of fanglomerates with anisotropic fabrics. Sandstones characterized by horizontal stratification, isolated cross-bedding, and segregated gravel bars were deposited by braided streams to the south of the fanglomerates. Viscous mudflows characterized by a dispersed framework and monomict composition were deposited close to the source area.

McGowen and Groat (1971) present an excellent investigation of the Van Horn Sandstone (Cambrian) of West Texas. They defined lateral facies relationships in the Van Horn sequence through a detailed study of sedimentary structures, textures, thickness and lateral continuity of sedimentary

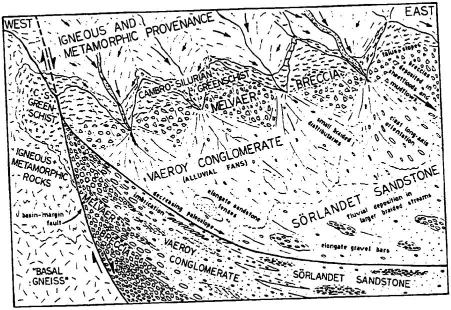

Figure 4. Devonian paleogeographic diagram of the Buelandet-Vaerlandet district, Norway. (After Nilsen, 1969.)

units, and geologic setting. They concluded that the Van Horn was deposited as a widespread alluvial fan system. The sediments were deposited by high-gradient, short-duration peak discharge streams which transported sand, gravel, and minor amounts of clay and silt. The fans were constructed solely by fluvial processes. Direction of transport was established by studying trends in grain size as well as paleocurrent indicators such as cross-bedding and imbrication.

Three main sedimentary facies defined by McGowen and Groat are the proximal, mid-fan, and distal facies. The proximal facies includes gravel or interbedded gravel and sand with 15 percent or more of the section being gravel in size. Other characteristics of the proximal facies include:

1. Coarse grain size.
2. Limited lateral bedding continuity in a direction perpendicular to transport, but persistent parallel to the transport direction.
3. Extreme lateral variation in texture and thickness.
4. Massive bounder beds 15-50 feet thick
5. Alternating gravel and sand beds 10-95 feet thick--the gravel beds commonly have a flat base and flat to slightly convex upper surface with gentle to abrupt slopes laterally. Sand units thicken toward the margins of the gravel beds where foreset bedding is common.

6. Minor amounts of thick sand and muddy sand.

The above characteristics led McGowen and Groat to conclude that the proximal facies was deposited by confined flow in well defined channels.

The mid-fan facies consists of interbedded gravel and sand with gravel comprising up to 15 percent of the facies. The gravel units occur as infilling of scour channels and as longitudinal bars with relatively flat bases and convex upper surfaces. Sand units occur in lows flanking gravel lenses in well defined, broad and shallow channels and as thick sand masses tens of feet thick in which no channel boundaries can be recognized. Foreset and trough cross-beds are common in all of the units. McGowen and Groat interpret the gravel lenses to have been formed as elongate bodies or longitudinal bars parallel to current flow in a braided stream which was transporting mostly sand. Individual channels are more apparent in the mid-fan sediments because of the diverse sediment types. They interpret the mid-fan facies as being deposited by migrating braided streams.

The distal facies consists of coarse and very coarse sand with local accumulations of gravel 1 foot in thickness. Foreset and trough cross-beds are the dominant stratification types. Relative to the mid-fan facies, there is a decrease in the scale of primary sedimentary structures as well as an increase in the abundance of trough cross-bedding

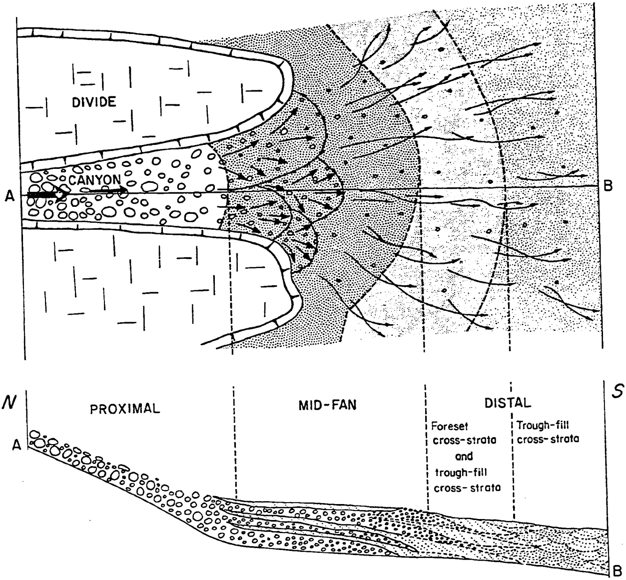

Figure 5. Alluvial-fan model for the Van Horn Sandstone, West Texas. (After McGowen and Groat, 1971.)

and finer grained units. Lower energy conditions relative to the mid-fan and proximal deposits in a braided stream distributary system were responsible for the deposition of the distal facies.

Figure 5 illustrates the depositional model proposed by McGowen and Groat for the Van Horn Sandstone. In this excellent paper, perhaps the best descriptive work on ancient alluvial-fan sediments, McGowen and Groat recognize a most important feature of alluvial-fan sequences. They thoroughly document the fact that the depth of flow and the confinement of flow and therefore the intensity of the physical processes decrease from the proximal to the distal portions of the fan system. The recognition of this phenomenon is essential for the recognition of alluvial-fan deposits in the stratigraphic record.

Areas of Study

Three areas of study were carefully chosen for this investigation because they exhibit good vertical exposures of alluvial fan sediments, and are easily accessible. They are the Recent Kyle Canyon and Lida Wash alluvial fans, and the late Tertiary Muddy Creek Formation.

Kyle Canyon Alluvial Fan

The Kyle Canyon alluvial fan, which is described geomorphically by Lattman (1971 and 1973), is located 12 miles northwest of Las Vegas, Nevada. This fan has formed at the base of Kyle Canyon, the largest canyon draining the

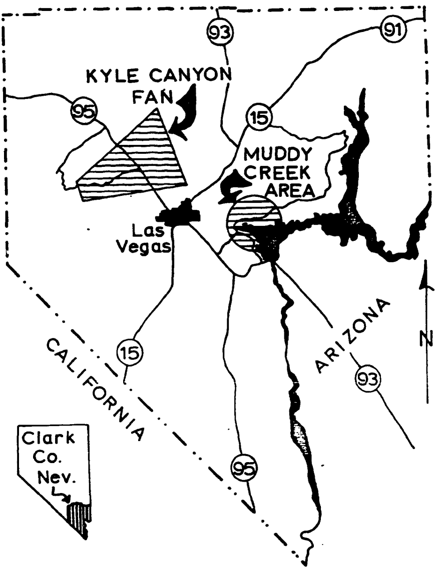

Figure 6. Map showing location of the Kyle Canyon and Muddy Creek study areas in Clark County, Nevada.

eastern flank of the Spring Mountains. The head of the canyon is at an altitude of nearly 12,000 feet and its mouth (head of the fan) is at 4,500 feet. The fan toe in the center of Las Vegas Valley reaches an elevation of 2,600 feet, yielding a fan relief of about 2,000 feet. (Figure 6.) The fan itself has an area of approximately 50 square miles and has an overall slope of 188 feet per mile, which is consistent with other fan slopes in Las Vegas Valley.

The source area for the Kyle Canyon fan sediments consists of 90-95 percent Paleozoic carbonates which contain some cherty units. The remaining 5-10 percent of the source rocks is red sandstone of Triassic age. (Figure 7.)

The topography of the area is fault controlled. The two steep scarps within the drainage basin are produced by the Griffith and La Madre faults. (Lattman, 1971.)

Aggradation and extensive canyon filling occurred in late Tertiary or Pleistocene time. Subsequent excavation of this canyon fill and transportation of the sediments down the fan has produced three distinct geomorphic surfaces that are present on most fans in the area. Lattman (1973) shows that the longitudinal profiles of the three surfaces of the Kyle Canyon fan fit an exponential curve of the form $y = be^{ax}$ with $r \geq .92$. They represent successive downcutting and erosion of the older canyon and upper fan sediments with a corresponding increase in fan area through

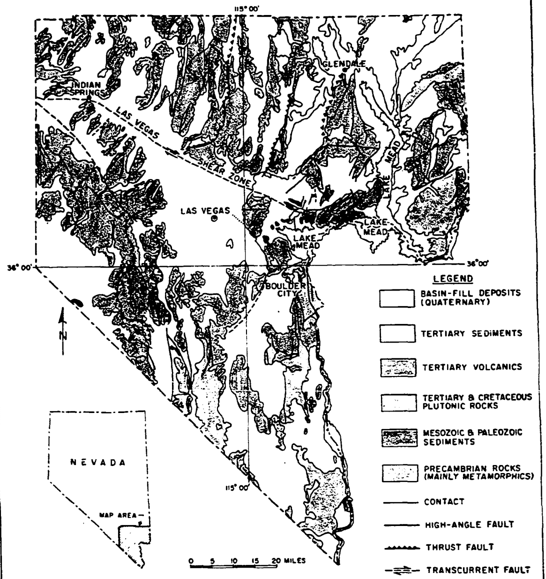

Figure 7. Geologic map of Clark County, Nevada. (After Longwell et al, 1965.)

deposition lower on the fan. This downcutting and incisement and case-hardening of the gully walls has produced excellent exposures of these alluvial fan sediments.

Lattman (1972) suggests that during times of aridity canyon incision and main basin aggradation take place and that wetter conditions produce canyon valley widening and degradation. Basin filling, of course, is dependent upon the absence of through flowing axial drainage such as may have existed in the Las Vegas Valley during the glacial pluvials. Haynes (1967) states that the Las Vegas Valley has been tectonically active at various times throughout the past 40,000 years and local tilting has occurred, possibly as late as 1,000 years ago. Haynes' study indicates a major through-flowing braided stream and flood plain system, which he calls the ancestral Las Vegas River, occupied the valley during the Pleistocene. This system produced several cycles of alluviation and erosion which produced the deposits at the toe of the Kyle Canyon fan. These deposits are characterized by alluvial silts, lacustrine mudstones and alluvial gravels. Haynes suggests that a pluvial lake occupied most of Las Vegas Valley at one time. Perhaps the Late Pleistocene deposits of the Las Vegas Valley may correlate with the Chemehuevi formation along the Colorado River (Longwell, 1946) and a small patch in Las Vegas Wash, thus indicating that Lake Las Vegas was an arm of a much larger lake, the cause of which

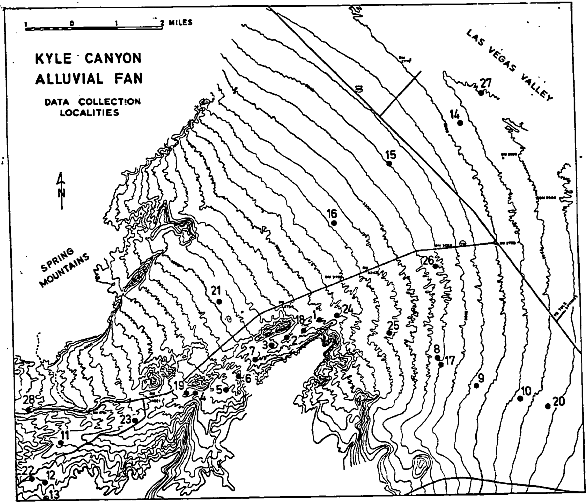

Figure 8. Data collection localities - Kyle Canyon alluvial fan. Numbers are prefixed by "KC" in the text tables.

remains unknown.

The Kyle Canyon fan is, therefore, a relatively large fan composed of partially cemented carbonate detritus that interfingers with alluvial and lacustrine sediments at its distal margin. The fan head area has been incised at least twice in succession, producing remnants of pre-existing fan surfaces as terraces in the canyon and caliche-capped surfaces on the fan proper.

Table 2 from Lattman (1973) shows the types of calcium carbonate cementation which occur on alluvial-fan surfaces in the Las Vegas, Nevada area. On older, inactive fan surfaces, soil horizons of secondary calcium carbonate accumulations more than 6 inches thick are very extensive. This zone is termed a calcic horizon by pedologists and a caliche by geologists. In later stages of development, further calcite cementation produces a hard layer that is impermeable. This process, which is pedogenic and widespread across certain fan surfaces, may be important in that it would produce, if preserved, a good stratigraphic marker in ancient fanglomerates. The fans in southern Nevada studied by Lattman (1973) and Bull (1972, p. 65) have either appreciable amounts of carbonate rocks in their source areas or are close enough to carbonates to receive wind-blown carbonate material. Fossil caliche horizons would also indicate that there was not enough water available to flush authigenic carbonate from the soil system, thus giving a clue to the climatic conditions

Table 2. Summary of characteristics of carbonate cement in southern Nevada.

Type	Origin	Occurrence	Characteristics
Calcic horizon	Pedogenic	Continuous and widely distributed (80 to 100 percent of a fan surface)	Highly variable thickness and amount of cement
Petrocalcic horizon	Pedogenic	Continuous but less widely distributed than calcic horizons (30 to 80 percent of a fan surface)	A late stage in development of calcic horizons. Hard and nonslaking. May be formed from calcic horizons by case hardening of exposures
Laminar horizons	Pedogenic and nonpedogenic	Generally discontinuous and of restricted distribution (10 to 50 per- of fan surface)	Laminated deposit consisting of >90 percent carbonate. Forms on top of petrocalcic horizons and in topographic lows on fan surface. Hard and nonslaking
Case hardening	Nonpedogenic	Restricted to surface exposures on vertical faces. Surface hardening also occurs on gently sloping exposures	Forms rapidly on carbonate-rich material, especially calcic horizons. Decreases inward from surface of exposure
Gully-bed cementation	Nonpedogenic	Restricted to beds and lower banks of fan washes	Resembles laminar layers but generally more crudely laminated. Hard and nonslaking
Caliche rubble	Nonpedogenic	Extensive on abandoned fan surfaces underlain by laminar layers and petrocalcic horizons	Angular rubble derived by mechanical breakup

which existed at the time of deposition. Figure 8 is a topographic map of the Kyle Canyon fan showing data collection localities along the two presently active channels.

Lida Wash

Lida Wash, which drains the Silver Peak Range in Esmerelda County, Nevada, is located 5 miles south southeast of Silver Peak, Nevada. (Figure 9.) This area was chosen because it drained into a closed basin, was remote but accessible, and provided locations for the study of braided stream sediments.

The area is tectonically active as can be seen in Plate IX-3 where several fault scarps are evident cutting the bajada sediments. Hot mineral brines are being pumped from the subsurface and a Holocene basaltic cinder cone protrudes above the bajaha at the north end of Clayton Valley. Whereas Las Vegas Valley has through flowing drainage, Clayton Valley is an intermontaine basin enclosed by the Silver Peak Range, the Palmetto Mountains, the Weepah Hills and Clayton Ridge. The valley-floor sediments are composed of playa clays, silts, evaporites, and sand dunes. Several "islands" of faulted Paleozoic strata project through the sediments of the valley floor.

Robinson and others (1968) report that samples from a well drilled near Lida Wash indicate more than 850 feet of Pleistocene and Holocene playa sediments beneath the valley floor. In addition, gravity profiles indicate that bedrock

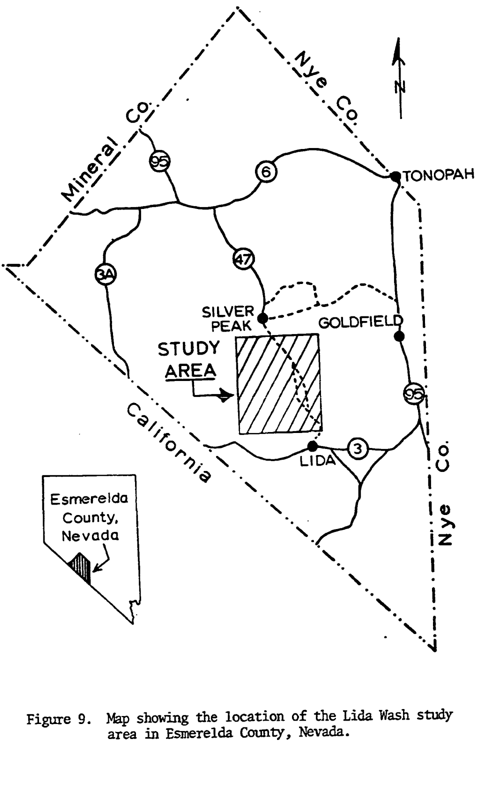

Figure 9. Map showing the location of the Lida Wash study area in Esmerelda County, Nevada.

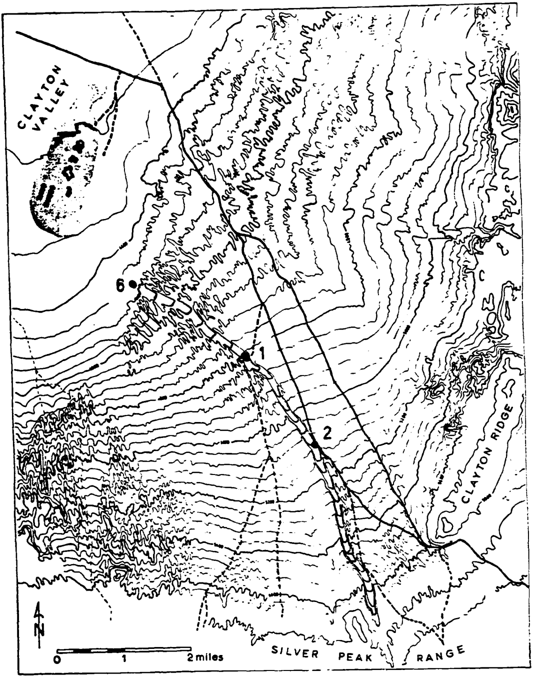

Figure 10. Topographic map of the Lida Wash area showing data collection localities. Numbers are prefixed by "LW" in the text.

is at least 1,350 feet below the surface.

The source area of the Lida Wash sediments, the Silver Peak Range, consists of Tertiary volcanics (flows, breccias, and welded tuffs) and some Paleozoic sediments that are dominantly carbonates.

Since carbonate rocks do not predominate in the area, caliche cementation of the alluvium is very poorly developed and vertical exposures of Pleistocene and Holocene gravels are not present. Field work in this area was limited to the braided streams only. Figure 10 shows the location of sample and mapping stations.

Muddy Creek Formation

A thick section of alluvial fan and playa sediments is exposed west and northwest of Lake Mead on the east and north flanks of the River Mountains. (Plate X .) This mass of basin fill deposits has been mapped by Longwell (1963) as the Muddy Creek Formation. Anderson et al. (1972) dated the extrusive igneous rocks associated with Muddy Creek sediments and assigned an early to middle Pliocene age to the formation. Deposited in closed basin conditions, it has since been highly dissected in response to the lowering of local base levels by the incision of the Colorado River thus creating excellent exposures of alluvial-fan and associated sediments.

The sandier lower units of the section locally contain secondary manganese deposits that were mined during the late 1940's. Hunt et al. (1942) and McKelvey et al. (1949)

described the stratigraphy of the Muddy Creek Formation and the following stratigraphic table (Table 3) was modified by Longwell (1963) from their reports.

Vertical displacements accompanied the deposition of the Muddy Creek Formation and are reflected by at least two angular unconformities. (Plate XIII.) Locally, dips of faulted beds are greater than 60°. Bedded gypsum associated with fine sands and red clays is found at several localities at high elevations in close association with the bedrock of the River Mountains suggesting that the basin once extended over a much larger area. This study is restricted to Member 3 of Table 3 because it is the least disturbed and best exposed.

Sediment types of Member 3 consist of coarsening upward sequences of alluvial-fan sediments which interfinger basinward with siltstones, clays, tuffs, and gypsum. (Plates X and XI.)

Methods

The analysis of alluvial-fan sediments was approached in two ways. First, a study of Recent braided streams was conducted on alluvial-fan surfaces. Random segments of braided streams were mapped using a plane table and alidade, particle size and shape measurements were made in the field, and sediment samples for laboratory analysis were collected at each mapping station. The plane table maps were drawn at a scale of 1 inch = 10 feet, using as many stations as

Table 3. Sequence of Tertiary Rocks Near Lake Mead from Longwell (1963).

Age	Formation	and Member	Description	Thickness (ft.)
Pliocene (?)	Muddy Creek formation	Member 3	Marginal conglomerate and sandstone, grading into siltstone, clay, tuff, and gypsum. Includes thick sheets of basalt; these form cap of Fortification Hill, and their probable equivalents to east and south are mapped separately as the Fortification basalt member of the Muddy Creek.	0-2,000
		Unconformity		
		Member 2	Conglomerate, sandstone, shale and gypsum	0-300
		Unconformity		
		Member 1	(c) Gypsum (locally manganiferous), limestone, clay, siltstone, and sandstone.	0-1,500
			(b) Tuffaceous sandstone and siltstone, generally magnaniferous, some beds with high content of manganese.	0-150
			(a) Bedded conglomerate, with some locally interlayered basal flows.	0-500
		Unconformity		
Miocene (?)	Mount Davis volcanics		Basalt and andesite flows and agglomerate. Coarse sedimentary debris included locally.	0-2,000+
		Unconformity		
Oligocene or Eocene (?)			Complex of volcanic rocks, latites to rhyolites, with much glass and tuff. Cut by dikes, stocks, and irregular intrusive bodies.	Thousands of feet

necessary until channel patterns and bed forms were well defined. Sediment distribution and type descriptions were recorded directly on the field map. Pebble shape studies were made using a large wooden caliper that allowed quick and accurate measurement of the long, short and intermediate axes of at least 50 pebbles from each locality. The computer was utilized to analyze data whenever possible. Textural analyses at ¼ phi sieve intervals were made on from 5 to 10 random samples from each locality. Finally, the long axis orientation of 100 pebbles was measured at seven localities. Elongated pebbles in the size range 5-25 cm were studied.

Secondly, where outcrops exist, a study of lithified alluvial-fan sediments was conducted by describing over 80 vertically measured sections in detail. Panoramic photography was used to construct cross sections showing bedding characteristics; some relatively long outcrops required up to 36 overlapping photographs.

The study was designed to provide an understanding of alluvial fan sediments that would facilitate their recognition in the geologic record. Once some criteria for their recognition have been established, one can use trends in bedding characteristics, grain size, particle shape and orientation, and current indicators to provide a basis for predicting paleogeography in ancient alluvial-fan associations.

Acknowledgments

Several organizations cooperated with me in support of this study. The Geological Society of America provided a generous grant from the Penrose Bequest. The Sedimentation Fund and the Geology Department of the University of Cincinnati contributed to my support while in the field. The Desert Research Institute in Las Vegas, Nevada, provided a room with plenty of cool air and offered the use of their map library and surveying equipment.

Dr. Laurence Lattman of the University of Cincinnati offered transportation to and from Nevada in 1971, introduced me to the alluvial fans and has donated considerable time and interest to the completion of this study. My advisor, Dr. Wayne Pryor, of the University of Cincinnati, without whom this study could not have been completed, helped considerably with the field work and offered valuable criticism of the manuscript. Dr. Burke Maxey of the University of Nevada's Desert Research Institute loaned me his personal car for transportation during the first field season.

Grateful acknowledgment is made to the above organizations and individuals. Special thanks go to Katharine Riggs Van Wie for taking notes through many, many hot days in the desert.

RECENT ALLUVIAL-FAN SEDIMENTS

Particle Morphology

Three measurements can be made on a pebble to give a numerical representation of its shape and also of its actual size. In the following discussion, these three dimensions of a pebble will be designated as:

L = the length, the distance between the two points on the surface of a particle that are farthest from each other.

I = the breadth, which is the same as the smallest round hole in a sieve that just lets the particle pass.

S = the thickness, which corresponds to the narrowest opening of a sieve with slits through which the particle may pass.

In 1922, Wentworth introduced single numbered indices that are accessible to mathematical or graphical analysis. Up to that time reports on shape were qualitative descriptions. Using the three aforementioned dimensions, particle morphology can be expressed as a single number or a point on a graph. Zingg (1935) proposed the most widely used method for designating particle form. He plotted the ratio I/L against the ratio S/I and proposed four form classes (spherical, discoidal, rodlike, and bladed). (Figure 11.) Sneed and Folk (1958) criticized this classification on the basis that there were too few classes to be useful, and the rodlike field was disproportionately small. Instead, they proposed ten form classes, with boundaries fixed so that there is a geometrically equal likelihood of pebbles being either rods or blades or discs. (Figure 12.) Adding to this, Dobkins and Folk (1970) developed a form index ($\overline{OP}$ index) based mainly on the value (L-I/L-S), which defines whether the intermediate axis is closer in size to the short axis or to the long axis. Their resulting formula is

$$\overline{OP} = \frac{10\left(\frac{L-I}{L-S} - .50\right)}{S/L}$$

Using this formula, all perfect blades have $\overline{OP} = 0.0$ whether they have axes of 10:9:8 or 10:6:2. Discs (oblate pebbles) have negative values. Rods (prolate pebbles) have positive values.

Sphericity

Sphericity is defined by Dobkins and Folk (1970) as "the ratio between the three major dimensions of a particle and reflects hydraulic behavior such as settling or traction velocity." Wentworth (1922b) devised the first sphericity measurement (L + I)/2S, which expresses the "flatness" of a particle. Wadell (1932) compared the surface area of a pebble with that of the equivalent sphere; then in (1934a) he devised the measure IS/L^2 which compared the volume of a pebble to the volume of a circumscribing sphere. Folk

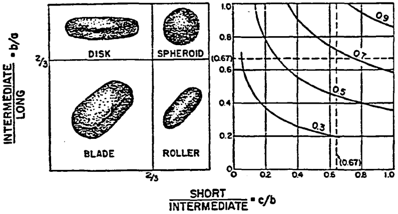

Figure 11. Zingg's classification of pebble shapes (left) based on ratios of intercepts. Relation of intercept sphericity to Zingg's classification of pebble shapes is shown at right.

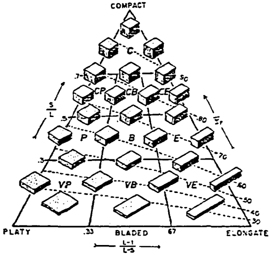

Figure 12. Form triangle. Shapes of particles falling at various points on the triangle are illustrated by a series of blocks with axes with the correct ratio; all blocks have the same volume. (After Folk, 1965.)

(1955) devised a formula for maximum projection sphericity. This measure compares the maximum projection area of a pebble with the maximum projection area of a sphere with the same volume. Sneed and Folk (1958) found that the correlation between the maximum projection sphericity and settling velocity was +.97, whereas Wadell's measure only yielded +.76. Humbert (1968) also found MPS to be the most satisfactory. In this study, the following indices were calculated with the aid of a computer:

1. The flatness index (L + I/2S)
2. The S/I ratio
3. The I/L ratio
4. The sphericity index $\frac{IS}{L}$
5. The maximum projection sphericity index $\frac{S}{LI}$
6. The (L-I)/(L-S) ratio
7. The S/L ratio
8. The $\overline{OP}$ index

Procedure

To test whether there is any significant shape sorting on the fans studied L, I, and S axis determinations were made on at least 50 pebbles at each sample locality. A metric tape was laid perpendicular to the flow direction and pebbles lying directly beneath each ½ meter mark were measured. A large wooden caliper allowed quick and accurate readings to be made. The computer was used to calculate the various shape indices, their averages for each sample, and the standard deviation of the distributions of the MPS, size, and the $\overline{OP}$ index. A summary of the data is given in Appendix vii. Zingg diagrams for each sample were plotted using a computer and the percentage of each shape class calculated. Also, each pebble was plotted on a Sneed and Folk (1958) form diagram.

Results

Shape distribution using Zingg's classification is summarized in Table 4 and figures 13 and 15. Discoid pebbles are the most common on the Kyle Canyon fan. Ranging from 46 to 26 percent of the population, discs are very abundant (up to 46%) in the upper reaches of the southern main channel feeding the fan. Their abundance decreases toward the fan proper where again they increase in abundance to 40%.

Spheroidal pebbles generally make up the lowest percentage of pebbles in the alluvial fan gravels, ranging from 28% to 6% of the total number measured. They exhibit a low percentage in the uppermost sample in the canyon, increase to a high of 28% towards the apex of the fan, drop off sharply on the fan surface, increase and then decrease towards the toe of the fan.

Blade shaped pebbles range in abundance from 40 to 12 percent. They are relatively abundant in the channel above the fan apex, decrease on the fan surface and show a slight

	KC - 13	KC - 12	KC - 11	KC - 4	KC - 5	KC - 6	KC - 7	KC - 3	KC - 2	KC - 1	KC - 8	KC - 17	KC - 9	KC - 10	KC - 21	KC - 16	KC - 15	KC - 14	LW - 2	LW - 1	LW - 6
PERCENT SPHEROIDS	14	18	14	16	10	12	14	28	24	6	20	20	18	16	20	26	20	10	20	22	22
PERCENT BLADES	24	34	30	30	40	28	22	34	20	30	26	18	14	18	16	24	12	26	22	24	22
PERCENT DISCS	46	34	30	30	30	34	32	26	26	42	30	38	38	40	42	32	36	40	26	30	24
PERCENT ROLLERS	16	14	26	24	20	26	32	12	30	22	24	24	30	26	22	18	32	24	32	24	32

Table 4. Zingg classification of pebble shapes.

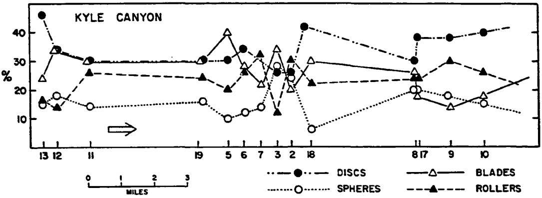

Figure 13. Variations in pebble shape across the Kyle Canyon fan surface.

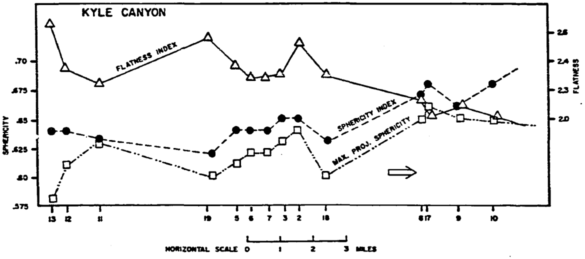

Figure 14. Variation in sphericity and flatness across Kyle Canyon fan. Downstream is to the right.

increase toward the toe of the fan.

Roller abundance seems to parallel that of the spherodial pebbles but their range of percentages is somewhat higher (12 to 32%). Their percentage increases in the channel above the fan apex, increases on the fan surface and decreases towards the toe of the fan.

Using the form diagram of Sneed and Folk (1958) (Figure 12), shape development across the fan surface can be examined in more detail. (Tab le 5.) By far the most common form is bladed, averaging 25.6 percent and ranging from 12 to 36 percent of the sample. Although the results are highly variable, Figure 16 shows a shape distinction between samples from above the fan apex and samples from the fan proper. Sample means increase towards more compact forms with slightly higher sphericities on the fan surface. Downfan changes in form can be summarized as follows:

1. Very elongate pebbles are present above the fan apex in variable percentages. They decrease rapidly to zero across the fan surface towards the toe.
2. Very bladed pebbles decrease downfan.
3. Very platy pebbles decrease downfan to zero abundance at the toe of the fan.
4. Elongate pebbles exhibit a high variability with their highest percentages occurring towards the toe of the fan.

	COMPACT	COMPACT PLATY	COMPACT BLADED	COMPACT ELONGATE	PLATY	BLADED	ELONGATE	VERY PLATY	VERY BLADED	VERY ELONGATE
All Samples	4.2	1.5	10.7	11.5	9.9	25.6	16.0	4.0	10.7	4.8
Kyle Canyon Fan	4.6	3.8	10.8	11.7	10.2	27.2	16.7	3.1	10.2	2.0
Kyle Canyon - Above Apex	3.5	2.0	8.7	10.2	10.0	21.9	14.5	6.2	14.2	8.0
KC - 13	0	2	16	8	12	20	12	12	16	4
KC - 12	4	2	6	14	10	12	18	6	20	8
KC - 11	4	0	10	4	6	36	16	2	10	12
KC - 4	4	2	6	12	6	18	14	12	12	14
KC - 5	4	0	8	8	20	24	12	4	14	6
KC - 6	2	0	10	12	14	20	20	6	14	2
KC - 7	2	2	8	14	6	28	18	4	18	0
KC - 3	8	8	6	10	12	18	6	4	10	18
KC - 2	8	2	10	10	10	28	14	6	8	4
KC - 8	4	2	16	18	10	20	14	4	6	6
KC - 17	4	6	8	22	10	30	6	6	8	0
KC - 9	2	4	14	4	10	28	28	4	6	0
KC - 10	2	6	12	8	14	32	22	0	8	0
KC - 21	4	0	12	12	12	28	16	0	14	2
KC - 16	4	6	12	14	2	34	14	2	8	4
KC - 15	10	2	10	10	12	26	18	2	8	2
KC - 14	4	6	4	8	12	20	16	4	26	0
LW - 2	4	0	20	12	2	32	20	2	2	8
LW - 1	4	8	16	16	12	34	8	0	0	2
LW - 6	6	2	10	14	6	24	28	0	6	4

Table 5. Particle form classification after Sneed and Folk, 1958.

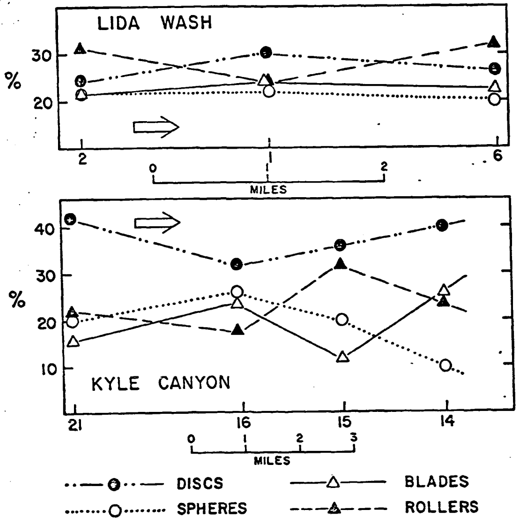

Figure 15. Variations in pebble shape, Lida Wash and Kyle Canyon. Arrow indicates downstream direction.

5. Bladed pebbles show variable percentages and make up the largest group in all samples.
6. Platy pebbles percentages remain fairly constant in the samples studied.
7. Compact elongate pebbles increase in the channel above the fan apex to their highest percentage on the fan apex, then decrease downfan.
8. Compact platy pebbles increase in abundance downfan.
9. Compact platy pebbles increase in abundance downfan.
10. Compact pebbles do not exhibit a regular trend but remain fairly constant in abundance.

Figure 16 also shows that the general size of the pebbles (> or < 64 mm) has no consistent relationship with pebble shape. Solid dots and open circles show no separation.

Sphericity and Flatness

Figure 14 expresses the change in pebble sphericities from the upper reaches of the channel above the fan apex to the fan toe. Sphericity values show a gradual increase toward the fan apex, a decrease on the fan surface and then an increase towards the toe of the fan.

The total distribution of sphericity values of all alluvial fan pebbles is expressed in Figure 17, which also depicts the distribution of river pebble sphericities from

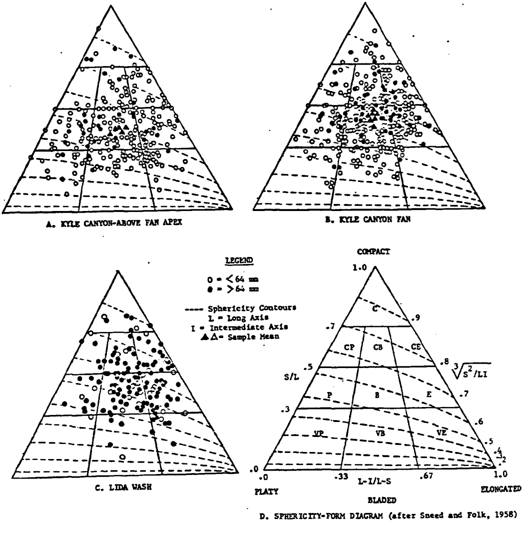

Figure 16. Sphericity - form classification of alluvial-fan pebbles. See Figure 12 for explanation of Triangle D.

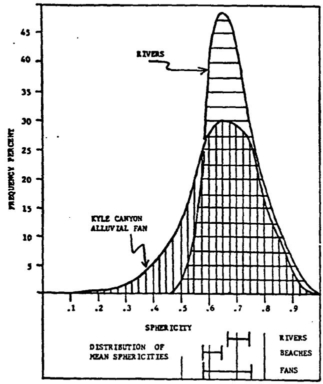

Figure 17. Distribution of sphericity values obtained on the Kyle Canyon fan compared with sphericity values observed in river and beach sediment.

Krumbein and Sloss (1963). The alluvial fan distribution has a mean of .65, and is skewed toward lower sphericity. The river sphericity distribution, on the other hand, exhibits a much lower standard deviation and is skewed toward higher sphericity values. At the base of Figure 7 the distribution of mean sphericities of rivers and beaches (Dobkins and Folk, 1970) is compared with the distribution of mean sphericities found in this study and by Bluck (1964). Dobkins and Folk found a segregation of beach and river sphericity values, however, alluvial fan sphericities cover the entire range of sphericity means of these environments.

Oblate Prolate Index

To further define pebble form development, the oblateness versus prolateness of the particle can be expressed using the $\overline{OP}$ index of Dobkins and Folk (1968 and 1970).

Dobkins and Folk (1970) found that beaches generally have negative mean $\overline{OP}$ values, whereas rivers have slightly positive mean $\overline{OP}$ values. In their study, the mean $\overline{OP}$ value for river pebbles is + 0.18 with a standard deviation of 4.93. Mean $\overline{OP}$ values for beaches range from -.81 to -2.13 with standard deviations ranging from 5.20 to 5.68 (Table 7, p. 189). Alluvial fan samples described in this study generally have positive mean $\overline{OP}$ values, and range from -1.19 (KC - 13) to 2.72 (LW - 2). (Appendix v.)

Standard deviations range from 3.97 to 9.71; much higher than those observed by Dobkins and Folk.

Figure 18 is a graphic representation of the distributions of $\overline{OP}$ values in three general areas. The uppermost curve shows a slightly prolate distribution but has tails that show some percentages of discoid and rodlike pebbles.

When the upper curve (samples above the apex) is compared with the distribution of $\overline{OP}$ values on the fan proper, a marked decrease in rod and discoid shaped pebbles on the fan surface with an evolution toward blade shaped pebbles can be observed. (Perfect blades have $\overline{OP}$ = 0.0.)

Lida Wash pebbles have a high mean $\overline{OP}$ value of 2.20.

Plotting mean sphericity against mean $\overline{OP}$ index yields an interesting distribution (Figure 19). This segregation of fan samples from samples above the apex also indicates a tendency towards blade shapes with higher sphericities in a downfan direction.

Discussion

The obvious drawback to shape studies of particles on alluvial fans is that characteristics of the bedrock in the source area control particle shape to some degree. Bedding thickness, for example, may put an upper limit on resultant particle thicknesses. Thinly bedded sediments would yield flatter particles to the sediment regimen than those with

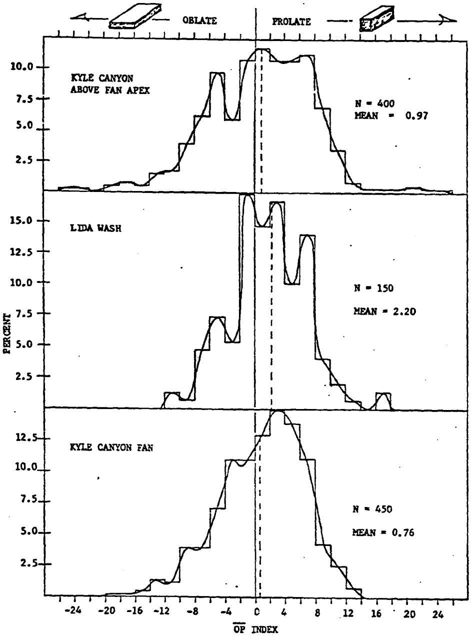

Figure 18. Distribution of oblate and prolate pebbles in Kyle Canyon and Lida Wash gravels.

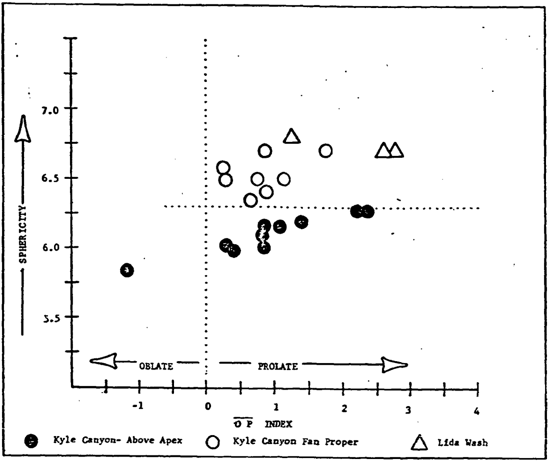

Figure 19. Plot of mean $\overline{OP}$ Index vs. mean sphericity of Kyle Canyon and Lida Wash gravels.

more massive bedding characteristics. Also, as Sneed and Folk (1958) have shown, lithology controls the rate of particle morphogenesis.

The frequency and intensity of the transporting floods and the relatively short distances from source area to depositional area in arid or semi-arid environments also decrease effective shape sorting on alluvial fans. Flooding of alluvial fan channels is not a periodic event and flow is not maintained at a constant level for long periods of time. Hence, high volume intense flows may transport larger immaturely shaped particles farther downfan than smaller more frequent floods.

Other processes that tend to disrupt downstream shape sorting on alluvial fan surfaces are fan head trenching and the break-up of particles on abandoned fan surfaces by freeze-thaw. Fan-head trenching creates a new sediment source from pre-existing fan deposits that may be less mature. Thus sediments introduced to the stream regimen from older fan deposits disrupt the "normal" size and shape sorting of a particular braided stream.

The "in-situ" break-up of particles on alluvial fan surfaces because of freeze-thaw also modifies shape development on alluvial fan surfaces. This process is very evident on the surfaces of fans in the Las Vegas Valley, and may actually cause a decrease in sphericity values down the fan. Large boulders are frequently broken into several pieces with an obvious effect on the resulting particle shapes and sizes.

Owing to these factors, shape sorting is by no means well developed but some general trends are evident. Elongated particles, blades and rods increase downfan, however, average sphericity and flatness increase and decrease respectively. Because of ease of transportation, blades and rods are transported farther downfan increasing their percentage in the distal portions of the fan. However, wear during transport increases their sphericities and decreases their flatness to a slight degree.

Texture

Methods

The problem of textural analysis of alluvial fan sediments that have high proportions of gravel sized particles (> 2 mm) was approached in two ways. First, at each locality studied at least 50 pebbles were measured in the field using a set of calipers. The long, intermediate, and short axes of each pebble that was directly under the 1/4 meter mark of a tape laid perpendicular to the channel were measured. The intermediate axis measurements were converted to phi units ($-\log_2$ of grain size in mm) using a computer.

The second approach consisted of taking random samples from the stream channel (from 5 to 10 at each locality) and sieving them at ¼ phi intervals. Again, a computer was used to analyze the data. Gravel-sand-silt ratios were calculated and plotted in triangular diagrams. Weight percentage distribution curves were drawn from the ¼ phi sieve data, first using the entire distribution and second using the portion of the sample less than 2 mm in size, thus removing the effects of the heavier gravel particles. Textural parameters (mean diameter, standard deviation, skewness, and kurtosis) were calculated using linear interpolation on the weight percentage distributions and the following formulas of Folk and Ward (1957):

$$\text{Mean diameter} = \frac{P_{16} + P_{50} + P_{84}}{3}$$

$$\text{Standard deviation} = \frac{P_{84} - P_{16}}{4} + \frac{P_{95} - P_{5}}{6.6}$$

$$\text{Skewness} = \frac{P_{16} + P_{84} - 2P_{50}}{2(P_{84} - P_{16})} + \frac{P_{5} + P_{95} - 2P_{50}}{2(P_{95} - P_{5})}$$

$$\text{Kurtosis} = \frac{P_{95} - P_{5}}{2.44\,(P_{75} - P_{25})}$$

Where P_{16}, P_{50} etc. are the grain sizes in phi units corresponding to the 16th, 50th, etc. percentiles on the cumulative curve of grain-size distribution. X-Y plots of all possible pairs of parameters were made using a library plotting subroutine.

Results

Figure 20 A, B, and C graphically displays the observed distribution of pebble sizes on the fan profiles studied. Lida Wash displays a very systematic decrease in particle size downstream, whereas the Kyle Canyon Fan profiles exhibit a very different pattern. On the Kyle Canyon Fan a systematic decrease in particle size downfan is not apparent until the distal portions of the fan are reached where the grain size decreases rapidly.

The southernmost active channel on the Kyle Canyon Fan has an almost constant percentage of -4ø and -5ø pebbles making up most of the distribution. These two size groups drop in percentage starting at point B, which is the point where the braided channel loses its confinement. This loss of channel restriction causes a dispersal of flow, loss of flow depth, and there is a rapid change in the competence of the stream. This can also be seen in the northern profile of Kyle Canyon.

So far this discussion has dealt only with sizes greater than 2 mm. When samples were sieved using quarter phi intervals, three general types of curves were found (see Figure 21). Curve A represents samples from braid bars within the channels. This distribution has two basic modes. One, a primary gravel mode with a secondary sand mode or matrix that is commonly trapped within the coarser

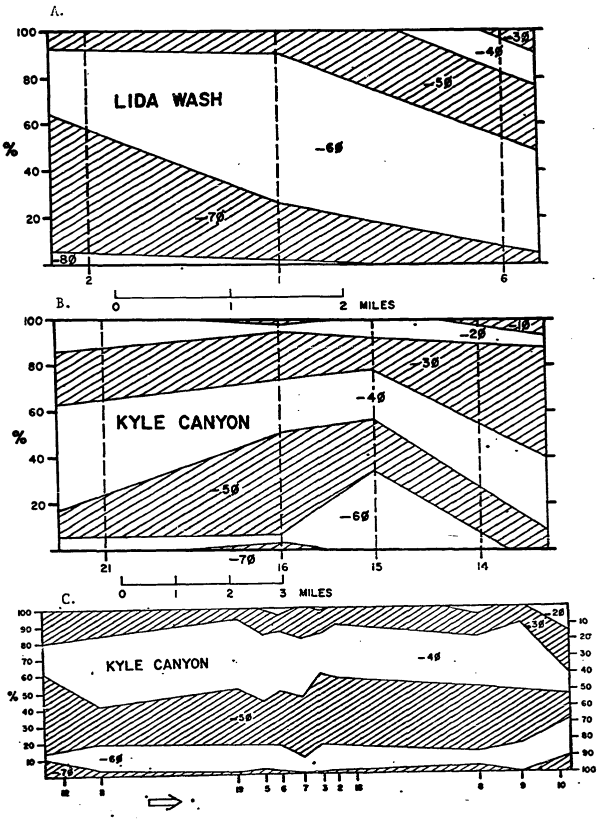

Figure 20. Particle size distribution in washes. Downstream direction is to the right.

gravel.

Curve B represents the fairly well-sorted channel samples that flank the braid bars. These channel samples typically have high percentages of fine gravel and coarse sand.

Curve C is a sample taken from the sand dunes at the distal end of Lida Wash and is typical of wind blown material commonly found associated with alluvial-fan deposits.

Further classification of the analyzed samples can be made using a classification scheme employing a triangular diagram for coarse sediments devised by Folk (1965) (see Figure 22). This classification is based on the relative percentage of gravel (> 2mm), sand (< 2mm and > .063 mm), and silt and clay (< .063 mm). Forty-seven percent of the samples were classified as muddy sandy gravel, 18% as sandy gravel, 17% as gravel, 7% as sandy mud, 2.8% as muddy gravel, 2.8% as gravelly sand, 2.8% gravelly muddy sand, 1.4% gravelly mud, and 1.4% muddy sand.

The grain size distributions were truncated and the percentages below -2 phi recalculated to 100%, yielding new distributions characteristic of the matrix in the gravels studied. In general, the matrix becomes progressively finer in a downfan direction. Figure 23 illustrates several groups of curves from the Kyle Canyon Fan. There is a progressive shift from coarsely skewed curves in the

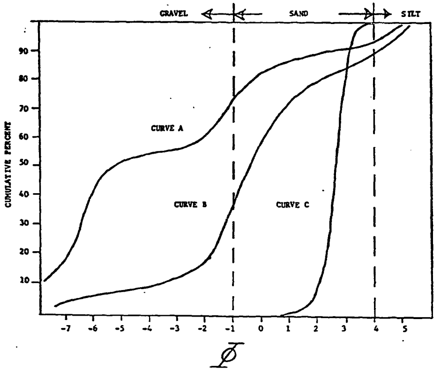

Figure 21. Three general types of cumulative distribution curves showing variations in sorting and particle size in alluvial fan and associated sediments.

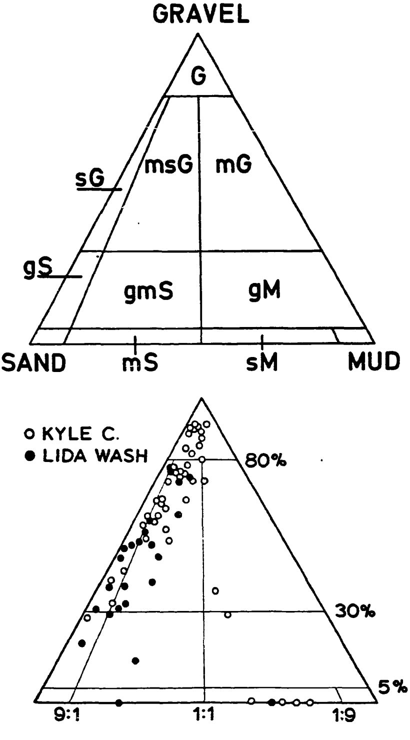

Figure 22. Triangular diagram used in the classification of alluvial-fan sediments. (After Folk, 1965.)

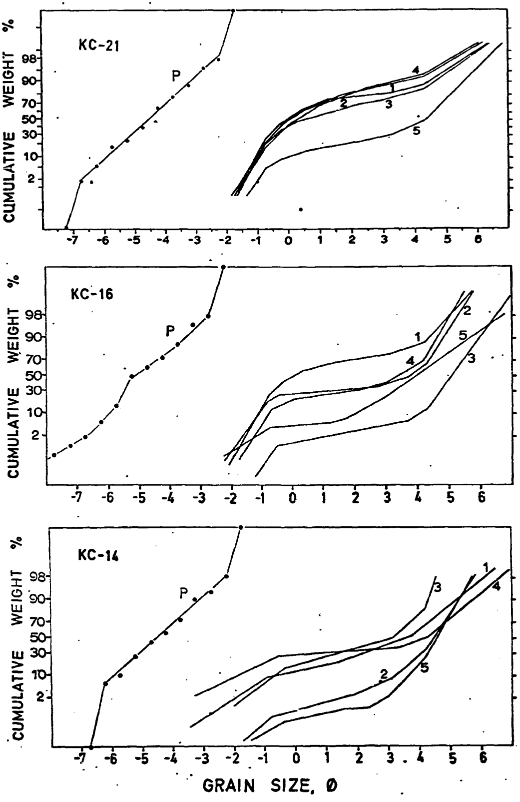

Figure 23. Particle size variation from fan apex KC-21 to fan toe KC-14. Curve P = pebble size distribution. Numbered curves on right based on 1/4 phi analyses of fine fraction (less than -3 Ø).

in the apical region of the fan to finely skewed curves in the distal reaches of the fan. This fining downfan is also illustrated in Figure 24, which indicates that the matrix may not always show a systematic size decrease downfan.

Finally, textural parameters of the grain size distributions were calculated using the previously described formulas, and several parameters were plotted against each other in various combinations (Figure 25). For the textural parameters calculated, see Appendix v.

Skewness measures the degree of asymmetry as well as indicating whether a curve has an asymmetrical tail on the coarse or fine ends of the distribution. Those curves with excess fine material have positive skewness and those with excess coarse material have negative values. Folk (1965) suggests the following verbal limits on skewness: from +1.00 to +.30, strongly fine-skewed; +.30 to +.10, fine-skewed; +.10 to -.30, coarse-skewed; and -.30 to -1.0, strongly coarse-skewed. Skewness values for the alluvial fan sediments studied range from -.63 to +.66, and can be summarized as being 15% strongly coarsely skewed, 13% coarsely skewed, 14% near symmetrical, 18% fine skewed, and 40% strongly fine-skewed. Maximum fine-skewed samples have coarser mean sizes than the coarse-skewed samples.

Kurtosis or peakedness measures the ratio between the sorting in the "tails" of the curve and the sorting in the central portion. If the central portion is better sorted

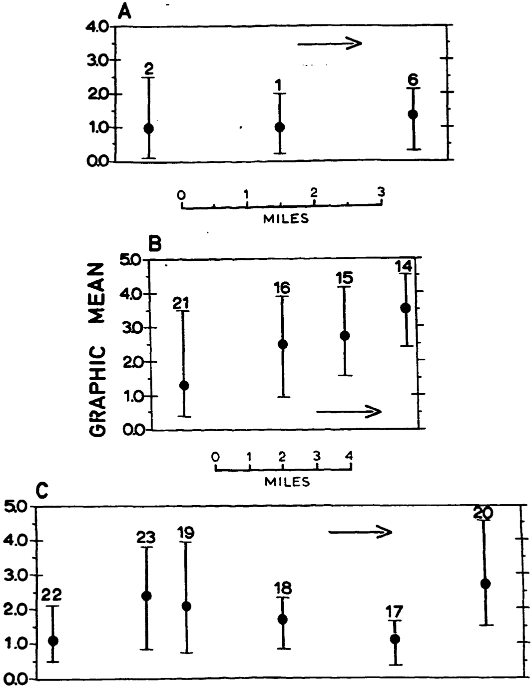

Figure 24. Variations in graphic mean values in three washes. Downfan direction is to the right. Graphic mean values are in Ø units. A = Lida Wash; B & C = Kyle Canyon.

than the tails, the curve is said to be excessively peaked or leptokurtic. If the tails are better sorted than the central portion, the curve is flat-peaked or platykurtic. Five percent of the samples studied are very leptokurtic, 29% are leptokurtic, 24% are mesokurtic (similar to a normal distribution), 21% are platykurtic, and 21% are extremely platykurtic. Strongly platykurtic curves are often bimodal with subequal amounts of the two modes.

The inclusive graphic standard deviation of Folk (1955) is used here to define the degree of sorting in the samples studied. Two percent fell between 0.5 and 0.71 ϕ standard deviations and are moderately well-sorted. Nine percent fell between 0.71 and 1.0 ϕ and are moderately sorted. Forty-eight percent fell between 1.0 and 2.0 ϕ standard deviations and are poorly-sorted. Forty-one percent have standard deviations between 2.0 and 4.0 phi and are very poorly sorted.

Landim and Frakes (1963) attempt to distinguish between tills and other diamictons using textural characteristics. In order to quantify observed separations between alluvial fan deposits and tills they applied discriminant functions to their data and they present the following equation:

$$D(M_2, G_I, SK_I, k_G') = 0.00405M + 0.002381$$

$$- 0.05616Sk + 0.10365\ k'$$

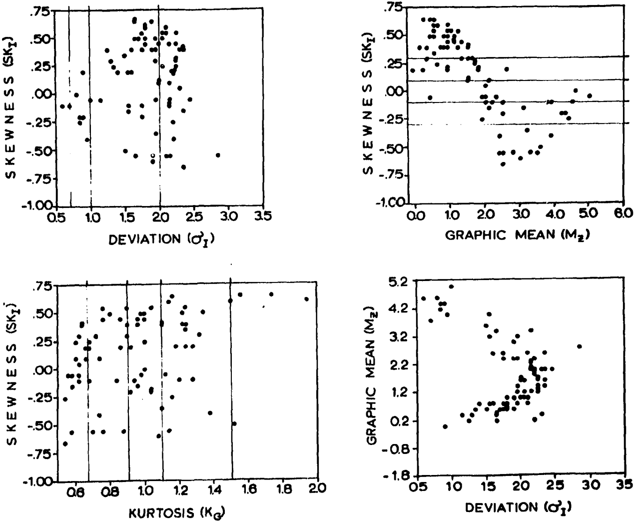

Figure 25. Textural parameters of alluvial fan sediments.

In the alluvial fan discrimination, D = 0.12809. Values less than this number would indicate formation on an alluvial fan. When this equation is applied to the Kyle Canyon fan sediments D = 0.0931. This suggests that the equation derived by Landim and Frakes (1968) may be useful for distinguishing between these types of sediments.

Pebble Orientation

The long-axis orientation of 100 pebbles was studied at 7 localities: 4 on the Kyle Canyon fan and 3 on Lida Wash. Only elongated pebbles in the size range 5 cm - 25 cm were studied. Figures 26 and 27 show rose diagrams constructed for the data collected relative to their location on the fan. In general, elongated pebbles have their long axes oriented perpendicular to stream flow and are imbricated upstream. Imbrication ranges from 27 to 76 percent of the pebbles studied.

Observed pebble orientations are, of course, dependent upon the intensity of the last flood to occupy the channel. High velocity, high volume flows that are more likely to affect the fan bay and fan head portions of the channels would produce poorly oriented large bars with poorly oriented pebbles. But as the flow subsides, the upper layers of the sediment deposited may be modified to produce better pebble orientations. Whereas in the distal portions of the fan less intense flooding would be expected and pebble orientation should increase. In other words, in middle and distal

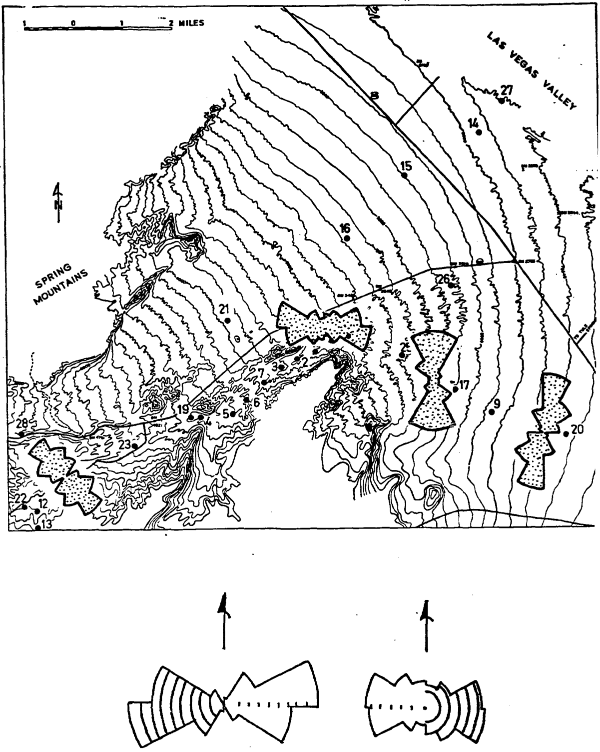

Figure 26. A. Particle long-axis orientations on the Kyle Canyon fan.
B. Summation of particle orientations-Kyle Canyon (left), Lida Wash (right)-relative to current direction (arrows). Increments = 5%.

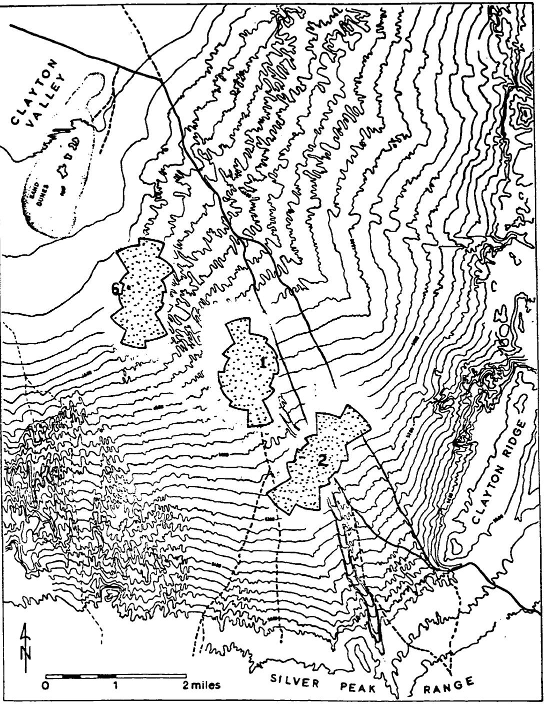

Figure 27. Particle long-axis orientations - Lida Wash area.

VECTOR	LW-1	LW-1 Sum	LW-2	LW-2 Sum	LW-6	LW-6 Sum	KC-17	KC-17 Sum	KC-18	KC-18 Sum	KC-20	KC-20 Sum	KC-22	KC-22 Sum
0-10°	7		5		7		24		2		12		8	
11-20	6	18	12	25	6	20	12	41	0	4	21	50	0	10
21-30	5		8		7		5		2		17		2	
31-40	12		11		2		3		4		12		0	
41-50	2	15	16	35	1	9	0	3	3	12	9	26	0	0
51-60	1		8		6		0		5		5		0	
61-70	6		6		2		0		7		5		0	
71-80	7	14	5	14	2	7	0	0	14	33	1	8	2	6
81-90	1		3		3		0		12		2		4	
91-100	4		0		1		0		20		0		5	
101-110	5	10	5	8	6	9	0	1	11	41	0	0	6	21
111-120	1		3		2		1		10		0		10	
121-130	7		2		11		3		10		1		13	
131-140	1	14	2	6	6	25	5	14	2	12	0	1	11	36
141-150	6		2		8		6		0		0		12	
151-160	11		2		6		13		2		3		5	
161-170	7	29	3	12	14	30	12	41	1	3	3	15	8	22
171-180	11		7		10		16		0		9		9	
Total # of Measurements	100		100		100		100		105		100		95	
% Imbricated	27		30		34		55		76		70		63	

Table 6. Pebble orientation data.

portions of the fan, the hydraulic properties are more important than in the fan bay and fan head portion of the fan.

In comparing the data from the Kyle Canyon fan with that from Lida Wash, it is evident that imbrication is better developed on the Kyle Canyon fan. This suggests that particle shape may control the degree of imbrication and the quality of the orientation data obtained by this type of measurement. The more compact pebble forms present in the Lida Wash sediments yielded low imbrication percentages. Rose diagrams exhibit more scatter than the Kyle Canyon samples but the resultant orientations are still normal to stream flow (Figure 26b).

Geometry of Braided Stream Segments

Methods

The plane table and alidade were employed to systematically study several segments of braided stream channels on alluvial fans. The objectives of this mapping procedure were to (1) record the distribution of sediment types within the channels, (2) measure the geometry and size of sedimentary features within the channels, (3) measure the dimensions of the channels themselves, (4) determine downfan changes in channel characteristics, and (5) make deductions as to the resultant geometry and size of individual sedimentary units if they were preserved in the geologic record.

In many cases, where confined by steep banks, the channels are well defined. This is generally true of the incised channels in the upper reaches of the fan. Channels lower on the fans are less confined and eventually exhibit a distributary pattern. In the cases where no definite confining banks were present, the channel was defined as the area of fresh uncoated sediments.

The maps were originally made at a scale of 1" = 10 feet. As many observations as necessary were taken until the channel patterns and bar forms were delineated clearly. Rod points were always recorded along with elevation differences and sediment types were noted and recorded directly on the field map. Finally, a profile of the channel perpendicular to the flow direction was made.

Morphological Units in Braided Channels

The most common features present as topographic highs in the channel segments studied are accumulations of coarse detritus that have their long dimensions parallel to stream flow. These bars do not appear to have simple histories, but display several erosional and depositional episodes, hence the bars cannot be simply classified.

The largest or lobate forms are by far the most common. They have irregular boundaries and broad irregular surfaces, cut by numerous minor channels. These larger features are probably the result of the larger volume flows that reach the fan surface and are able to move cobble sized and larger particles. The axes of the lobate bars are more or less parallel to main flow, and their final resting morphologies are dependent upon the degree of erosion subsequent to deposition. Bar margins may gradually grade into finer grained adjacent channels or they may abruptly terminate as erosional scarps. Sinuous boulder ridges left by the near complete erosion of lobate bars are common.

Whereas the lobate bars are the result of both depositional and erosional processes, the longitudinal bars appear to be solely depositional. These features are smaller than the lobate bars and occur within the smaller channels. They are lenticular in plan view, streamlined, or tapered downstream, and fine in a downstream direction. Their cross profile is convex.

Transverse bars have their long axes perpendicular to flow and are usually found at the intersection of two large channels. An example of these bars was observed at locality 14 on the Kyle Canyon fan. (Figure 28.)

General bar morphologies are summarized in Table 7. The plane table maps produced are shown in Figures 28 through 36 with further discussion of bedforms.

Figure 28. Plane-table map of locality 14 on the Kyle Canyon fan.

This map was made at the juncture of two channels. Average bar dimensions are 10 meters in length and 1.6 meters in width. Maximum bed relief is 0.45 meters. The largest bars are termed longitudinal and are oriented with their long axes parallel to flow (to the right) and are dissected by several small channels. The confluence has produced several small bars that are oriented perpendicular to the flow direction, herein called transverse bars.

The grain size curves are skewed toward the finer size fraction with graphic means of 3.2, 4.4, 2.4, 2.8, and 4.5 ∅ (average of 3.4 ∅). The mean pebble size along profile A-A' (Curve P) is -4.4 ∅.

Deposition of the large, coarse gravel bars at this locality seems to be related to the increased channel width caused by the confluence of the two channels. A previous high volume flow, upon encountering the increased channel width lost its capacity to transport the coarser fraction of its load. Subsequent lesser volume flows have partially dissected the bed forms.

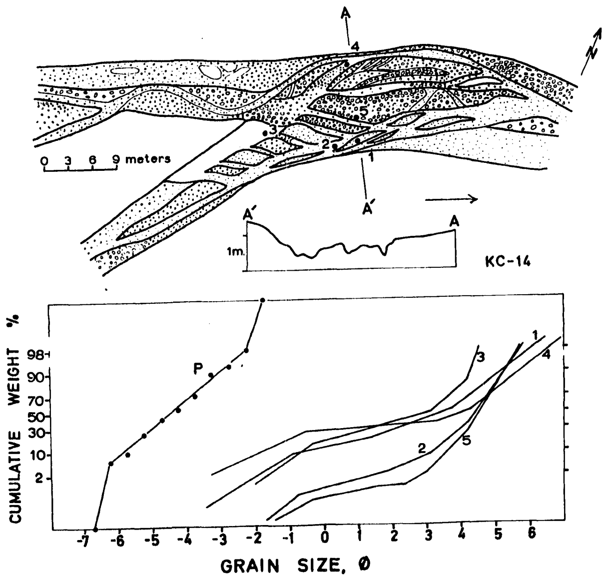

A
A'
1
2
3
4
5
0 3 6 9 meters
1m.
KC-14
CUMULATIVE WEIGHT %
98
90
70
50
30
10
2
P
GRAIN SIZE, Ø
-7 -6 -5 -4 -3 -2 -1 0 1 2 3 4 5 6

Figure 28.

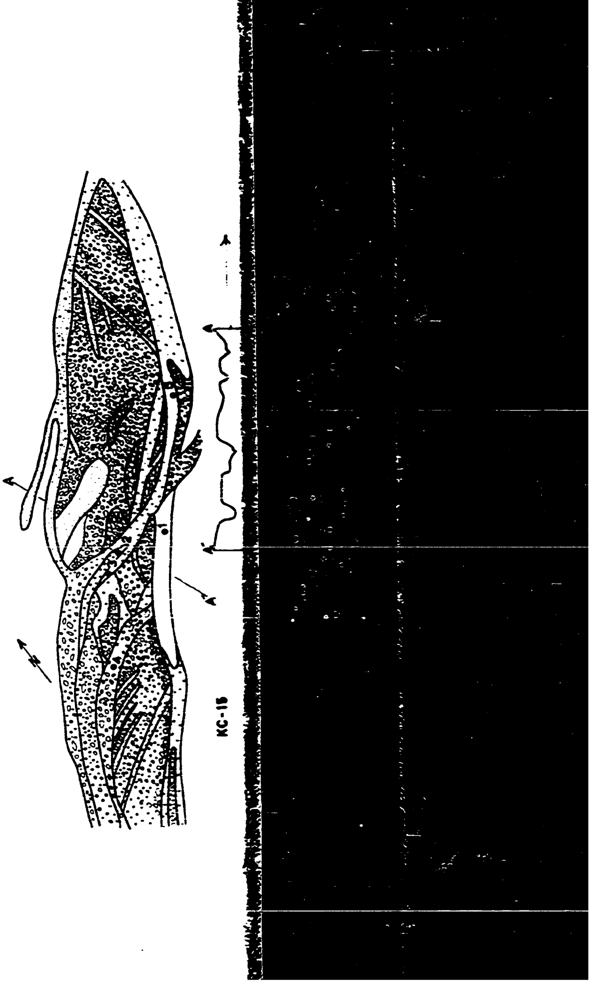
KC-15

Figure 29. Plane-table map of a braided channel segment at locality 15 on the Kyle Canyon fan.

Grain size at this locality is fairly coarse. Mean pebble size along profile A-A' is -5.3 ∅. Graphic means of the grain size cumulative curves are 4.2, 2.5, 3.6, 1.7, and 1.6 ∅ (an average of 2.7 ∅); coarser than KC-14.

This area of the fan is characterized by large bars that occupy most of the channel proper. They average 36 m in length and 8 meters in width. Maximum bed relief is 0.6 meters. The bars are roughly oriented parallel to flow (to the right) and they exhibit little dissection by cross-cutting channels. It appears that the large bar to the right of A-A' formed first, diverted flow around it, and influenced the deposition and erosion of the bar to the left of A-A'.

Low areas such as #1 acted as traps for fine grained sediments by creating low velocity eddy zones.

Note the poorly sorted nature of curves 2-5 which implies that selective size sorting of the less than -1 ∅ range was not taking place. This suggests that the ebbing flow ceased rather rapidly losing much of its volume through infiltration into the gravels.

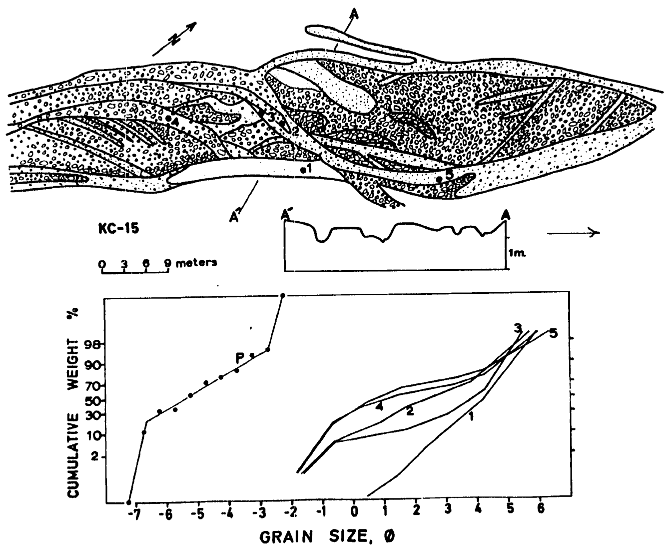

N
A
A'
KC-15
0 3 6 9 meters
1m
P
1
2
3
4
5
CUMULATIVE WEIGHT %
98
90
70
50
30
10
2
-7 -6 -5 -4 -3 -2 -1 0 1 2 3 4 5 6
GRAIN SIZE, Ø

Figure 29.

Figure 30. Plane-table map of braided channel segment at locality 16 on the Kyle Canyon fan.

This locality is closer to the apex of the fan and exhibits an increase in grain size and bed relief relative to localtiy 15. The mean pebble size along profile A-A' is 5.2 ∅ and the distribution has a coarse tail approaching -8 ∅ in size. The graphic mean of the cumulative distribution curves are 0.98, 2.5, 2.5, 3.9, and 5.0 ∅ (average 2.9 ∅). Areas of fine sediment accumulation such as #3 are small, and boulders are beginning to become numerous on the larger bars.

Average bar length is 17 meters and average width is 2.9 meters. Maximum bed relief is 0.8 meters. The large bar traversed by profile A-A' is lobate and roughly parallel to flow (to the right). The bar is cut by several small channels giving it a chevron-like appearance. Channels of this type are throught to be formed during ebbing flow over the bar. They are oblique to and often flow towards the thalweg of the channel.

Along the upper edge of the map, to the left of A-A', is what is probably best described as a natural level deposit. These deposits are not common but where present, they are located opposite the thalweg where flow has been deflected from the channel by a large bar.

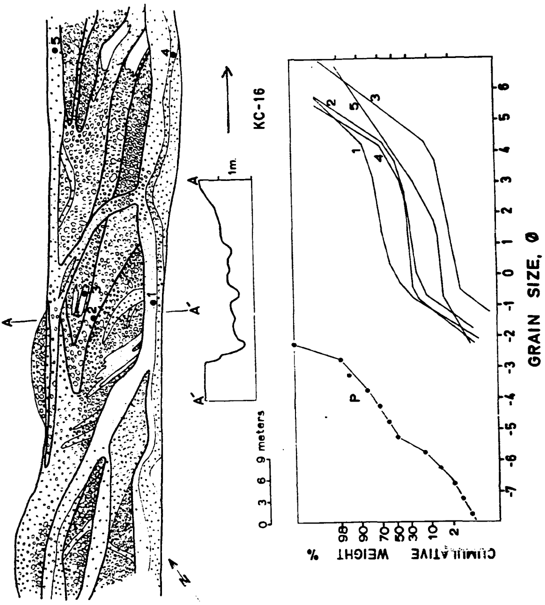
A
A'
1m.
KC-16
0 3 6 9 meters
N
CUMULATIVE WEIGHT %
98
90
70
50
30
10
2
GRAIN SIZE, Ø
-7 -6 -5 -4 -3 -2 -1 0 1 2 3 4 5 6
P
1
2
3
4
5

Figure 30.

Figure 31. Plane-table map of braided channel segment at locality #21 on the Kyle Canyon fan.

As evidenced by this map, braid bar histories are far from simple and their shapes may be modified to a great degree after deposition. In this case, a small but deep channel is superimposed on the larger scale bed forms. Obviously unrelated to the flow that deposited the large bars, the small channel has small longitudinal bars that decrease in size from their downstream end (to the right) to their upstream end where the sediment is similar in size to that of the channel. (Note the small bar just below B.)

Grain sizes in this area are coarsely skewed with cumulative curves having graphic means of 0.52, 0.88, 1.27, 0.42, and 3.5 ∅ (an average of 1.3 ∅).

The bars average 14 meters in length and 2.5 meters in width. The maximum bed relief is 0.7 meters.

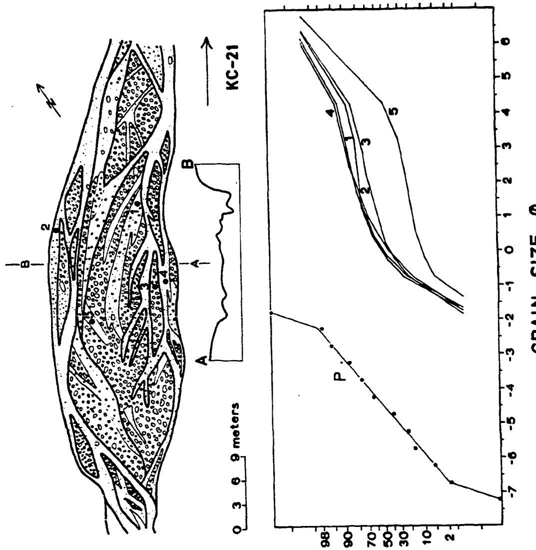

Figure 31.

Figure 32. Plane-table map of braided channel segment at locality 17 on the Kyle Canyon fan.

Locality 17 is an area where broad complex bar forms are the main channel features. The bars are lobate and are cut by numerous small channels which splay out over the bar surfaces. The most recent channel is located at the upper edge of the map and encompasses data points 2 and 3. Again, the smaller longitudinal bars in this channel appear to be the most recent and unaffected by past depositional erosion.

This locality is along the main channel of the Kyle Canyon fan and the grain size is fairly coarse. Graphic means of the cumulative curves are 1.3, -0.05, 1.65, 1.07, and 0.37 ∅ (an average of 0.87). Maximum bed relief is 0.8 meters. Pebble sizes approach the -8 phi interval.

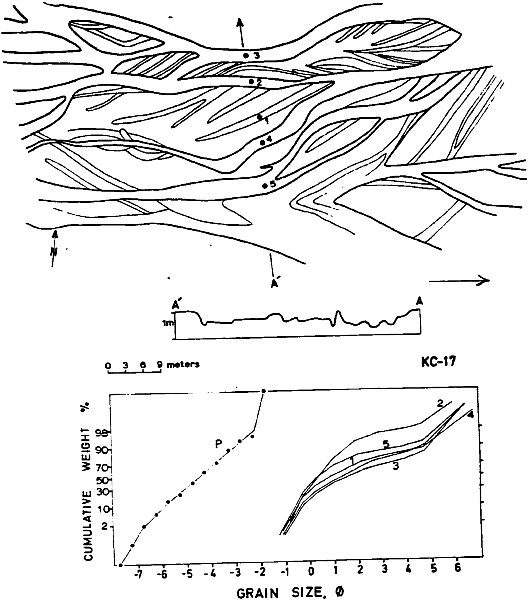
A
3
2
1
4
5
N
A'
A'
A
1m
0 3 6 9 meters
KC-17
CUMULATIVE WEIGHT %
98
90
70
50
30
10
2
P
2
5
1
3
4
-7 -6 -5 -4 -3 -2 -1 0 1 2 3 4 5 6
GRAIN SIZE, Ø

Figure 32.

Figure 33. Plane-table map of braided channel segment at locality 20 on the Kyle Canyon fan.

This locality is near the toe of the fan and it is highly dissected by numerous small channels. Several areas of fine sediment accumulation in lows such as at #1 exist in the area. This fining is also evident in the cumulative curves which have graphic means of 4.56, 2.4, 1.5, 3.1, and 2.04 ϕ (an average of 2.7 ϕ). Compared with the previously discussed locality 17 there is a drastic difference in grain size. Maximum bed relief here is 0.3 meters.

When fluid flows reach this far down fan they probably lack enough energy or competence to create the large scale bar forms observed closer to the apex. If large scale features were formed, the time between the high volume flows that create them is great and their depositional features are probably destroyed completely.

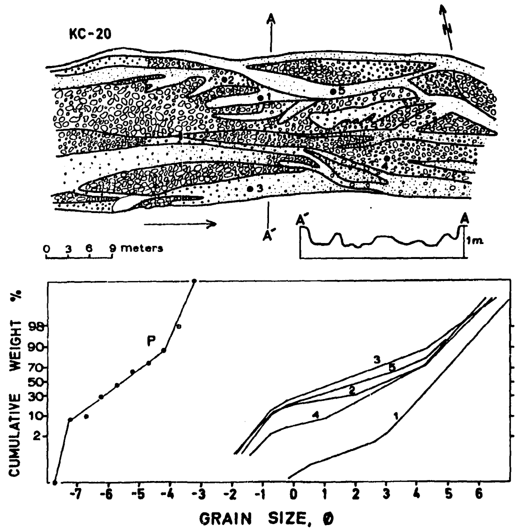
KC-20
A
A'
N
1
2
3
4
5
0 3 6 9 meters
A'
A
1m.
CUMULATIVE WEIGHT %
98
90
70
50
30
10
2
P
1
2
3
4
5
-7 -6 -5 -4 -3 -2 -1 0 1 2 3 4 5 6
GRAIN SIZE, Ø

Figure 33.

Figure 34. Plane-table map of locality 2 in Lida Wash.

Bar morphologies found in Lida Wash are similar to those present on the Kyle Canyon fan. They are somewhat simpler in that the complex lobate forms present in the Kyle Canyon washes are not as common here. The bars are more longitudinal and small channels have fairly long straight segments. Bed relief at this locality is almost 2 meters, much greater than that present in the Kyle Canyon area. The average bar here is 29 meters in length and 3.3 meters wide. The average clast size along a transverse profile is - 7.3% Ø and the average graphic mean of the cumulative curves is 1.0 Ø.

Sinuous boulder ridges are present as erosional remnants of bars deposited during periods of high velocity, high volume flow. The long axes of the ridges are almost always parallel to flow.

Rapid lateral textural changes present in the Kyle Canyon fan channels is also a feature in Lida Wash. Coarse gravel and bouldery bars are bounded by sandy, fine-gravel channels.

Bed relief, maximum particle size and the straightness of bars and channel segments indicate higher volume, higher velocity flows are more common in Lida Wash than in the Kyle Canyon area.

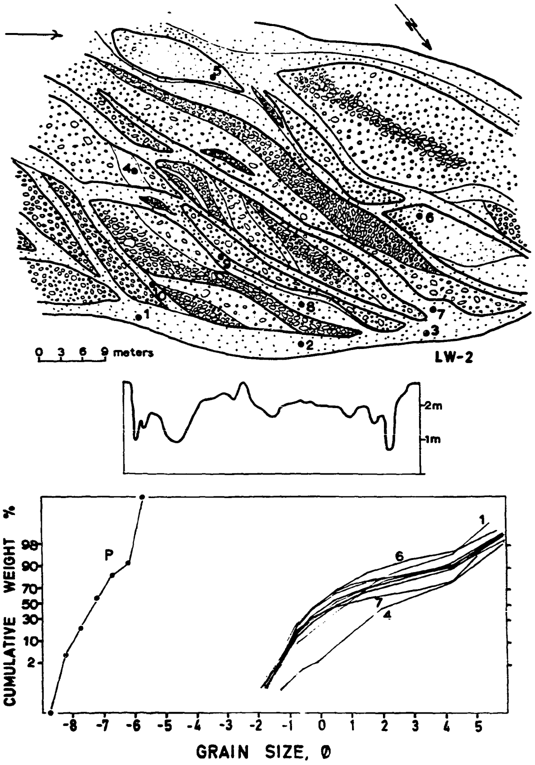
N
1
2
3
4
5
6
7
8
9
10
0 3 6 9 meters
LW-2
2m
1m
CUMULATIVE WEIGHT %
98
90
70
50
30
10
2
P
1
6
7
4
-8 -7 -6 -5 -4 -3 -2 -1 0 1 2 3 4 5
GRAIN SIZE, Ø

Figure 34.

Figure 35. Plane-table map of braided channel segment at locality 1 in Lida Wash.

Bed relief at this locality reaches a maximum of 1.1 meters and the average bar size is 28 meters in length and 6.3 meters in width. Boulders are still common as evidenced by curve "P" in which clast sizes approach -9 Ø .
Boulder ridges are still common at this locality.

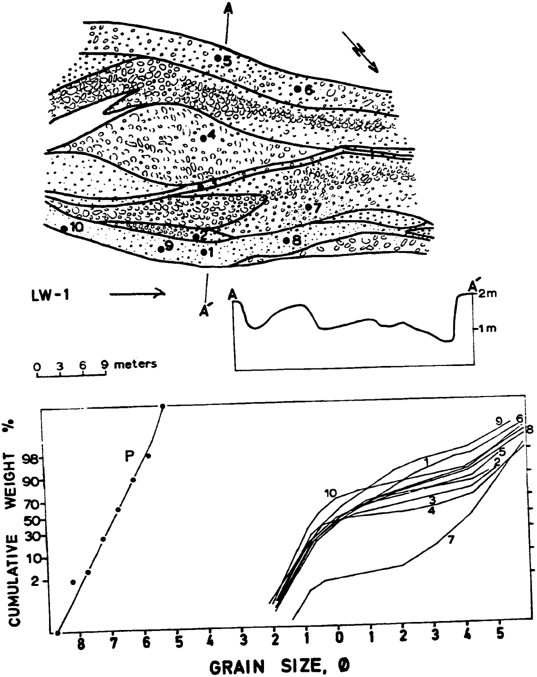
A
5
6
4
3
7
10
2
9
1
8
LW-1
A'
A
A'
2m
1m
0 3 6 9 meters
CUMULATIVE WEIGHT %
98
90
70
50
30
10
2
P
10
1
9
6
8
5
2
3
4
7
8 7 6 5 4 3 2 1 0 1 2 3 4 5
GRAIN SIZE, Ø

Figure 35.

Figure 36. Plane-table map of braided channel segment at locality 6 Lida Wash

As previously noted, the majority of bars present in Lida Wash can be classified as longitudinal, whereas those of the Kyle Canyon area are more lobate and are highly dissected. Most of the bars at this locality are very lenticular and exhibit little dissection by cross-cutting channels. Several factors may account for the difference in bar morphologies between Lida Wash and the Kyle Canyon area. Flow regimes may be higher and flows more frequent in Lida Wash. The volcanic sediments in the source area (vs. mainly carbonates in Kyle Canyon) supply abundant sand and finer material to the regimen of Lida Wash. Thus the distinction between bars and channels may be more pronounced in Lida Wash.

Compared with localities 1 and 2 which are farther "upstream," locality 6 exhibits a smaller maximum bed relief of 0.5 meters, a smaller average clast size, and smaller bedforms. The average bar size is 18 meters in length and 2.5 meters in width.

The random gravel size profile "P" does not reflect the anomalous presence of mega boulders present near this locality. Shown in Plate IX-4, the boulders which approach 2 meters in diameter may be remnants of a large magnitude mudflow.

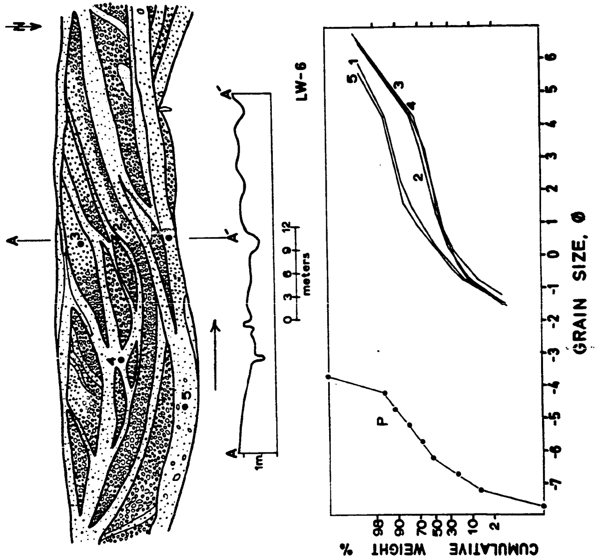
N
A
A'
0 3 6 9 12
meters
1m
LW-6
1
2
3
4
5
P
CUMULATIVE WEIGHT %
98
90
70
50
30
10
2
GRAIN SIZE, Φ
-7 -6 -5 -4 -3 -2 -1 0 1 2 3 4 5 6

Figure 36.

Figures 37, 38, and 39 show three series of cross-channel profiles on the alluvial fans studied. In all three series there is a marked decrease in bed relief from the proximal to the distal profiles. This is accompanied with a decrease in channel width and an increase in small scour channels relative to boulder bars and ridges.

Outcrop Studies

When studying ancient sediments, the geologist deals with outcrops of generally well lithified materials in which the third dimension is introduced. Sedimentologists can often enlarge their perspective of these ancient deposits by excavating their Recent analogs (i.e., point bars, beaches, dunes, etc.), but alluvial-fan gravels present a great problem in this respect. Good natural exposures must be found, but in most cases incised streams on fan surfaces have gently sloping sides that rarely produce outcrops. Fans such as the Kyle Canyon fan, which have an abundance of carbonate rocks in their drainage basins, have proved to have good outcrops as a result of case hardening of the walls of incised streams. (See Lattman and Simonberg, 1971.)

Panoramic photographs were taken of good exposures at various locations across the Kyle Canyon alluvial fan. Bedding, highlighted by textural variations, was traced from these photos and studied in detail. The following fold-out illustrations illustrate the bedding characteristics found

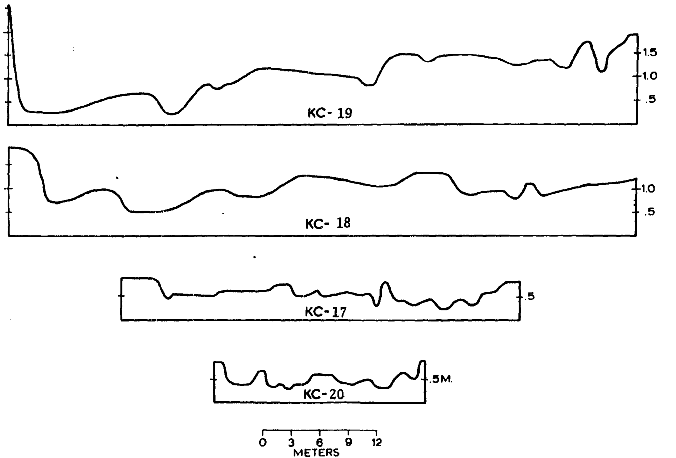

Figure 37. Series of cross-channel profiles along main wash of the Kyle Canyon alluvial fan. Vertical exaggeration = 5x.

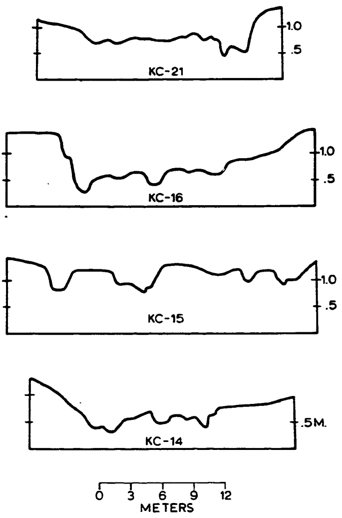

Figure 38. Series of cross-channel profiles on the Kyle Canyon fan.
Proximal profile = KC-21;
Distal profile = KC-14.

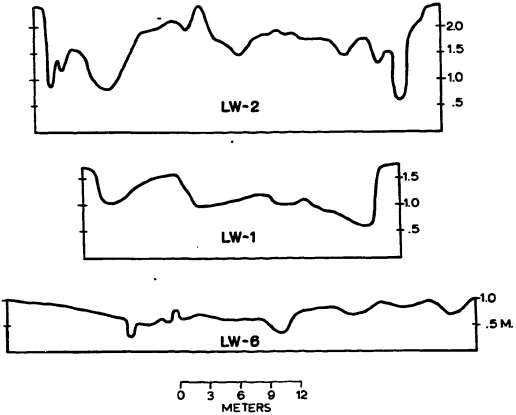

Figure 39. Series of cross-channel profiles in Lida Wash.
Proximal = LW-2; Distal = LW-6.

on the Kyle Canyon fan. Numbers I and II are located near the apex, III, IV, and VII are from the mid-fan region and numbers V and VI were taken at its distal margin.

Foldouts I and II

Panoramic views of sediments in the fan bay area of the Kyle Canyon fan (for photo see Plate VI). The conglomerates are characterized by the following:

a. Abundant channel scours which are frequently infilled with large scale cross-bedding, highlighted by pebble orientations.

b. Massive, poorly sorted, bouldery bar deposits commonly greater than one meter thick which are discontinuous laterally.

c. More continuous, thinner (<40 cm) fine to medium gravel channel deposits.

The large scale inclined bedding features seem to be related to lateral bar migration. Thinner beds of fine gravel exhibit internal cross-stratification related to lesser flows that are confined to inter-bar channels. Bed relief is at a maximum and sorting is better developed than in the deposits on the fan proper. Boulder bars are the dominant feature in this area.

I

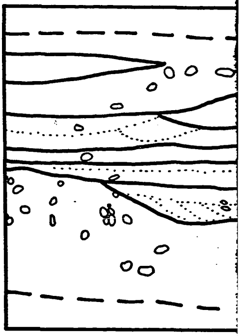

II

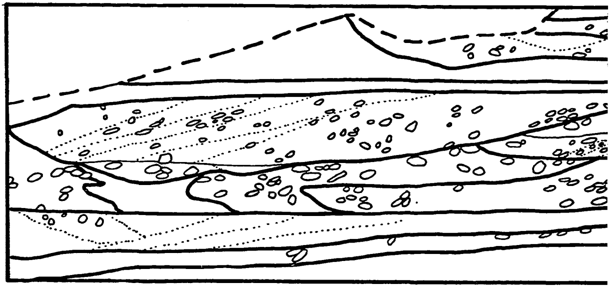

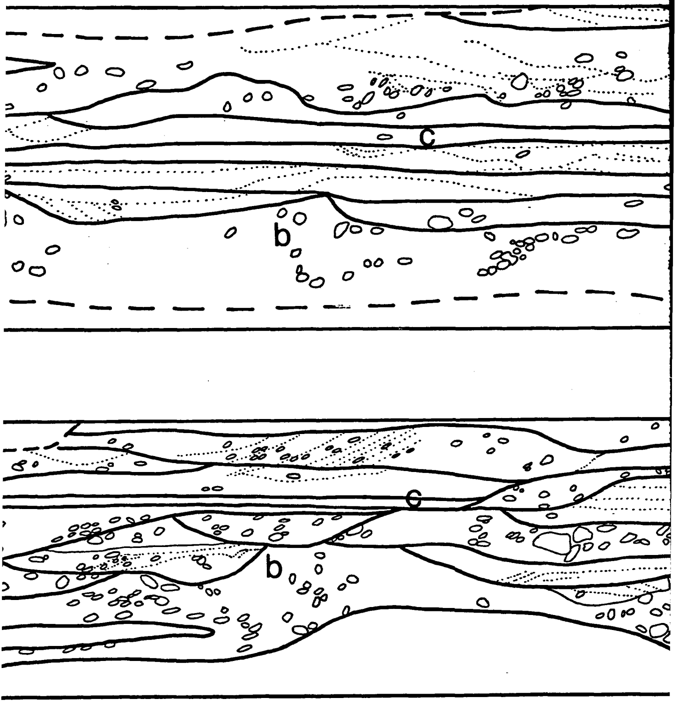
c
b
c
b

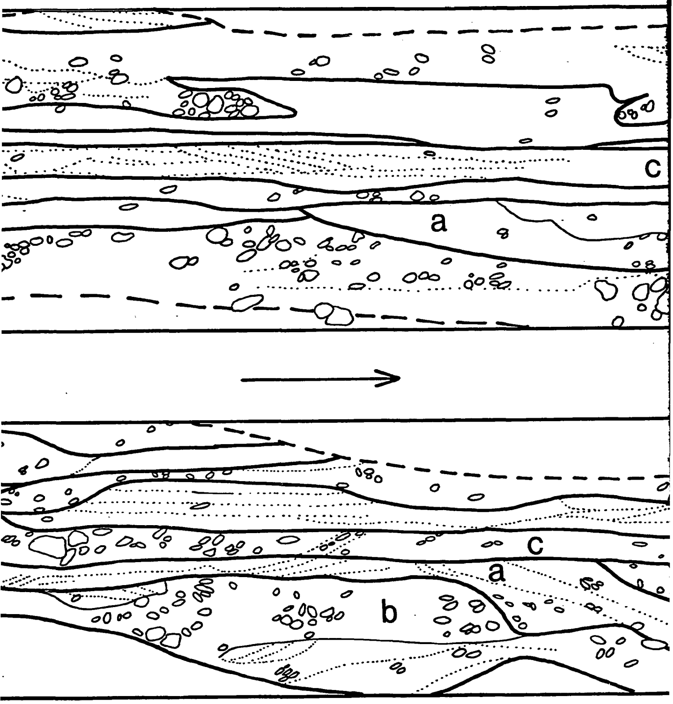
c
a
c
a
b

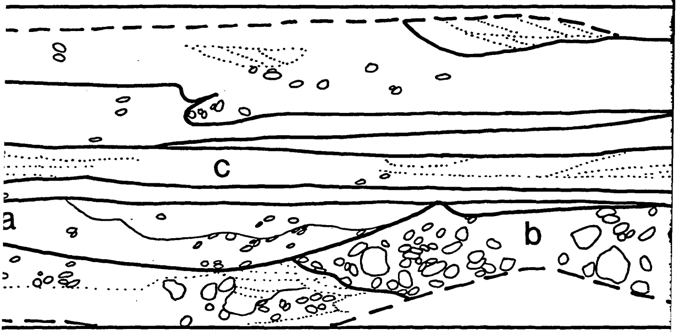
c
a
b

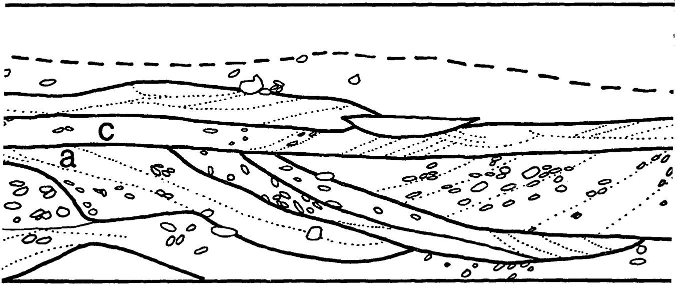
c
a

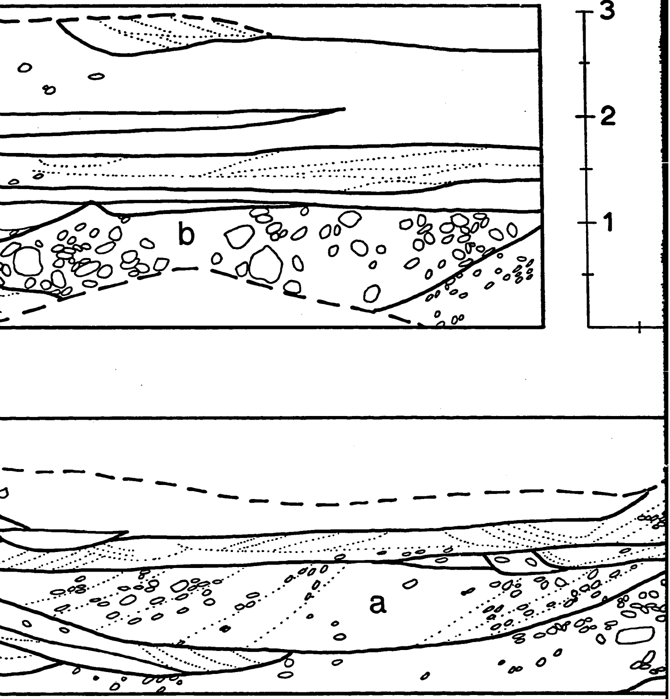
3
2
1
b
a

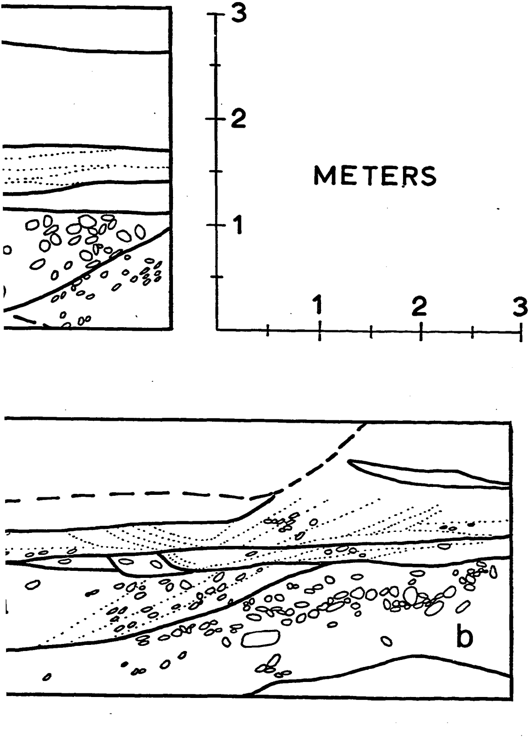
3
2
1
METERS
1
2
3
b

Foldout III and IV Mid fan region

Bed relief is diminished relative to that present in the upper fan area. Large scale channel fills and lateral bar migration features are rare to absent. The average clast size is much diminished with less abundant cobble sized material present.

The mid-fan area sediments (III, IV, and VII) are characterized by the following:

a. A lesser proportion of bouldery bar deposits.

b. An increase in small width scour-and-fill structures.

c. An increase in fine to medium gravel, thin lenticular channel deposits with low angle cross-stratification.

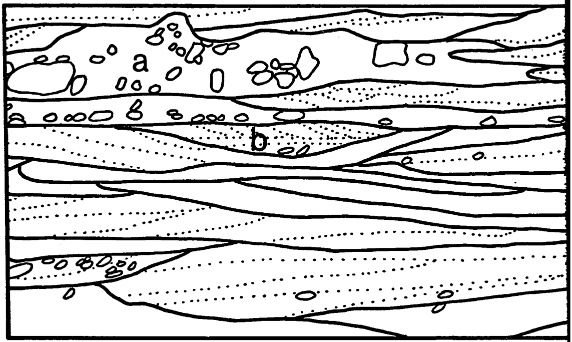

III

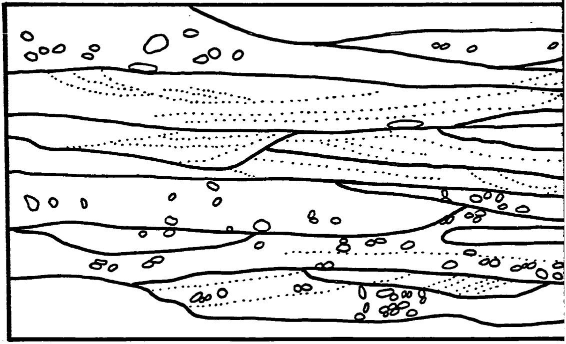

IV

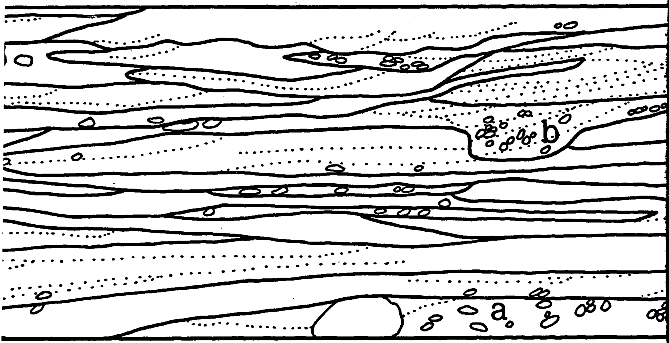
b
a

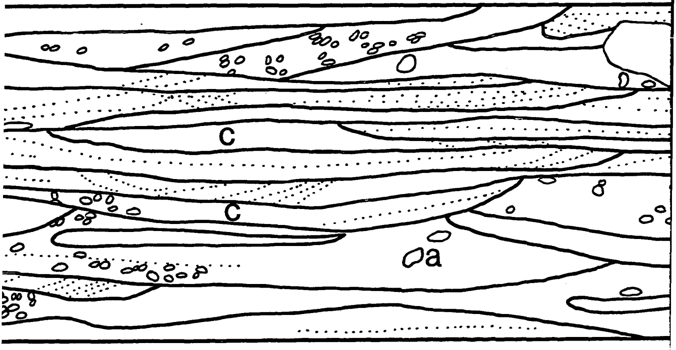
c
c
a

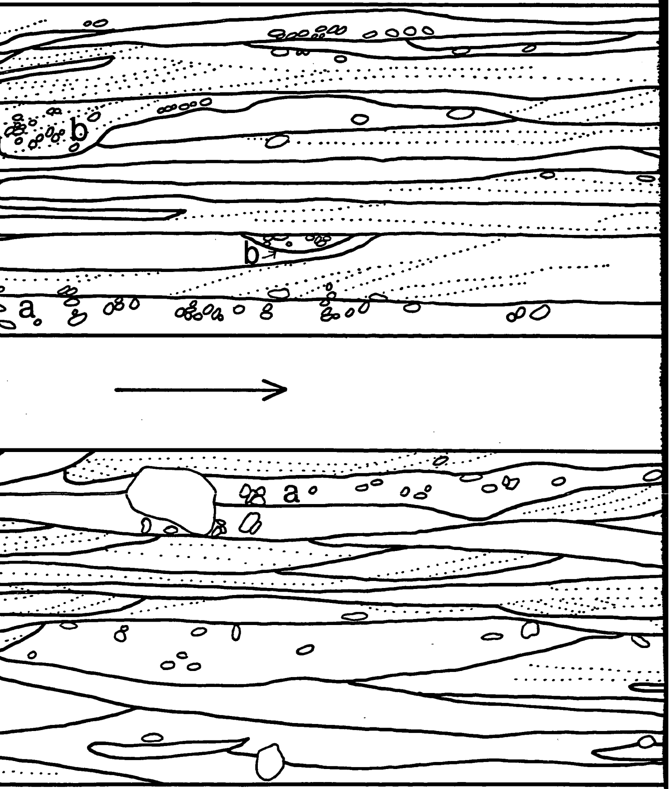
b
b
a
a

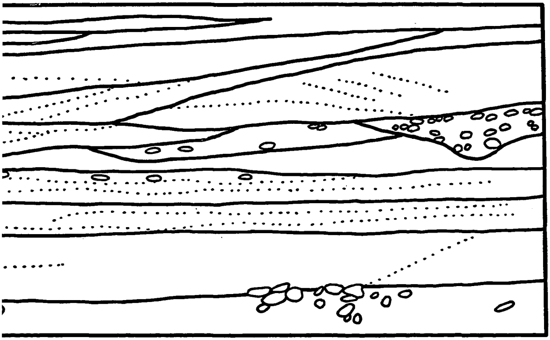

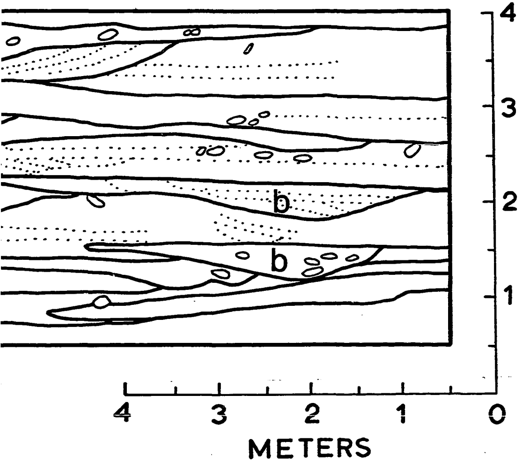
b
b
4
3
2
1
4
3
2
1
0
METERS

Foldout V and VI Distal Fan Area

The distal portion of the Kyle Canyon fan is characterized as discussed previously by an interfingering of fan sediments with pluvial lake sediments. The grain size in this area is again diminished with a complete absence of boulders. Much silt sized material is present in the section as distinct beds and as matrix in the gravels. Gravel beds are very thin and distinguishing individual beds on the scale in the foldout is difficult.

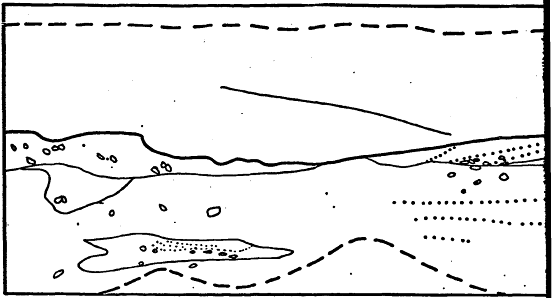

V

VI

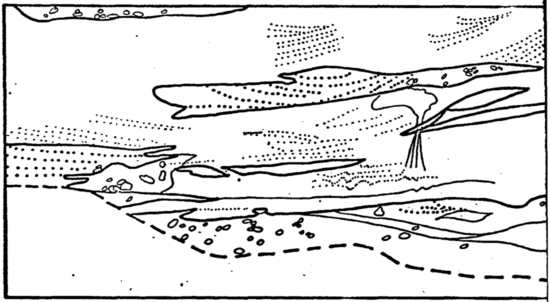

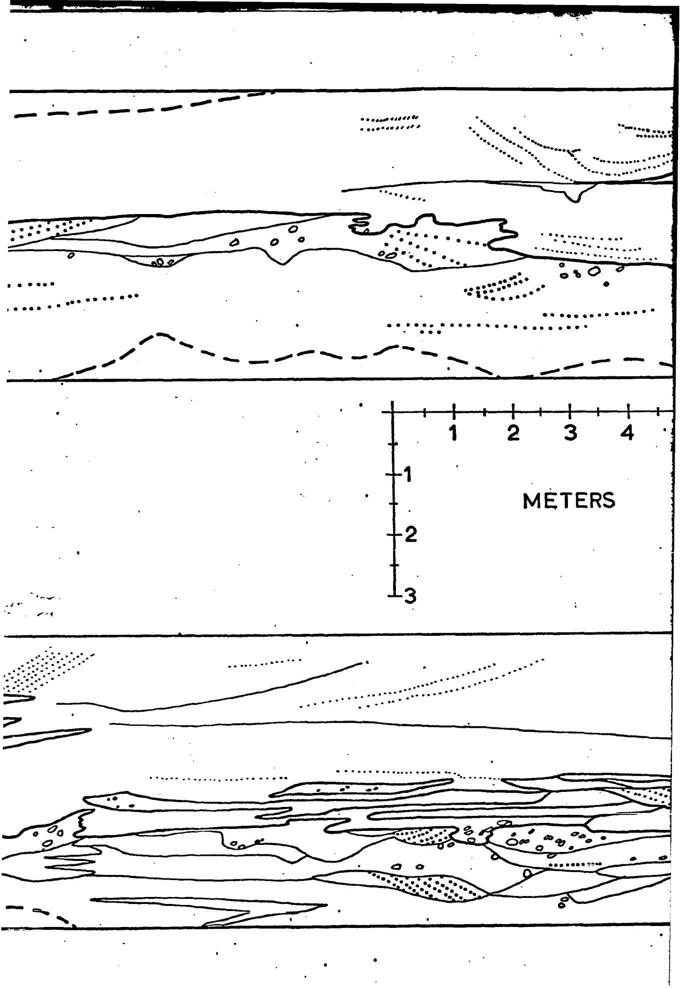
1
2
3
4
1
2
3
METERS

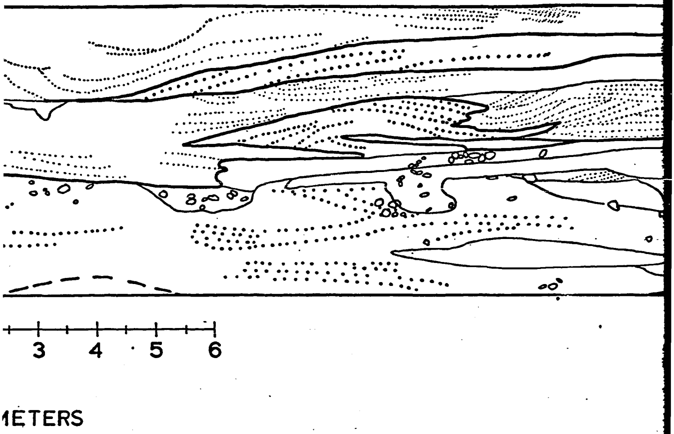
3
4
5
6
METERS

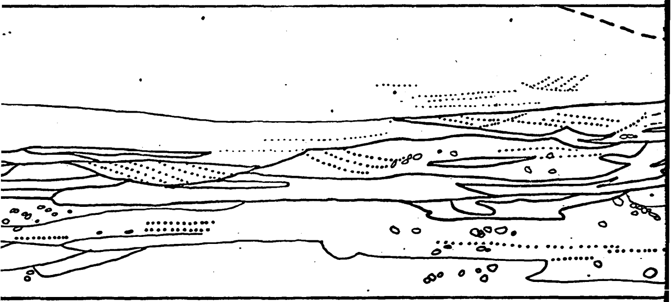

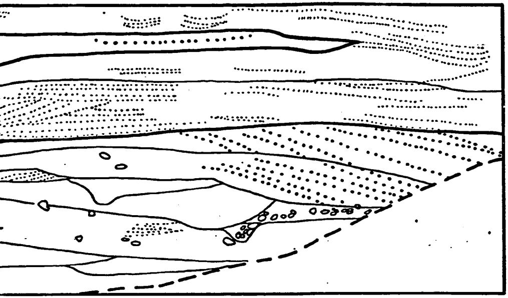

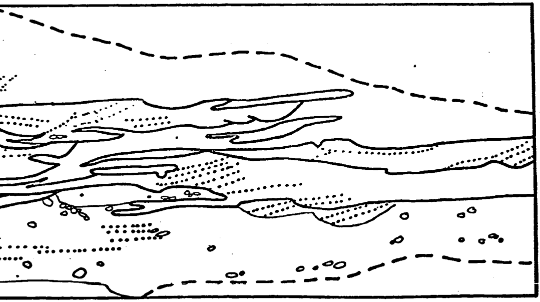

Foldout VIII

For comparison purposes an example of a fossil mudflow is given in this foldout series. The outcrop is located at locality number 28 on Figure 47. The large clasts are andesitic in composition and are surrounded by sand, silt, and clay size material. Several of the large clasts have their long axes parallel to bedding and some project into the overlying bed. The mudflow units in this area are often overlain by thin well-sorted sand beds (a on VIII) that are discontinuous laterally.

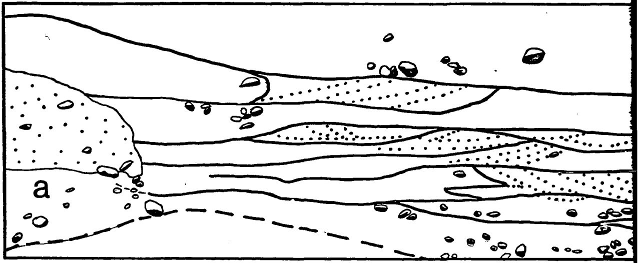

VII

VIII

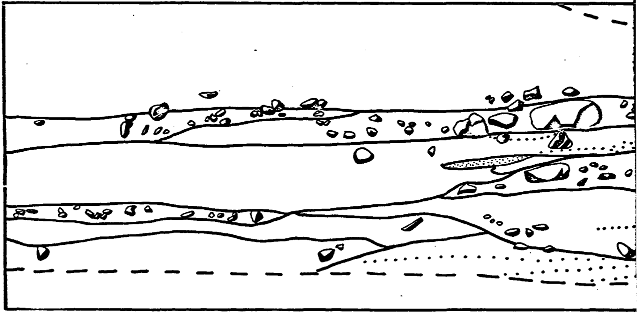

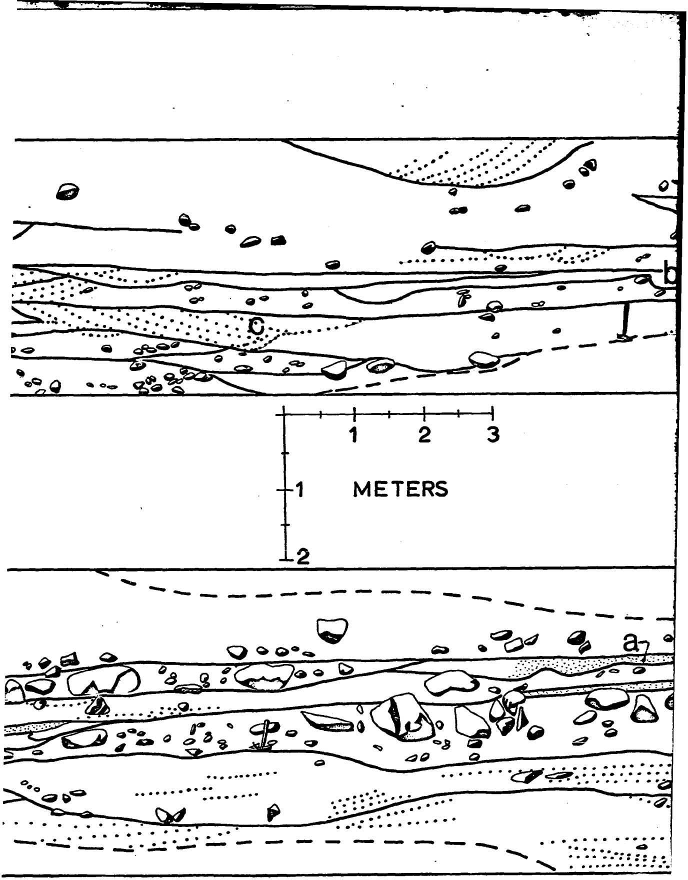

b
c
1 2 3
1 METERS
2
a

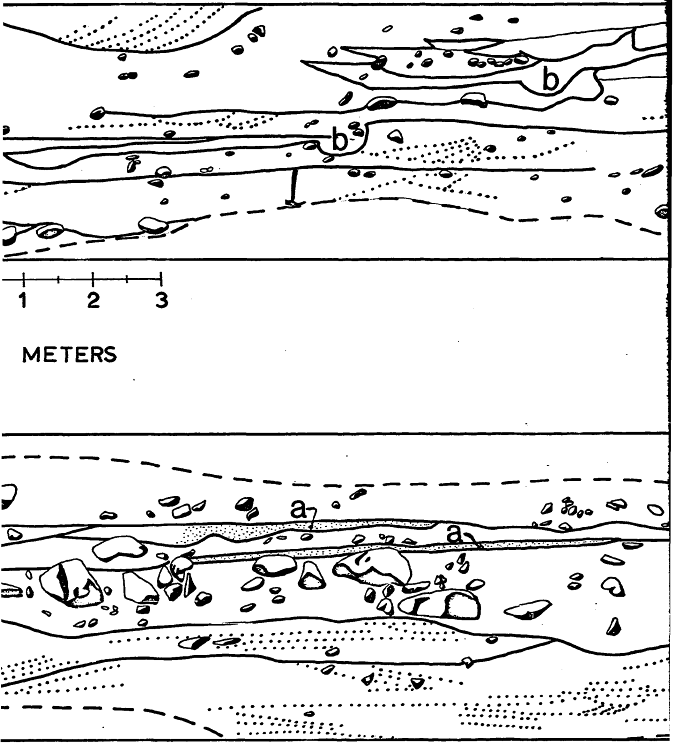
b
b
1 2 3
METERS
a
a

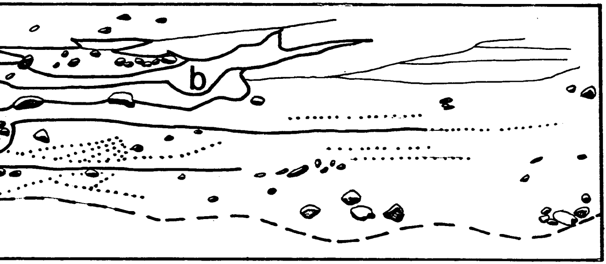
b

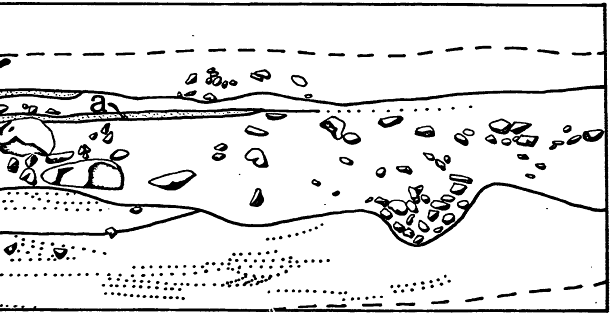
a

Down fan changes in bedding characteristics appear to be related to the frequency, duration, intensity, and discharge rate of floods reaching the fan. Most precipitation occurs in the mountains, not on the fan proper, hence the proximal areas of the fan have a greater probability of being affected by flooding of higher intensity and longer duration than the distal portions. Water flowing from the mountains is confined in definite channels until it is well out on the fan surface. Unconfined flow across the fan surface does not have the competence to transport boulders and cobbles for any great distance. Spring melt water runoff coupled with possible intense spring rains could produce enough discharge for flooding to reach the distal portions of the fan. However, because of down-fan increases in infiltration and channel width with a corresponding decrease in channel depth and slope, the flow loses competence.

The bedding characteristics observed on the Kyle Canyon fan reflect this down-fan decrease in the intensity of flow. The proximal sediments exhibit several distinct features. Cross stratification is common and often occurs on a large scale (up to 1 meter). (Plate XII.) The conglomerates are relatively well sorted and there is an absence of sand and silt interbedded as distinct beds within the gravels. Bedding units are generally impersistent laterally, but thin fine gravel beds may be very continuous. Erosional bedding planes

Table 7. Bar and channel dimensions (in meters) measured from plane-table maps. KC = Kyle Canyon; LW = Lida Wash.

Station Number	Bar Width	Bar Length	Channel Width	Channel Length
KC - 19	4.0 M	18.5 M	4.0 M	34 M
	5.5	24.0	2.3	25
	10.0	33.0	4.5	20
	4.0	18.0	6.5	40
	5.0	24.0	0.5	13
	6.5	16.0	1.0	16
	10.0	25.0	2.5	40
	11.0	28.0	2.5	22
	3.0	14.0	1.5	16
	6.0	28.0		
	Average 6.5	22.9	2.8	25
KC - 18	4.5 M	32.0 M	2.7 M	32 M
	6.0	30.0	2.2	25
	5.2	24.0	2.7	18
	8.0	34.0	1.2	15
	4.5	28.0	3.5	36
	5.2	32.0	1.0	17
	7.0	35.0	4.0	34
	2.5	16.0	1.5	32
	15.0	28.0	2.0	31
	2.0	10.0		
	Average 6.0	26.9	2.3	27
KC - 16	4.5 M	22.0 M	2.5 M	32 M
	3.0	20.0	2.2	20
	2.0	13.0	1.5	26
	3.0	10.0	1.0	26
	3.0	17.0		
	2.5	20.0		
	2.5	20.0		
	Average 2.9	17.4	1.8	26

Table 7 (Continued).

Station Number		Bar Width	Bar Length	Channel Width	Channel Length
KC - 15		13.0 M	49.0 M	2.0 M	23 M
		3.4	30.0	2.4	23
		8.0	30.0	1.5	19
				2.5	16
				4.0	31
				.8	15
	Average	8.1	36.3	2.2	21
KC - 14		1.5 M	14.0 M	3.0 M	34 M
		1.0	9.0	1.0	13
		3.0	22.0	1.0	14
		3.3	18.0	1.5	21
		1.8	7.0	0.9	20
		1.5	6.0	1.2	12
		1.8	6.3		
		.5	6.5		
		.8	7.0		
		.7	8.5		
	Average	1.6	10.4	1.4	19
KC - 17		4.5 M	16.0 M	2.1 M	28 M
		3.8	15.0	1.5	34
		2.3	18.0	3.2	38
		8.0	28.0	2.0	20
		10.0	37.0	1.0	20
		4.5	20.0	2.5	28
		9.5	28.0	1.2	24
	Average	6.1	23.1	1.9	27
KC - 20		3.8 M	31.0 M	2.0 M	25 M
		1.8	12.0	1.1	27
		3.8	25.0	3.0	24
		1.5	18.0	2.3	30
		1.8	27.0		
		3.0	11.0		
	Average	2.6	21.0	2.1	26

Table 7 (Continued).

Station Number		Bar Width	Bar Length	Channel Width	Channel Length
KC - 21		1.6 M	15.0 M	1.5 M	18 M
		2.0	8.0	1.5	18
		1.5	8.0	0.8	17
		3.0	11.0	1.2	13
		5.0	16.0	1.5	17
		1.3	12.0	1.2	16
		1.4	13.0	.5	9
		6.0	27.0		
		1.0	14.0		
	Average	2.5	13.8	1.2	15
LW - 2		3.0 M	36.0 M	1.5 M	48 M
		5.4	42.0	3.8	39
		2.4	20.0	1.0	26
		2.0	41.0	1.5	21
		2.4	24.0	2.1	20
		4.8	20.0	1.0	22
		3.0	21.0	1.0	18
				3.0	27
	Average	3.3	29.1	1.9	28
LW - 1		3.6 M	25.0 M	3.0 M	28 M
		9.0	30.0	0.9	27
				3.6	42
	Average	6.3	27.5	2.5	32
LW - 6		2.3 M	21.0 M	1.2 M	12 M
		4.8	19.0	2.0	27
		1.8	14.0	1.5	31
		3.6	23.0	3.0	31
		2.0	15.0	3.0	29
		2.3	24.0	1.5	25
		1.2	13.0		
	Average	2.5	18.4	2.0	26

are also common but less abundant than in the midfan sediments. Because flows affecting the proximal fan areas are more constant, "imbrication" and orientation of pebbles is greater. Beds are thicker reflecting more continuous sedimentation. Near structureless coarse gravel and boulder bars are flanked by coarse sand to coarse gravel channel fill deposits that exhibit large scale cross-stratification, probably as a result of lateral infilling of channels by bar growth.

Table 8. Summary of bed length and bed thickness measurements

Profile Number	L Bed Length	T Bed Thickness	L/T
I and II	7.5 M	.50 M	15/1
III	8.0 M	.42 M	20/1
IV	5.6 M	.42 M	13/1
VII	5.4 M	.37 M	14/1
V and VI	5.8 M	.44 M	13/1

Discussion

To gain a better insight into the processes active in forming the sedimentary associations found on the Kyle Canyon alluvial fan, a discussion of studies of Recent braided stream sediments would be beneficial. Because of the infrequency of stream flow on alluvial fans, there is an absence of published data relating the sedimentary structures found in alluvial fan deposits to their formative processes. In the following discussion I will apply the observations of several students of braided streams to the interpretation of the Kyle Canyon fan sediments.

Doeglas (1962) carried out detailed investigations on the Durance and Ardeche Rivers, France. This paper documents the distributions of sedimentary structures and vertical sequences in rivers carrying coarse material.

Macrostructures of the deposits of the Durance and Ardeche Rivers show that horizontal parallel bedding is not common. In cross sections of the deposits, Doeglas found that channel structures or festoon laminations will prevail. This structure is depicted in Figure 40. He observed that at the beginning of floods, cross channels are present in abundance and coarse material from upstream is trapped in them. If the cross channels are shallow, no steep-dipping oblique lamination can be formed. The pebbles are deposited as soon as they roll over the edge into deeper water and the fines travel a bit farther before settling giving each layer a grading by size in a downstream direction. If the channel has a steep concave bank which points upstream, oblique lamination may be formed. Figure 40.

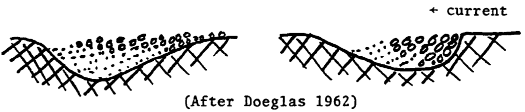

(After Doeglas 1962)

This type of bedding structure has also been frequently observed in sandier deposits in the Netherlands by Augustinus and Riezebos (1971). It is a good explanation for similar structures present in the mid-fan and proximal sediments on the Kyle Canyon fan (see Plate V). The dip of the observed structures was always in a downfan direction. This particular structure appears to be a very good indicator of the extremely variable flow conditions found on alluvial fans of semi-arid regions. In the interpretation of ancient sediments it could be used as a paleocurrent indicator as well as indicating deposition by a braided stream with fluctuating discharge.

Apparent oblique laminations (channel laminations) parallel to the bottom profiles of channels are also common in the sediments studied by Doeglas (1962). These originate at the downstream ends of braid bars in places where they are being built out with a tail into a secondary channel. This structure is also very evident in exposures of alluvial fan sediments, and is most common towards the fan apex where flows are more likely to be of longer duration, enabling bar growth (Plate VI).

Orientation studies conducted by Doeglas revealed that the long axes of cobbles, pebbles and sand grains are generally normal to the current direction and that they are imbricated upstream. This is in good agreement with pebble orientation data from Kyle Canyon fan and Lida Wash.

Another detailed study of a braided stream was presented by Williams and Rust in 1969. Their work on the Donjek River of the Yukon Territory, Canada, provides additional data on channel and bar characteristics, facies relationships and directional features.

Williams and Rust recognize three types of bars present in the Donjek River: longitudinal, transverse, and point bars. Longitudinal bars are the most common, but no percentage figures are given (Figure 41).

Particle sizes ranged from clay to boulders with the average size being around 1.0 ∅ and a maximum diameter in excess of 22 cm. The graphic standard deviation and sorting values show the sediment to be moderately to poorly sorted, positively skewed, and predominantly mesokurtic to leptokurtic. This indicates an excess of fines, a general lack of current winnowing and a tendency for better sorting for the central portion of the grain size distribution (Figure 42). CM plots permit Williams and Rust to divide the braided-stream sediment into three main groups: silt and mud of low energy environments such as abandoned channels, gravel of high energy channel-bar complexes, and a variable intermediate group which fills channels under medium energy conditions. Their CM plots give support to the braided stream CM field from alluvial fans as defined by Bull (1964a).

The sedimentary structures recognized by Williams and

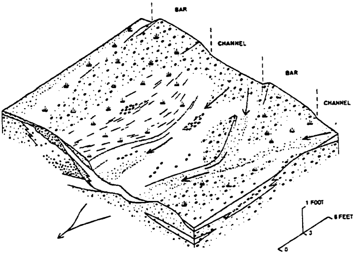

Figure 41. Schematic diagram showing the interrelationships of braided stream lithologies. (After Williams and Rust, 1969.)

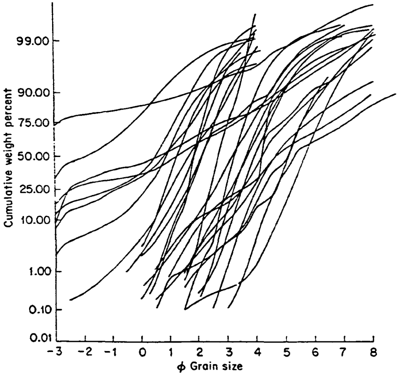

Figure 42. Cumulative size-frequency curves of sediment samples from the Donjek River. Note the extreme variation in both sorting and grain size. (After Williams and Rust, 1969.)

Rust are small-scale ripples, large-scale ripples, cross-stratification, ellipsoidal scours, current crescents, silt volcanoes, bars, channels and bar-avalanche faces. They combined the distribution of these and other attributes into 7 facies.

Few authors have attempted plane table mapping of braided stream segments. Fahnestock (1963) mapped several segments of the White River, a glacial stream in Washington. Two of his maps, which indicate the distributions of current across the bar surfaces as well as the fining downstream of the individual bars, are shown in Figure 43. In his analysis of the White River channel patterns, Fahnestock concludes that a braided pattern may result from the reoccupation of numerous old channels owing to deposition within the main channel as well as to high flows that raise the water surface. Leopold and Wolman (1957) describe the formation of a braided pattern in a flume channel by the deposition of a central bar that subsequently became an island. The common element in most explanations of braiding appears to be a movement of bed load with local deposition within the channel causing a diversion of flow from one channel into one or more other channels or causing the deposition of channel bars and islands. Braided channel segments can occur, as noted by Fahnestock, in reaches where the stream is aggrading, poised or degrading and the pattern alone does not conclusively define the regimen of the stream. White River braiding took

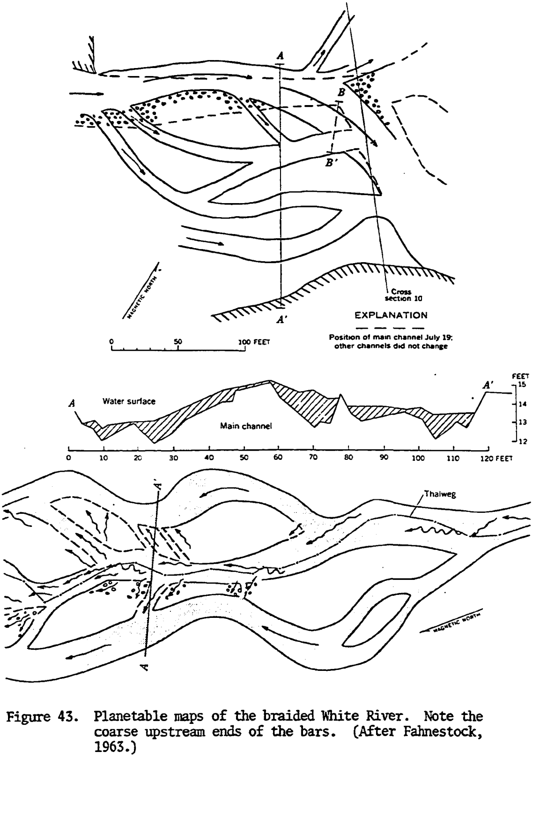

Figure 43. Planetable maps of the braided White River. Note the coarse upstream ends of the bars. (After Fahnestock, 1963.)

place most actively at times of high discharge and large loads.

Rubey (1952) and Leopold and Wolman (1952) recognized that braiding (channel division and island formation) could be a possible equilibrium condition in a channel. Leopold and Wolman also suggested that braiding does not indicate an excess of total load within a stream system. Ore (1964) and Smith (1970) concluded that braiding is created mainly by the accretion of longitudinal bars composed of coarse, poorly sorted sediments, and by the dissection of transverse bars.

Krumbein and Orme (1972) used field mapping techniques and computer simulation to analyze a braided stream segment. Their field observations fully support the idea that braided stream systems often consist of reaches in which a single channel carries all the discharge, followed by a braided pattern of varying complexity, ultimately rejoining to form single channel, and so on in succession downstream.

Smith (1970) used the braided Platte River as a Recent analog of a lower Silurian clastic sequence in New Jersey and Pennsylvania. Smith found that the distribution of bars depends on the texture of the bed load; coarse, poorly-sorted sediment favors formation of longitudinal bars and finer-grained, better-sorted materials form transverse bars. The abundance of transverse bars increases in a downstream direction. This is accompanied by an increase in the ratio of planar cross-stratification to horizontal stratification and a decrease in cross-channel topographic relief (Figure 44). These downstream trends were employed by Smith to compare the Silurian clastics to the Platte River sediments (Figure 45). Although the distances involved are much smaller, similar "downstream" reduction in bed relief was noted on the alluvial fans studied in this report. Other studies of ancient braided-stream deposits are summarized in Table 9.

Table 9. Published examples of ancient braided stream sediments.

Age	Area	Author
Tertiary	Llano Estacado	Bretz and Horberg, 1949
	Wyoming	Spearing, 1969
Cretaceous	Maryland	Hansen, 1969
	Mississippi	Berg and Cook, 1968
	Montana	Gwinn and Mutch, 1965
Devonian	New York	Buttner, 1968
	Northwest Territories Canada	Miall, 1970
	Spitsbergen	Moody-Stuart, 1966
Silurian	New York, New Jersey Pennsylvania	Smith, 1970
Precambrian	Scotland	Williams, 1966, 1969

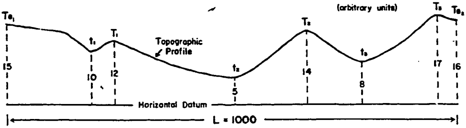

An example of the calculation of a bed-relief index (BRI).

$$BRI = \frac{(15-10)+(12-10)+(12-5)+(14-5)+(14-8)+(17-8)+(17-16)}{1000} \times 100$$

$$= \frac{2[(12+14+17)-(10+5+8)]+15-16}{1000} \times 100$$

$$= 3.9$$

Figure 44. Smith's method for the calculation of the bed-relief index. (After Smith, 1970.)

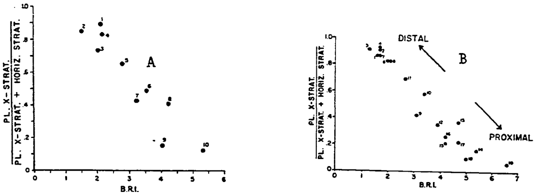

Figure 45. Diagrams showing the relationship between stratification and bed relief. A. For localities on the South Platte River and B. For Silurian clastics. Bed relief decreases in a downstream direction. (After Smith, 1970.)

MUDDY CREEK FORMATION

Geologic Setting

The basin-fill sediments of the Muddy Creek Formation in the vicinity of Lake Mead, Nevada were chosen for inclusion into this investigation because of the availability of excellent exposures over a wide area. The area included in this study is shown in Figure 47. It lies southeast of the Rainbow Gardens area of the Frenchman Mountains and to the north and northeast of the River Mountains in Clark County, Nevada.

The Muddy Creek sediments lie unconformably on sedimentary rocks of the Thumb and Horse Spring Formations in the Rainbow Gardens area and a Tertiary volcanic sequence in the River Mountains area. The Thumb Formation consists of a complex assemblage of clastic rocks ranging from coarse fanglomerates to siltstones. Included at the top of the sequence are large landslide masses of brecciated metamorphic and granitic rocks that Longwell (1974) thinks are related to movement on the Las Vegas shear zone. Fresh water limestones and gypsum beds are also included in the formation, which exhibits an overall coarsening upward trend. The lower sequence from fresh water limestone at the base grades upward into bedded gypsum overlain by a coarse fanglomerate containing Paleozoic limestone clasts. This entire section dips uniformly to the southeast at an angle of

50° (Figure 46a). The relation of the chaotic landslide deposits, which contain some blocks the size of compact cars, is not clear.

In the Rainbow Gardens area, igneous rocks are found only in the upper part of the Thumb, where they form several north-trending sill-like masses (Anderson et al. 1972) (Figure 46a). Anderson and others believe the igneous sequence to be extrusive and therefore the date of the upper Thumb Formation would be Miocene (17 my$\pm$). The lower part of the Thumb is thought to be Cretaceous.

The Horse Spring Formation is composed of carbonates and clastics interbedded with gypsum, borates, and other evaporites. Much volcanic ash found in the Horse Spring Formation gives it a distinctive white coloration. Like the Thumb Formation, the Horse Spring Formation is highly deformed by major movements along normal and transcurrent faults with the major portion of the deformation occurring between 15 and 11 million years before present (Anderson et al. 1972).

Volcanic rocks of the River Mountains range in composition from rhyolite to basalt, are mainly extrusive in origin, and range in age from 11.8 to 13.2 million years. Armstrong (1970) indicates that there is a progression from silicic to mafic rocks in each active area of the Great Basin. A similar trend seems to be indicated in the Lake Mead area where the last phase of volcanism was almost

a

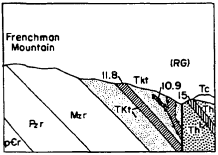

Frenchman Mountain-Rainbow
Gardens (RG) areas

Legend

Tc - Muddy Creek Fm.
Tkt - Thumb Fm.
Mzr - Mesozoic rocks
Pzr - Paleozoic rocks
Th - Horse Spring Fm.
Tcf - Fortification Basalt
Tm - Mount Davis Volcanics

b

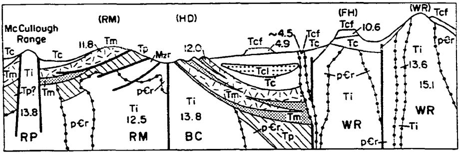

McCullough Range-River Mountains (RM)-Hoover Dam (HD)-Fortification Hill (FH)-
Wilson Ridge (WR) areas

Figure 46. Dimensionless east-west sketches of some stratigraphic and structural relationships in the Lake Mead area. Note that the Muddy Creek Formation is bracketed by age dates of 4.9 and 12.0 m.y. (After Anderson et al, 1972.)

exclusively basaltic.

Figure 46b illustrates the position of the Muddy Creek Formation related to the isotopic ages of Anderson et al. (1972). The sediments of the Muddy Creek Formation are bracketed by ages of 4.9 and 12.0 million years, which spans the Pliocene. Although no distinct lava flows occur within the Muddy Creek Formation, vitric tuffs are interbedded with the fine-grained distal fan sediments at several localities. Chemical compositions of these tuffs are shown in Appendix iv. The Muddy Creek Formation was deposited in closed-basin conditions created by block faulting at the close of the Miocene.

Sediments

The conglomerates of the Muddy Creek Formation rarely exhibit marked erosive contacts at their bases (Plate XIII). Braided stream deposition as seen on the Kyle Canyon alluvial fan does not appear to have been the dominant process active in the initial deposition of the Muddy Creek conglomerates. They are characterized by very poor sorting, good lateral bedding continuity, large boulders that are matrix-supported and an absence of internal bedding. Pebbles are frequently oriented with their long axes parallel to the bedding planes. These attributes are commonly associated with mudflow or debris flow deposits (Bull 1964a, Bluck 1964), implying that the major transporting and depositing

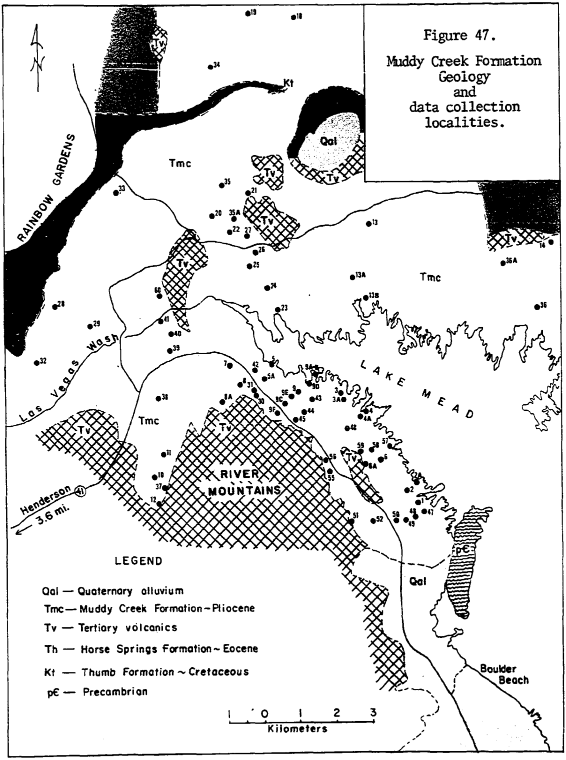

Figure 47.
Muddy Creek Formation Geology and data collection localities.

medium was a fluid with very high sediment to water ratio that lacked sufficient turbulence to erode previously deposited sediments. This also implies that a sufficient amount of fine grained mineral was available in the source area.

In many cases, individual mudflow units are overlain by thin, often channelized, well-sorted sandstones that frequently exhibit scour into the underlying flow (see Foldout VIII). Sharp and Nobles (1953) state that low concentration flood waters often follow mudflows on Recent alluvial fans. This post mudflow flooding would winnow fines from the mudflor gravels producing discontinuous and often channelized sand and silt layers superjacent to the mudflow.

Methods

Indurated ancient conglomerates do not lend themselves to detailed textural analyses. Therefore, this study was limited to measuring those attributes easily observed in the field. Maximum particle size, bedding characteristics, and sedimentary structures were noted and measured at 60 localities around Las Vegas Bay of Lake Mead. Data collection localities are shown in Figure 47.

Results

Paleocurrent directions and variations in clast lithology (Figure 48) indicate three sediment sources for the area studied. Area I is characterized by southerly paleocurrent directions and abundant clasts of Precambrian granite gneiss.

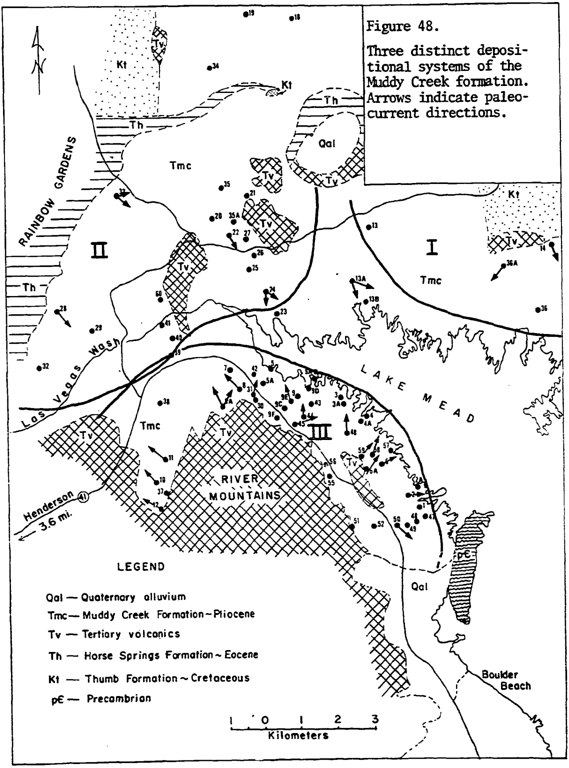

Figure 48.

Three distinct depositional systems of the Muddy Creek formation. Arrows indicate paleocurrent directions.

from the Cretaceous Thumb Formation (landslide deposits). Area II is characterized by southeasterly current directions and a distinctive clast suite consisting of white tuffs and buff-colored fresh water limestones from the Horse Spring Formation, detrital gypsum from the Thumb Formation, and red sandstones from the Jurassic in the Rainbow Gardens area of the Frenchmen Mountains. Area III exhibits northerly current vectors and is entirely composed of detrital volcanics from the River Mountains.

Plate XVII (in pocket) shows the abrupt lithologic variation present in the Muddy Creek Formation. The term diamictite (Flint, 1960) is used here to describe the non-sorted to poorly-sorted clastic sediments consisting of sand and larger particles in a finer-grained matrix.

The coarse grained diamictites rapidly grade basinward into and in part interfinger with playa deposits. The Muddy Creek playa sediments reflect frequent flooding and dessication and consist of evaporites (Plate XVI), slickensided red, smectite rich clays (see Appendix ii), finely laminated to massive siltstones and silty clays (Plate XII), vitric tuffs (Plate XIV), aeolian sand, pebbly siltstones and mudstones. Clasts larger than pebbles are extremely rare. The playa sediments grade vertically into distal fan deposits (Plate XI). This phenomenon (vertical coarsening), the frequent occurrence of tuffs in the section, and local angular unconformities (Plate XIII) reflect continued uplift in the source area with a corresponding progressive infilling of the basin.

Simple linear regression and correlation analyses were applied to the bed thickness and particle size data from each measured section of the Muddy Creek Formation. Average bed thickness and maximum particle size were also calculated and the results are summarized in Appendix iv.

Bed Thickness

The distribution of average bed thickness of the Muddy Creek Formation is shown in Figure 49. Thicknesses decrease away from the source areas. The lobate 50 centimeter maximum east of the River Mountains seems to indicate a major depositional trend. The dominant trend to recognize, however, is the rapid decrease in bed thickness away from the mountain front.

Maximum Particle Size

The mean largest grain contours shown in Figure 50 closely parallel the bed thickness trends and indicate an infilling of the Muddy Creek basin from three sides as mentioned previously. The averaging method was used to smooth the particle size data; the value for a particular locality is the average maximum particle size for the entire section. Much higher values could be obtained by using the size of the largest grain in a particular section of beds. For example, the largest particle encountered in Section 9 C

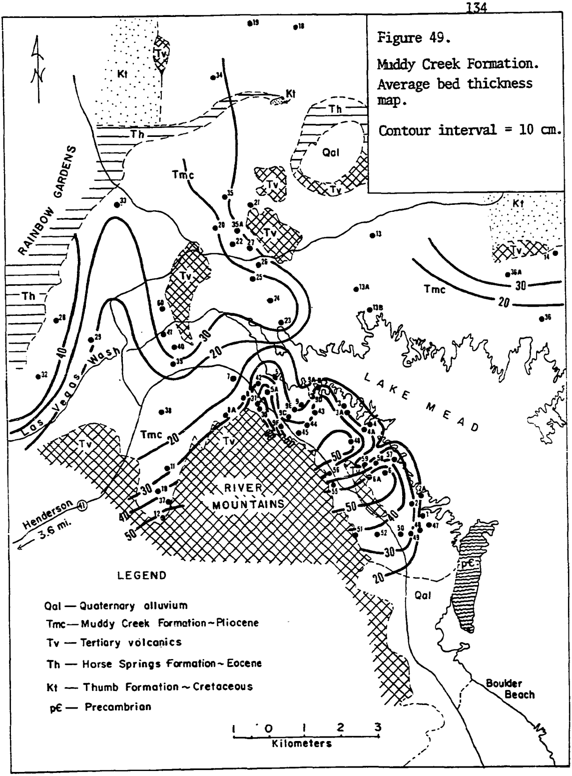
Figure 49.
Muddy Creek Formation.
Average bed thickness map.
Contour interval = 10 cm.
RAINBOW GARDENS
Las Vegas Wash
LAKE MEAD
RIVER MOUNTAINS
Henderson 3.6 mi.
Boulder Beach
LEGEND
Qal — Quaternary alluvium
Tmc — Muddy Creek Formation ~ Pliocene
Tv — Tertiary volcanics
Th — Horse Springs Formation ~ Eocene
Kt — Thumb Formation ~ Cretaceous
p€ — Precambrian
1 0 1 2 3
Kilometers

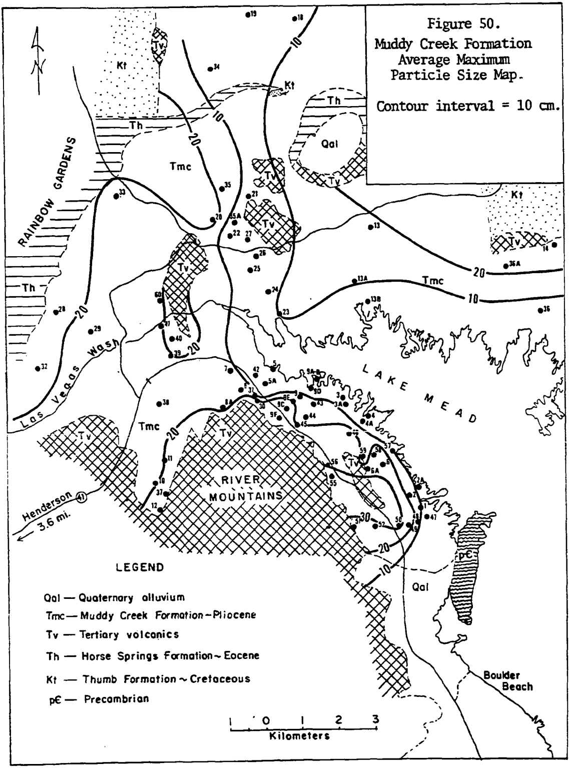

Figure 50.
Muddy Creek Formation
Average Maximum
Particle Size Map.

Contour interval = 10 cm.

is 65 cm. and the mean largest grain value for section 9 C is 25 cm. It is believed that this approach gives a better description of particle size trends by vertically averaging anomalous values. Only conglomeratic units were included in this analysis.

Discussion

For each outcrop studied, bed thickness was plotted against maximum particle size. The correlation coefficient, regression line, and regression coefficient were computed for each outcrop. A correlation coefficient of + 1.0 would indicate that bed thickness is directly proportional to maximum particle size. Likewise, a coefficient of determination (R^2) of 1.0 indicates that the established linear regression equation passes through every point plotted establishing a perfect linear relationship between the two variables. Examples of linear and non-linear relationships are shown in Figure 52.

Figure 51 illustrates the lateral variation in the correlation between bed thickness and maximum particle size. In general, the proximal outcrops yielded the highest correlation between the two variables. The decrease in the correlation coefficient away from the source areas may indicate that different processes were active across the fan surface. Mudflows rarely exhibit basal scour, indicating that individual beds are distinct depositional units. Little reworking in

Figure 51.
Muddy Creek Formation
Correlation between
bed thickness and
maximum particle size.

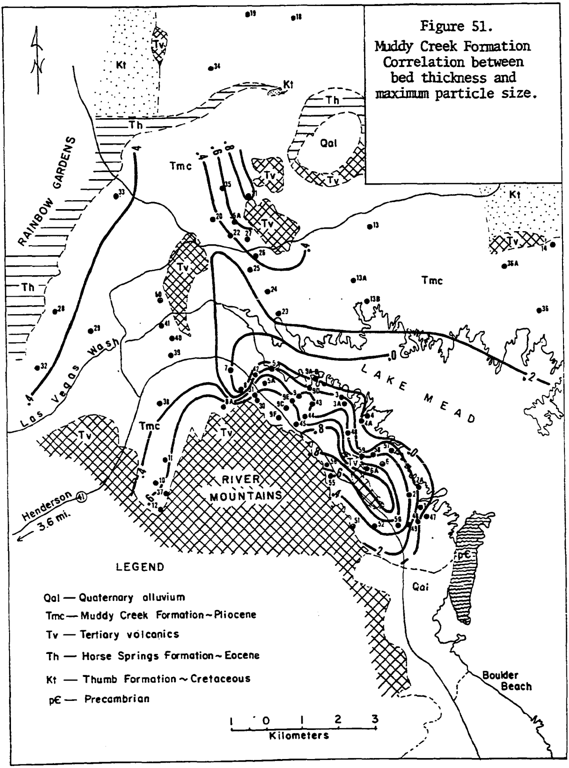

areas of dominant mudflow deposition would yield good correlations between bed thickness and maximum particle size. If the initial mudflow deposits were progressively reworked down-fan by running water in small braided channels heading on the fan surface, the correlation between maximum particle size and bed thickness would be progressively destroyed. Chemical and mechanical weathering processes which occur on inactive fan surfaces (Denny, 1965) produce clasts with anomalously higher angularity (maturity) and smaller size. The growth of the mineral sepiolite (see Appendix iii), found in the Muddy Creek sediments as accumulations along angular unconformities, was observed as an agent of mechanical and chemical alteration of volcanic boulders. Flows originating on the fan surfaces would transport fines from the mudflow deposits and degraded weathering products from older surfaces to the distal reaches of the fans. This would also account for the very sharp decline in particle size toward the playa.

As previously discussed, mudflow deposition is replaced vertically and downslope by braided stream sediments. Plate XI shows a typical coarsening upward sequence with basin-center playa sediments overlain by distal braided stream gravels. The basal playa deposits in this area are laterally equivalent to mudflow sequences near the source area. It is this writer's opinion that Muddy Creek deposition began as

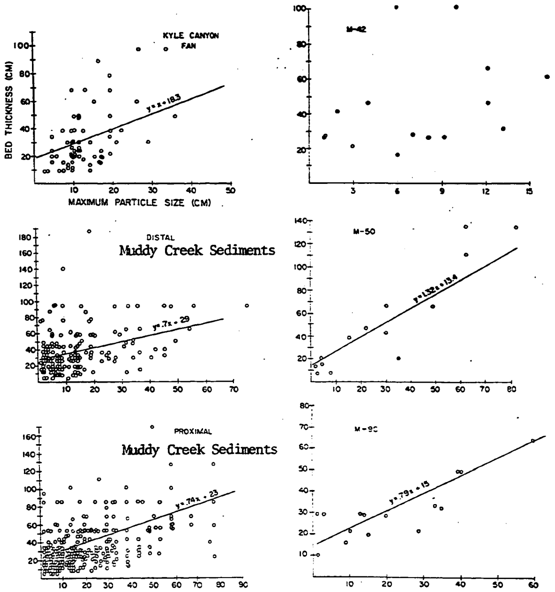

Figure 52. Plots of bed thickness vs. maximum particle size.

small mudflow fans that were reworked to some degree by channelized water. The initial playa size was at a maximum and as time progressed, the drainage basins enlarged and deepened causing a shift from mudflow to braided stream deposition on the fan surfaces.

SUMMARY AND CONCLUSIONS

In summarizing the characteristics of the alluvial-fan sediments studied in this investigation, the following general observations should be stated. The deposition of alluvial fans takes place in close proximity to source areas, hence, recognizing sediment sources of alluvial-fan deposits in the stratigraphic record should be relatively easy. Transportation of the sediment from the source area to the fan takes place under extremes of energy conditions that produce deposits containing particles ranging in size from clay to boulders. Correspondingly, overall sorting of alluvial-fan sediments is poor. Since the deposition of such deposits is almost always adjacent to the source area, the nature of the source rocks plays an important role in the textural and morphological characteristics of the clastic particles as well as controlling to a degree the type of transporting medium.

Source areas with shale or clay-rich rocks or a thick weathered zone in humid regions may yield high viscosity flows to the fan surface. Whereas source areas lacking fines (massive limestones, quartzites, etc.) will be dependent upon flood water to transport coarse particles to the fan surface. These two "end members" may be intermixed to varying degrees in any one source area yielding alluvial fans with differing percentages of debris flow or mudflow and stream-laid sediments. In this study, the Kyle Canyon source area lacks fine clay-sized material, the Lida Wash area contains more fines, and the Muddy Creek area contains appreciably more. This is reflected in the bedding characteristics of the deposits formed in these areas. A gradation from debris flow to water-laid sediments is noted in the Muddy Creek area. In the stratigraphic record, bedding variations along strike controlled by local source rock conditions may be appreciable from one fan to the next.

The alluvial-fan sediments studied in the Kyle Canyon and Lida Wash areas were deposited by channelized water. Plane table maps of random channel lengths revealed a braided pattern. The major bedforms are lobate and longitudinal gravel bars that vary from 2 to 40 meters in length and from 1 to 15 meters in width. Overall channel widths range from 70 meters to 10 meters, decreasing toward the fan toe. Individual braid channels were at a maximum 40 meters long, and averaged 25 meters long and 2 meters wide. Maximum bed relief was on the order of 1.5 meters but averaged less than 0.7 meters. Using these measurements from plane table maps a prediction can be made about the geometry of resulting deposits. Channel and bar measurements were maximums and if preserved, accounting for erosion and the attitude of the resultant outcrops, the unit thickness would be less than these values.

Since average maximum channel length is 25 meters and average channel depth is 0.7 meters, resultant bed length to bed thickness ratio would be 35/1. But since these are optimum channel lengths, and considering the increased degree of braiding and channel separation downfan, a more realistic number would be much less. Boulder bars averaging 22 meters maximum in length and 4.5 meters wide would yield thicker but more compact deposits with bed length/bed thickness ratios of less than 20/1.

Direct measurements taken from random outcrops of alluvial-fan sediments yielded an average bed length to bed thickness ratio of 15/1. As expected, bed lengths were much less than the maximum measured from the plane table maps. Bed thicknesses and bed lengths were observed to decrease downfan due to the loss of channel confinement and the increase in anastomosis of braided channels. Cross-channel profiles also exhibit a decrease in channel width and channel depth from fan head to fan toe.

Most of the bedding observed exhibits frequent scour that produced uneven bedding planes and lenticular bedded units. Cross-stratified channel-fills as well as oblique bedding arising from the migration of bars with low channelward dipping slopes are common. This festoon-type channel-fill deposit is important because it indicates infilling of a channel cut by a previous flow that was infilled by a flow of a higher magnitude. This evidence of low fluctuation has also been described in glacial outwash sediments that are similar to alluvial-fan sediments. This type of sedimentary structure is a good key to the fluctuating discharge conditions that occur on alluvial fans.

The gravels are all grain supported and voids have been infilled with matrices of coarse sand to silt. In the exposed outcrops openwork gravel fabrics are rare.

Minor bedded units consist of cross-stratified sand, ripple-laminated fine sand, and horizontally laminated silts deposited as surface veneers in low areas during reduced or zero discharge conditions. Their abundance increases in a downfan direction.

Measurements of pebble long-axis orientations indicate an overall tendency toward flow-transverse alignment. Dip azimuths of imbricated pebbles are also good indicators of current direction, but the abundance of imbricated pebbles decreases down the fan.

Gravel-sized material comprises over 85% of the sediment studied. Mean and maximum particle size decreases in a downfan direction, but in an inconsistant manner. Cumulative curves of channel sediments have polymodal distributions with a wide range of particle size. Particles less than medium sand occur in the mid- and upper-fan reaches and increase in the distal fan areas.

This system of bedding features, textures, orientations, all of which decrease in dimension in a downfan direction, can be related to the frequency of flows that reach the toe. Since most precipitation occurs in the mountain areas, the proximal fan areas have a higher probability of being affected by flooding whereas fan toe areas have a low probability of being flooded.

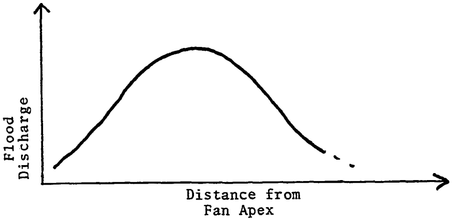

Figure 53.

A general curve is shown in Figure 53 which illustrates this point. As flood discharge increases the distance the flood travels downfan also increases until some break-over point where it reaches the playa. This would also mean that at times of low discharge floods, sediment would accumulate in the fan apex and would be flushed during floods of high discharge. The distal regions will be affected by less intense flows less often than the proximal fan areas thus accounting for the downfan trends observed in this study.

Chemical precipitates in the form of calcium carbonate "caliche" crusts are common on the Kyle Canyon fan. Aridic soils, in contrast to humid soils, are characterized by concentrations of calcium salts somewhere in the soil profile. Water from rains is only rarely abundant enough to move through the soil and into drainage channels. As a result, only the most soluble soil constituents are leached. Calcium carbonate is the most common, but gypsum may accompany it or replace it as is the case with the Muddy Creek Formation. Locally, accumulations of the mineral sepiolite (Papke, K. G., 1972) occur in the Muddy Creek Formation indicating relatively basic conditions ($3H_4SiO_4 + 2\ Mg^{++} \rightleftarrows Mg_2Si_3O_8 \times 4H_2O + 4\ H^+$). As is expected in basic environments (Krauskopf, 1967, p. 191), the stable clay mineral assemblage in the Muddy Creek Formation consists of predominantly smectite with minor amounts of illite.

The sediments of the Muddy Creek Formation were in part deposited by debris flows. The debris flow deposits are characterized by an absence of erosional surfaces, very poor sorting, good lateral bed continuity, matrix-supported boulders and the near absence of internal bedding. Some units exhibit graded bedding and often particles have their long axes parallel to bedding planes.

Average bed thickness for the Muddy Creek Formation ranges from 55 cm to 18 centimeters. Lengths of individual beds were difficult to measure mainly because they are so continuous (>50 meters). The resultant bed length/bed thickness ratio would therefore be considerably greater than those obtained for braided-stream sediments.

Figure 54 is a representation of the four general sedimentary associations observed in this investigation. Association "A" consists of debris flow or mudflow deposits which are poorly represented on the Kyle Canyon alluvial fan but make up a large percentage of the Muddy Creek sediments proximal to the source area. Associations "B", "C", and "D" represent the fluvially deposited proximal, mid-fan, and distal sediments observed on the Kyle Canyon and Lida Wash fans. As discussed previously, they exhibit a decrease in the mangitude of sedimentary features and particle size in a downfan direction. A similar phenomenon was observed by McGowen and Groat (1971) in the Cmabrian Van Horn Sandstone of Texas. The recognition of this feature is an important key . the interpretation of ancient conglomerates as being deposited in an alluvial fan environment.

The lateral variation in sedimentary associations can be used to construct three dimensional models of the Kyle Canyon and Muddy Creek fan systems. The probable vertical succession of the sedimentary associations observed on the surface of the Kyle Canyon alluvial fan is shown in figure 55 which reflects a gradual infilling of Las Vegas Valley. Future rejuvination of the fault system would cause a shift of the proximal association toward the center of the basin.

The Muddy Creek sediments have a more complex history

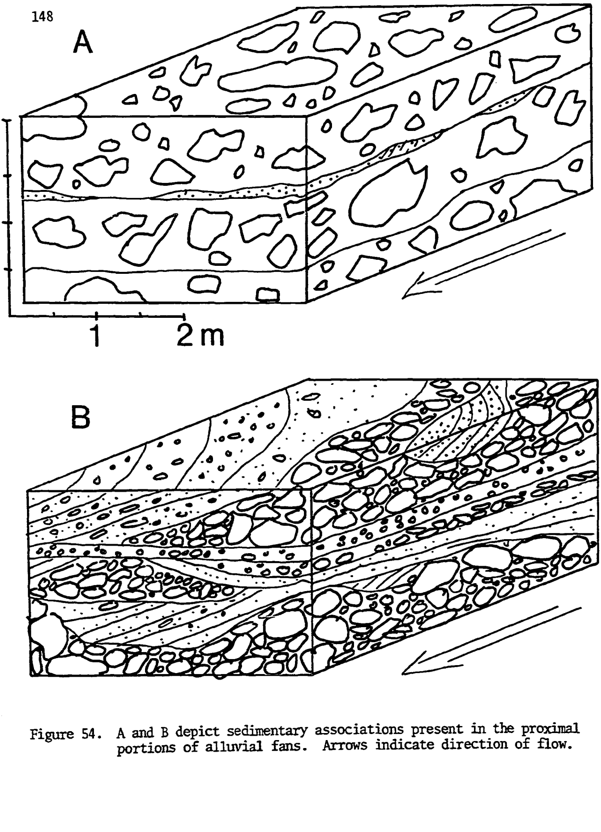

Figure 54. A and B depict sedimentary associations present in the proximal portions of alluvial fans. Arrows indicate direction of flow.

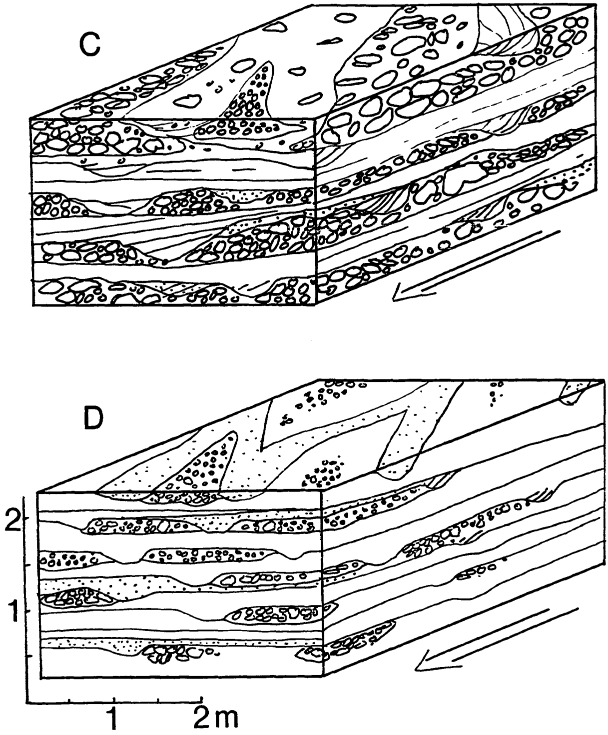

Figure 54 (Continued). C = mid-fan association. D = distal association. Arrows indicate direction of flow.

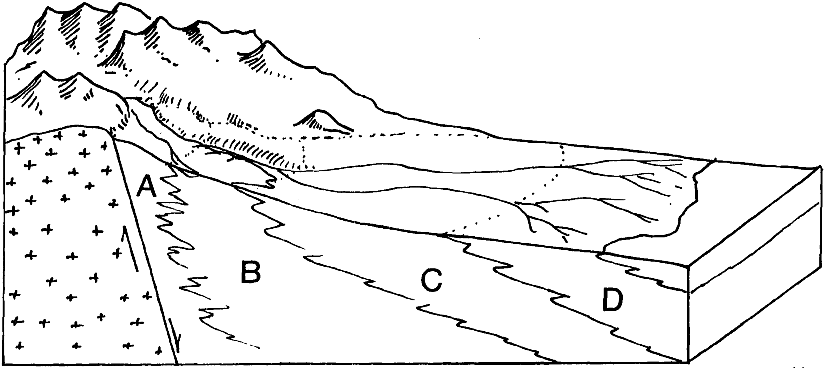

Figure 55. Probable spatial relationships between sedimentary associations present on the Kyle Canyon alluvial fan. Letters refer to associations shown in Figure 54.

that is evidenced by several unconformities. Figure 56 illustrates the development of the Muddy Creek fan system through time and depicts the lateral and vertical variations of sedimentary associations which were observed in outcrop. During the initial deposition of the Muddy Creek sediments (t_1) small fans constructed by debris flows ("A") and reworked by small braided streams at their distal margins ("D") graded laterally into evaporite playa lake sediments. Following additional uplift of the volcanic source area (t_2) there was a shift of the debris flow association basinward. Finally, (t_3) a thin deposit of predominantly fluvial associations "B" and "C" was deposited prior to the incision of the Colorado River. Whereas a vertical section through the Kyle Canyon fan sequence would probably yield a fining upward sequence with proximal associations overlain by distal associations, the Muddy Creek section is just the opposite. Other alluvial-fan sequences like the Tertiary Ridge Basin Group (Crowell, 1954) which is 25,000 feet thick and associated with continual movement of the San Gabriel Fault Zone may exhibit very little vertical variation in sedimentary associations.

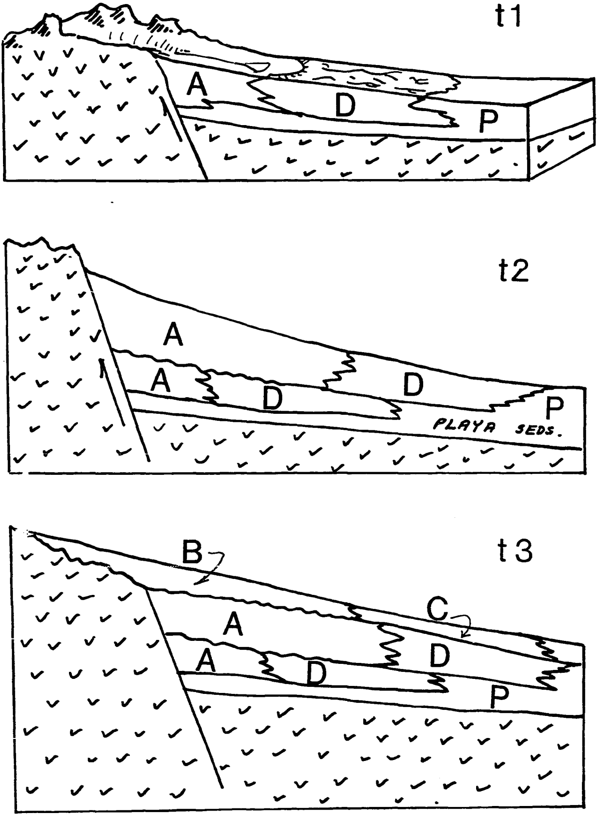

Figure 56. Spatial relationships of sedimentary associations present in the Muddy Creek Formation. P = playa deposits.

CONCLUSIONS

Geometry:

1. Because of their tectonic setting, alluvial fans may be several miles in radius and may coalesce with other fans to form sizable clastic accumulations thousands of feet thick. The deposit may be lenticular or a wedge that is either thickest or thinnest near the mountain front. (Bull, 1972)

Process:

2. Dominant processes active in alluvial fan depositions are flows that range from high to low viscosity depending upon the amount of clay material entrained in the flow. The dominant agent being stream action. Debris flows of higher viscosity are secondary and where frequent they decrease downfan from the apex. They seem important in the construction of smaller fan systems or as an agent that transports material to the fan apex to be reworked by water.

Bedforms:

3. Major bedforms in braided channels on alluvial fan surfaces are longitudinal to lobate bouldery gravel bars, and channels of better-sorted coarse to fine grave. The braided nature of the stream systems produces lenticular bedding with length thickness ratios on the order of 15/1. Beds are

commonly 0.5 meters thick and 7 meters in length. Bed thickness and bed length decrease in a downfan direction because of the loss of channel confinement and the increase in the anastomosis of braided channels.

Sedimentary Structures:

4. Parallel laminations produced by better sorted channel deposits and oblique or low angle cut-and-fill structures are the most common sedimentary structures on alluvial fans. Cross-stratified channel-fills as well as oblique bedding arising from migration of bars with low channelward dipping slopes are common in the apical and midfan regions. Cut and fill are more common in strike sections than in dip sections of alluvial fan sediments. Bedding continuity is also decreased in fan deposits along strike.

   Minor units of cross-stratified sand, rippled fine sand, and horizontally laminated silts less than 0.5 meters thick and discontinuous are deposited as surface veneers in low areas during reduced or zero discharge. Their abundance increases downfan.

Texture:

6. Eighty-five percent plus of the sediment of Kyle Canyon and Lida Wash is comprised of gravel-sized

debris. Cumulative curves drawn from ¼ phi sieve analyses of braided channel sediments are poly-modal with a wide range of particle sizes. The curves become skewed toward finer grain sizes toward the fan toe.

Pebble Orientation:

7. Pebble imbrication is well developed and long axis orientations indicate a flow-transverse alignment. The percentage of imbricated pebbles decreased downfan.

Debris Flows:

8. The debris flow deposits of the Muddy Creek Formation exhibit little preferred particle orientation, an absence of erosional surfaces, extremely poor sorting and good lateral bedding continuity. Occasionally, they are graded (coarse at the base) with particles aligned parallel to bedding planes.

Chemical Precipitates:

9. Chemical precipitates are common on alluvial fans in arid to semi-arid environments. Calcite, gypsum, and sepiolite were observed in association with alluvial-fan deposits.

Associated Sediments:

10. Depositional environments found in association with alluvial-fan deposits depend upon the geographic

setting in which the fans are formed. Sediments interbedded with distal fan deposits could be lacustrine, aeolian, or evaporitic if the fan formed in a closed basin. Fluvial sediments with current vectors perpendicular to the alluvial fan vectors may form where through flowing drainage exists. If the alluvial fans form in a coastal environment the potential exists for marine sediments to be interbedded with fan deposits.

Organics:

11. Fauna and flora are almost never preserved in alluvial fan sediments. Distal sediment associations as mentioned in number 10 have the best potential for preservation of fossils of vertebrates, ostracods, and algal charophytes.

REFERENCES

Anderson, R. E., 1972, Significance of K-Ar ages of Tertiary rocks from the Lake Mead region, Nevada-Arizona: Geological Society of America Bulletin, v. 83, p. 273-288.

Armstrong, R. L., 1970, Geochronology of Tertiary igneous rocks, eastern Basin and Range province, western Utah, eastern Nevada, and vicinity, U. S. A.: Geochimica et Cosmochimica Acta, v. 34, p. 203-232.

Augustinus, P. G. E. F., and Riezebos, H. T., 1971, Some Sedimentological aspects of the fluvioglacial outwash plain near Soesterberg (the Netherlands): Geol. Mijnbouw, v. 50, p. 341-348.

Beaty, C. B., 1963, Origin of alluvial fans, White Mountains, California and Nevada: Annals of the Association of American Geographers: v. 53, p. 516-535.

Beaumont, P., and Oberlander, T. M., 1971, Observations on stream discharge and competence at Mosaic Canyon, Death Valley, California: Geological Society of America Bulletin, v. 82, p. 1695-1698.

Berg, R. R., and Cook, B. C., 1968, Petography and origin of lower Tuscaloosa sandstones, Mallalieu field, Lincoln County, Mississippi: Gulf Coast Association of Geological Societies Transactions, v. 18, p. 242-255.

Blissenbach, E., 1954, Geology of alluvial fans in semi-arid regions: Geological Society of America Bulletin, v. 65, p. 175-190.

Bluck, B., 1964, Sedimentation of an alluvial fan in southern Nevada: Journal of Sedimentary Petrology, v. 34, p. 395-400.

________ 1965, The sedimentary history of some Triassic conglomerates in the Vale of Glamorgan, South Wales: Sedimentology, v. 4, p. 225-245.

________ 1967, Deposition of some Upper Old Red Sandstone conglomerates in the Clyde area; a study in the significance of bedding: Scottish Journal of Geology, v. 3, p. 139-167.

Boggs, S., 1966, Petrology of the Minturn Formation, east-central Eagle County, Colorado: American Association of Petroleum Geologists Bulletin, v. 50, p. 1399-1422.

Bretz, J. H., and Horberg, L., 1949, The Ogallala Formation west of the Llano Estacado: Journal of Geology, v. 57, p. 477-490.

Bull, W. B., 1964a, Alluvial fans and near surface subsidence in western Fresno County, California: United States Geological Survey Professional Paper 437A, 71 p.

________, 1964b, Geomorphology of segmented alluvial fans in western Fresno County, California: United States Geological Survey Professional Paper 352-E, p. 89-129.

________, 1972, Recognition of alluvial-fan deposits in the stratigraphic record, in J. K. Rigby and W. K. Hamblin editors, Recognition of ancient sedimentary environments: Society of Economic Paleontologists and Mineralogists Special Publication 16, 340 p.

Buttner, P. J. R., 1968, Proximal continental rhythmic sequences in the Genesee Group (lower Upper Devonian): Geological Society of America Special Paper 106, p. 109-126.

Crowell, J. C., 1954, Geology of the Ridge Basin area: California Division of Mines bulletin 170, Map sheet 7.

Denny, C. S., 1965, Alluvial fans in the Death Valley region, California and Nevada: United States Geological Survey Professional Paper 466, 62 p.

Dobkins, J. E., Jr., and Folk, R. L., 1968, Pebble shape development on Tahiti-Nui (abstract): American Association of Petroleum Geologists Bulletin, v. 52, p. 525.

________, 1970, Shape development on Tahiti-Nui: Journal of Sedimentary Petrology, v. 40, p. 1167-1203.

Doeglas, D. J., 1962, The structure of sedimentary deposits of braided rivers: Sedimentology, v. 1, p. 167-190.

Drew, F., 1873, Alluvial and lacustrine deposits and glacial records of the upper Indus basin: Geological Society of London Quarterly Journal, v. 29, p. 441-471.

Drewes, H., 1963, Geology of the Funeral Peak Quadrangle, California, on the east flank of Death Valley: United States Geological Survey Professional Paper 413, 78 p.

Fahnestock, R. K., 1963, Morphology and hydrology of a glacial stream, White River, Mount Ranier, Washington: United States Geological Survey Professional Paper 422-A, p. 1-70.

Flemal, R. C., 1967, Sedimentology of the Sespe Formation, southwestern California: Princeton, New Jersey, Princeton University, PhD thesis, 258 p.

Flint, R. F., 1960, Diamictite, a substitute term for symmictite: Geological Society of America Bulletin, v. 71, p. 1809.

Folk, R. L., 1955, Student operator error in determination of roundness, sphericity, and grain size: Journal of Sedimentary Petrology, v. 25, p. 297-301.

______ 1965, Petrology of sedimentary rocks: Austin, Hemphill, 170 p.

Folk, R. L., and Ward, W., 1957, Brazos River bar: a study in the significance of grain size parameters: Journal of Sedimentary Petrology, v. 27, p. 3-26.

Gwinn, V. E., and Mutch, T. A., 1965, Intertongued Upper Cretaceous volcanic and nonvolcanic rocks, central-western Montana: Geological Society of America Bulletin, v. 76, p. 1125-1144.

Hanson, H. J., 1969, Depositional environments of subsurface Patomac Group in southern Maryland: American Association of Petroleum Geologists Bulletin, v. 53, p. 1923-1937.

Haynes, C. V., 1967, Quaternary geology of the Tule Springs area, Clark County, Nevada: Nevada State Museum Anthropological Papers no. 13, part 1, 104 p.

Hooke, R. LeB., 1967, Processes on arid region alluvial fans: Journal of Geology, v. 75, p. 438-460.

Hoppe, G., and Ekman, S., 1964, A note on the alluvial fan of Ladtjovagge Swedish Lapland: Geografiska Annaler, v. 46, p. 338-342.

Howard, J. D., 1966, Patterns of sediment dispersal in the Fountain Formation of Colorado: Mountain Geologist, v. 3, p. 147-153.

Hubert, J. F., 1960, Petrology of the Fountain and Lyons Formations, Front Range, Colorado: Colorado School of Mines Quarterly, v. 55, p. 1-242.

Humbert, F. L., 1968, Selection and wear of pebbles on gravel beaches: PhD dissertation Rijksuniversiteit Te Groningen, University of Groningen Geologic Institute Publication 190, 144 p.

Hunt, C. B., McKelvey, V. E., and Wiese, J. H., 1942, The Three Kids manganese district, Clark County, Nevada: United States Geological Survey Bulletin 936-L, p. 297-319.

Klein, G. deV., 1962, Triassic sedimentation, Maritime Provinces, Canada: Geological Society of America Bulletin, v. 73, p. 1127-1186.

________ 1968, Sedimentology of Triassic rocks in the lower Connecticut Valley, in Guidebook for field trips in Connecticut, New England International Collegiate Geology Conference: Connecticut Geology and Natural History Survey Guidebook 2, p. 1-19.

Krauskopf, K., 1967, Introduction to geochemistry: McGraw-Hill, New York, 721 p.

Krumbein, W. C., and Orme, A. R., 1972, Field mapping and computer simulation of braided-stream networks: Geological Society of America Bulletin, v. 83, p. 3369-3380.

Krumbein, W. C., and Sloss, L. L., 1963, Stratigraphy and sedimentation, 2 nd edition: San Francisco, Freeman and Company, 660 p.

Laming, D. J. C., 1966, Imbrication, paleocurrents and other sedimentary features in the Lower New Red Sandstone, Devonshire, England: Journal of Sedimentary Petrology, v. 36, p. 940-959.

Landim, P. M. B., and Frakes, L. A., 1968, Distinction between tills and other diamictons based on textural characteristics: Journal of Sedimentary Petrology, v. 38, p. 1213-1223.

Lattman, L. H., 1971, Geomorphology of the east flank of the Spring Mountains, Nevada: Air Force Cambridge Research Laboratories, Report AFCRL-71-0326, 89 p.

________ 1973, Calcium carbonate cementation of alluvial fans in southern Nevada: Geological Society of America Bulletin, v. 84, p. 3013-3028.

________, and Simonberg, E. M., 1971, Case hardening of carbonate alluvium and colluvium, Spring Mountains, Nevada: Journal of Sedimentary Petrology, v. 41, p. 275-281.

Lawson, A. C., 1913, The petrographic designation of alluvial fan formations: University of California Publication, Department of Geology Bulletin, v. 9, p. 23-48.

Leopold, L. B., and Wolman, M. G., 1957, River channel patterns: braided, meandering and straight: United States Geological Survey Professional Paper 282-B, p. 39-85.

Lindsey, D. A., 1972, Sedimentary petrology and paleocurrents of the Harebell Formation, Pinyon Conglomerate, and associated coarse clastic deposits, northwestern Wyoming: United States Geological Survey Professional Paper 734-B, 68 p.

Longwell, C. R., 1946, How old is the Colorado River?: American Journal of Science, v. 244, p. 817-835.

________ 1963, Reconnaissance geology between Lake Mead and Davis Dam Arizona-Nevada: United States Geological Survey Professional Paper 374-E, 51 p.

________, 1974, Measurement and date of movement on the Las Vegas Valley Shear Zone, Clark County, Nevada: Geological Society of America Bulletin, v. 85, p. 985-990.

________, Pampeyan, B. B., and Roberts, R. J., 1965, Geology and mineral resources of Clark County, Nevada: Nevada Bureau of Mines Bulletin 62, 218 p.

McGowan, J. H., and Groat, C. G., 1971, Van Horn Sandstone, West Texas: an alluvial fan model for mineral exploration: Texas Bureau of Economic Geology, Report of Investigations no. 73, 57 p.

McKelvey, V. E., Wiese, J. H., and Johnson, V. H., 1949, Preliminary report on the bedded manganese of the Lake Mead region; Nevada and Arizona: United States Geological Survey Bulletin 948-D, p. 83-101.

Meckel, L. D., 1967, Origin of Pottsville conglomerates (Pennsylvanian) in the central Appalachians: Geological Society of America Bulletin, v. 78, p. 223-258.

Melton, M. A., 1965, The geomorphic and paleoclimatic significance of alluvial deposits in southern Arizona: Journal of Geology, v. 73, p. 1-38.

Miall, A. D., 1970a, Continental marine transgression in the Devonian of Prince of Wales Island, Northwest Territories: Canadian Journal of Earth Sciences, v. 7, p. 125-144.

________, 1970b, Devonian alluvial fans, Prince of Wales Island, Artic Canada: Journal of Sedimentary Petrology, v. 40, p. 556-571.

Moody-Stuart, M., 1966, High and low sinuosity stream deposits, with examples from the Devonian of Spitzbergen: Journal of Sedimentary Petrology, v. 36, p. 1102-1117.

Nilsen, T. H., 1969, Old Red sedimentation in the Buelandet-Verlandet Devonian district western Norway: Sedimentary Geology, v. 3, p. 35-57.

Ore, H. T., 1964, Some criteria for the recognition of braided stream deposits: Wyoming University Contributions to Geology, v. 3, p. 1-14.

Papke, K. G., 1972, A sepiolite-rich playa deposit in southern Nevada: Clays and Clay Minerals, v. 20, p. 211-216.

Robinson, P. T., McKee, E. H., and Moiola, R. J., 1968, Cenozoic volcanism and sedimentation, Silver Peak Region, western Nevada and adjacent California, in Coats, R. R., Hay, R. L. and Anderson, C. A. editors, Studies in volcanology: Geological Society of America Memoir 116, p. 577-611.

Rubey, W. W., 1952, Geology and mineral resources of the Hardin and Brussels quadrangles (Illinois): United States Geological Survey Professional Paper 218, 179 p.

Ruhen, R. V., 1964, Landscape morphology and alluvial deposits in southern New Mexico: Annals of the Association of American Geographers, v. 54, p. 147-159.

Ryder, J. M., The stratigraphy and morphology of paraglacial alluvial fans in south-central British Columbia: Canadian Journal of Earth Sciences, v. 8, p. 279-298.

Sharp, R. P., 1948, Early Tertiary fanglomerate, Big Horn Mountains, Wyoming: Journal of Geology, v. 56, p. 1-16.

________, and Nobles, L. H., 1953, Mudflow at Wrightwood, southern California: Geological Society of America Bulletin, v. 46, p. 547-560.

Smith, N. D., 1970, The braided stream depositional environment: comparison of the Platte River with some Silurian clastic rocks, north-central Appalachians: Geological Society of America Bulletin, v. 81, p. 2993-3014.

Sneed, E. D., and Folk, R. L., 1958, Pebbles in the lower Colorado River, Texas, a study in particle morphogenesis: Journal of Geology, v. 66, p. 114-150.

Spearing, D. R., 1969, Stratigraphy, sedimentation, and tetonic history of the Paleocene-Eocene Hoback Formation of Wyoming: Ann Arbor, Michigan, University of Michigan, PhD thesis, 179 p.

Troxell, H. C., et al., 1942, Floods of March 1938, in southern California: United States Geological Survey Water-Supply Paper 844, 399 p.

Vaughn, F. E., 1922, Geology of the San Bernadino Mountains north of San Gorgonio Pass, California: University of California Publications, Department of Geological Science Bulletin, v. 13, p. 319-411.

Wadell, H., 1932, Volume, shape, and roundness of rock particles: Journal of Geology, v. 40, p. 443-451.

________, 1934, Shape determination of large sedimental rock fragments: Pan-American Geologist, v. 61, p. 187-220.

Weaver, W. E., and Schumm, S. A., 1974, Fan-head trenching-an example of a geomorphic threshold: Geological Society of America Abstracts with Programs, v. 6, p. 481.

Wentworth, C. K., 1922a, A method of measuring and plotting the shapes of pebbles: United States Geological Survey Bulletin, v. 730-C, p. 91-102.

_______ 1922b, A field study of the shapes of River pebbles: United States Geological Survey Bulletin, v. 730-C, p. 103-114.

Wessel, J. M., 1969, Sedimentary history of Upper Triassic alluvial fan complexes in north-central Massachusetts: Massachusetts University, Department of Geology Contributions no. 2, 157 p.

Williams, G. E., 1966, Paleogeography of the Torridonian Applecross Group: Nature, v. 209, no. 5030, p. 1303-1306.

_______ 1969, Characteristics and origin of a Pre-Cambrian pediment: Journal of Geology, v. 77, p. 183-207.

Williams, P. F., and Rust, B. R., 1969, The sedimentology of a braided river: Journal of Sedimentary Petrology, v. 39, p. 649-679.

Wilson, M. D., 1970, Upper Cretaceous-Paleocene synorogenic conglomerates of southwestern Montana: American Association of Petroleum Geologists Bulletin, v. 54, p. 1843-1867.

Widner, C. G., 1965, Alluvial cone construction by alpine mudflow in a humid temperature region: Canadian Journal of Earth Sciences, v. 2, p. 270-277.

Zingg, Th., 1935, Beitrag zur schotteranalyse: Schweizer Mineralog U. Petrog, Mitt., Bd. 15, p. 39-140.

APPENDIX i

PLATES I-XVI

PLATE I. Kyle Canyon Fan: General

Figure 1. View of the drainage basin of the Kyle Canyon fan showing scarp of carboniferous carbonates. The road cut in the center of the photograph dissects crudely bedded colluvial deposits.

Figure 2. Close-up view of case-hardened colluvial deposits in the upper reaches of the Kyle Canyon drainage basin. The deposits are very poorly sorted and are probably of debris flow origin.

Figure 3. Aerial view of the braided nature of the deposits in the major sediment contributing channel of the Kyle Canyon fan near the apex in the fan bay. Downfan is to the left. The scarp bounding the channel is composed of older fan deposits which are being eroded and acting as a sediment source.

Figure 4. Braided channel on the fan surface. Downstream is to the left. Note abandoned channel which shows up as a slightly lighter area just above the present channel location. Most of the bed forms in the channels are elongate parallel to the direction of flow.

PLATE I

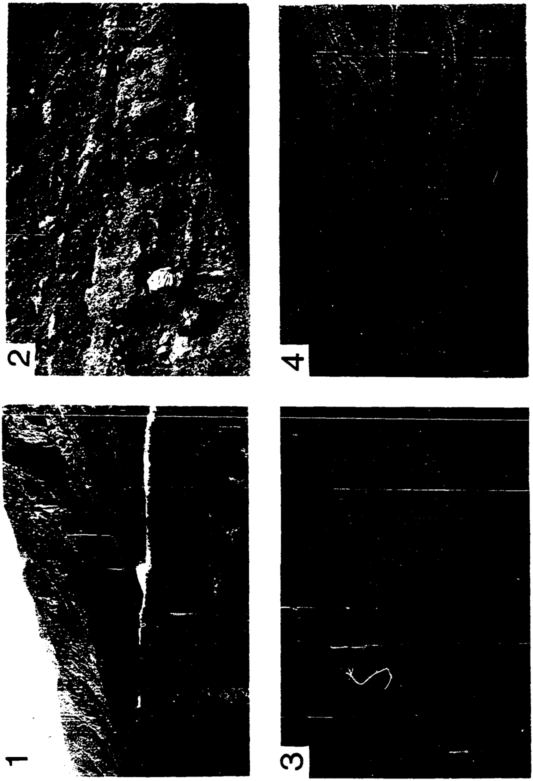

PLATE II. Kyle Canyon Alluvial Fan: Aerial Photographs

Figure 1. Aerial view of Kyle Canyon alluvial fan looking down the major channel near the apex of the fan. Note the elongate nature of the longitudinal braid bars. Channel width is approximately 50 meters.

Figure 2. Aerial view near the toe of Kyle Canyon fan which is characterized by numerous distributary channels.

PLATE II

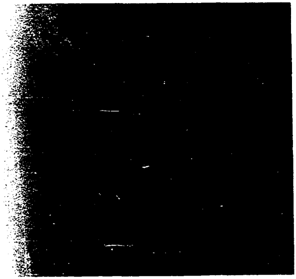

2

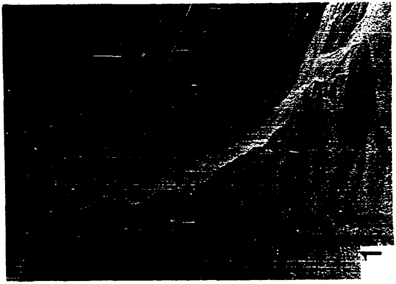

1

PLATE III. Kyle Canyon Fan: Channel sediment-textures

Figures 1 & 2. Oblique and plan views of the surface of a braid bar. Note horizontal variations in grain size and apparent good local sorting. Silt and fine sand fill the voids in the sediment just below the surface. White calcium carbonate coated pebbles and cobbles have been reworked from older fan sediments. Hammer is 40 cm. long.

Figure 3. View of the channel in the fan bay area. Note imbrication and the frequency of large boulders. (locality 23)

Figure 4. View of channel near fan apex showing low areas which have trapped fine grained sediments. (locality 19). Hammer is 40 cm. long.

PLATE III

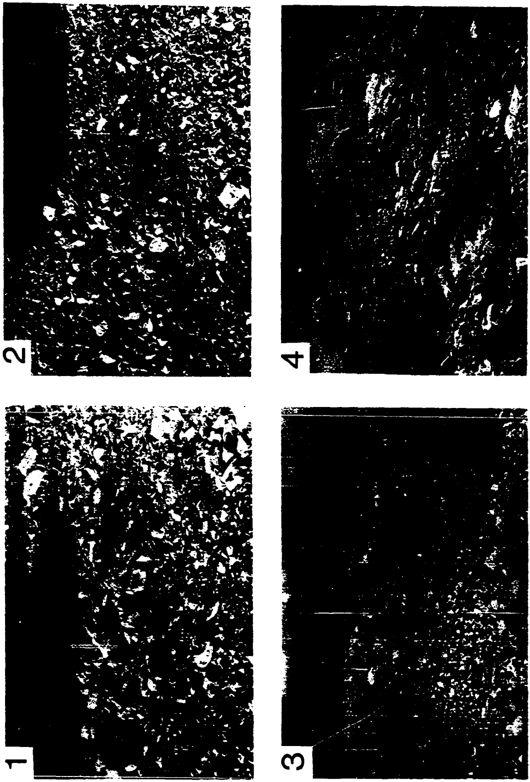

PLATE IV. Kyle Canyon Fan: Sediment textures

Figure 1. 20 centimeter bed of fine ripple-laminated sand interbedded with fine grained gravel near the toe of the fan. Percentage of this sediment type increases towards the distal fan margin. Wind may be the dominant agent responsible for the movement and deposition of the fines in the fan toe areas. (locality 20)

Figure 2. Cross-bedded medium to coarse sand interbedded with medium to fine gravel occurring as channel fill near the toe of the fan. (locality 10). Hammer is 40 cm. long.

Figure 3. Coarse gravel lens with sand and silt matrix. Silt and sand appear to have infiltrated an open-work gravel fabric creating a poorly sorted sediment. (locality 17)

Figure 4. Well developed imbrication in gravels in the mid-fan area (locality 25). Downfan is to the left.

PLATE IV

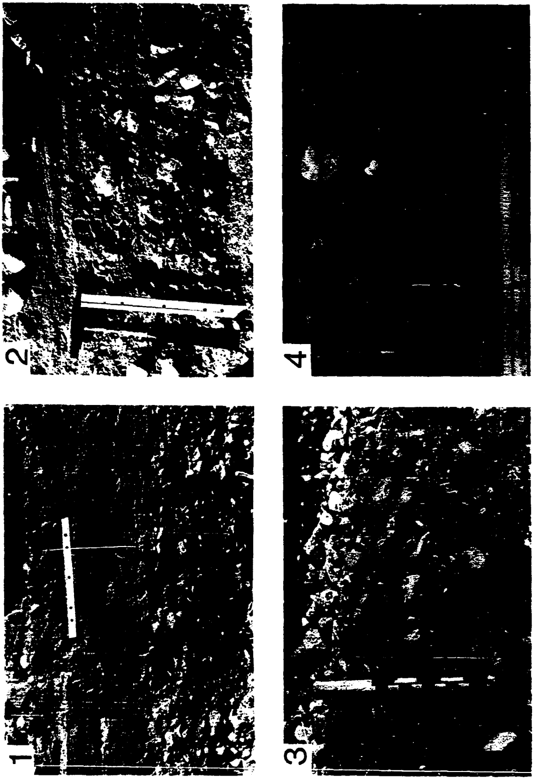

PLATE V. Kyle Canyon Fan: Cross-bedded channel fills

Figure 1. Cross-bedded channel fill exhibiting fining upward cycles. Previously scoured, the channel acted as a baffle to higher flows over the bar surface. Scale is 30 cm. long. Flow was from right to left. (locality 26)

Figure 2. This photo exhibits two distinct features present in alluvial-fan sediments; a buried fan surface at hammer level marked by a buried caliche zone, and a low angle channel fill. Hammer is 40 cm. long. (locality 25)

Figure 3. Scour and fill exhibiting laminae which fine upward and laterally. The coarser gravels in the channel fill deposits often exhibit an open-work fabric. (locality 11). Hammer is 40 cm. long.

Figure 4. Channel fill with caliche zone defining lower boundary. Channel has approximately 1 meter of relief.

PLATE V

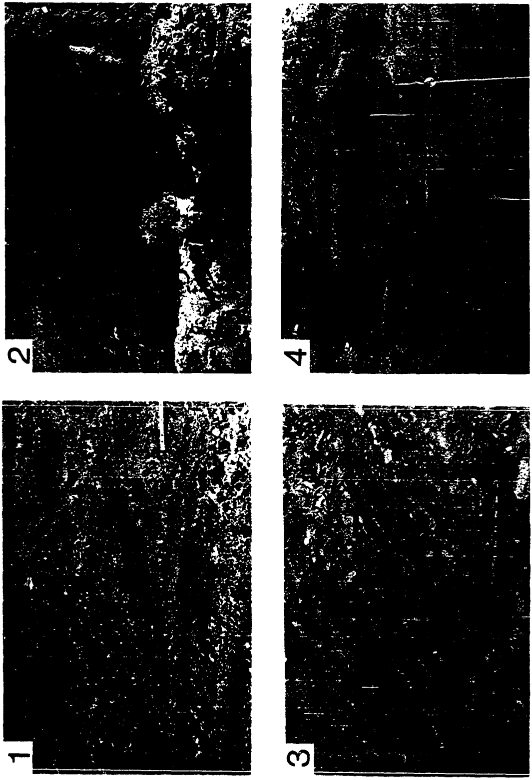

PLATE VI. Kyle Canyon Fan: Braid bars in outcrop

Figures 1 & 2. Zones of "imbricated" pebbles bounded by horizontal, continuous bedding units. Imbrication in these two examples appears to be the result of lateral bar migration. The long axes of the pebbles dip toward the thalweg of the channel. Downfan direction is to the right in both examples. Rod is two meters high; ruler is 30 cm. long. (locality 23)

Figure 3. Frequently, bar surfaces act as a baffle for finer grained sediment which infiltrates the gravel fabric. This photograph illustrates several zones (light areas) where this phenomenon is exemplified. Scale is 30 cm. in length. (locality 18)

Figure 4. Very coarse bouldery bar overlain by more laterally continuous channel deposits. Near fan apex at locality 23. Rod is 2 meters long.

PLATE VI

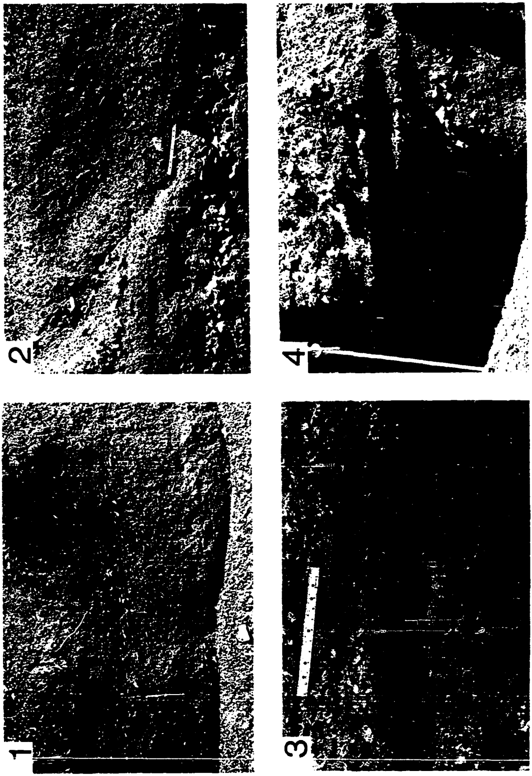

PLATE VII. Kyle Canyon Fan: General

Figure 1. View of incised channel looking towards fan apex from locality 1. Walls are 7 meters high. Talus accumulations at the base of the channel wall contribute large quantities of sediment to the regimen of the channel. Notice cloud buildup over the mountain peaks; a daily occurrence frequently accompanied by precipitation.

Figure 2. Distal fan deposits consist of very thin-bedded, discontinuous units. Bush is 1 meter high. (locality 26)

Figure 3. Plan view of caliche cemented fan surface. Carbonate pebbles have been abraded and dissolved forming a flat surface. (locality 8)

Figure 4. Photo taken in the mid-fan region shows coarse grained bar deposits (level of boulder) overlying finer grained channel deposits resting on a caliche surface. Boulder is 1 meter in diameter. (locality 25)

PLATE VII

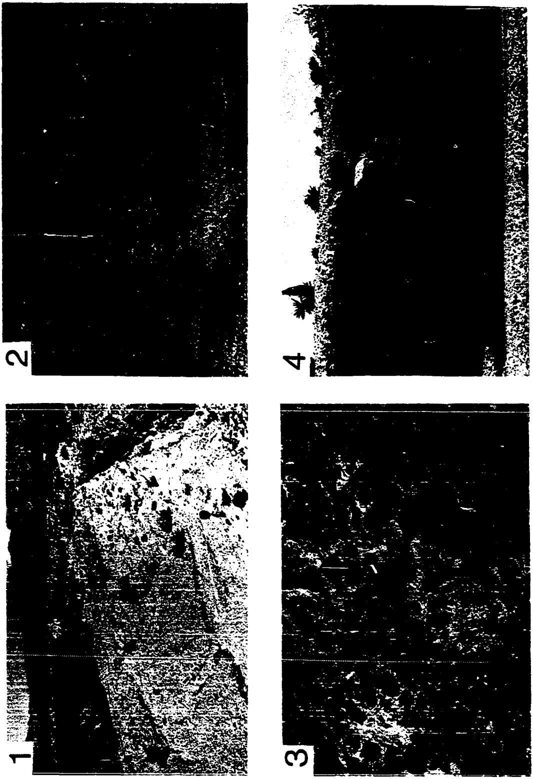

PLATE VIII. Lida Wash: Aerial view, sediment textures

Figures 1 & 2. Cut through gravel bar and channel deposits in Lida Wash (locality 1). Bars are rich in boulders and poorly sorted. Note fine material concentrated on the upper surface of the wash. Fines have partially infiltrated the boulder bar (just above hammer in Figure 1). Channel deposits are better sorted and finer grained. Hammer is 40 cm. long.

Figure 3. Aerial view of Lida Wash area. Star-shaped dunes (more than 10 meters high) are being buried by encroaching alluvial gravels. The Lida Wash area has a great supply of fine grained, easily eroded material in the source area.

PLATE VIII

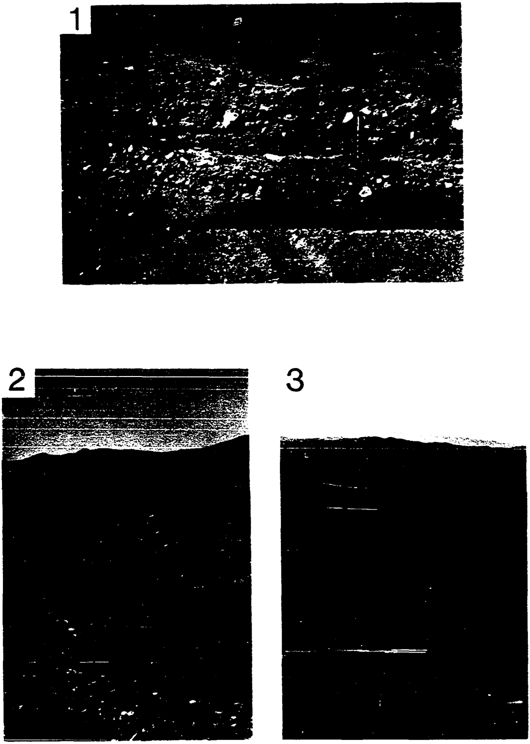

PLATE IX. Lida Wash

Figure 1. Aerial view of braided pattern in Lida Wash. Note streamlined nature of the braid bars. Typically the bars fine in a downstream direction. Flow was from upper left to lower right. Width of the wash is 80 meters. (locality 2)

Figure 2. View of the surface of area shown in Figure 1. Note elongate boulder bars, finer grained channels, and lighter areas of fine grained sediment accumulation. (locality 2).

Figure 3. Aerial view of channel patterns on bajada surface in vicinity of Lida Wash. Note obvious fault scarps.

Figure 4. Exotic boulders near the mouth of Lida Wash may be remnants of large magnitude flood or mudflow. The boulder near figure is two meters in diameter.

PLATE IX

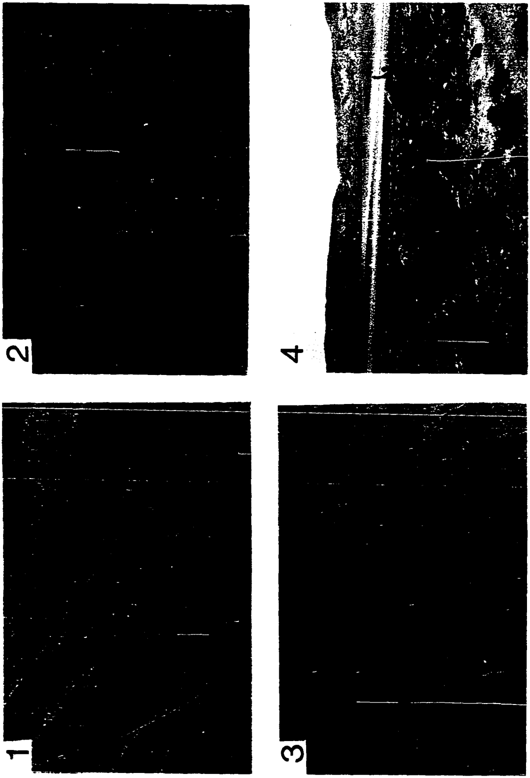

PLATE X. Muddy Creek Formation: General

Figure 1. Typical coarsening upward sequence of Muddy Creek sediments (locality 10). The lighter colored silty clays, silts, and fine sands are gradually replaced by coarse gravel conglomerates at the top of the section.

Figure 2. Aerial view of the River Mountains (dark area upper right) with Muddy Creek sediments outcropping along the periphery of Lake Mead. View is looking toward the southwest.

PLATE X

1

2

PLATE XI. Muddy Creek Formation: Distal fan sediments

This photograph exemplifies the typical distal fan facies of the Muddy Creek Formation at locality 33. Thick gypsum bed at the feet of observer at right grades upward into red slickensided, gypsiferous clays. The clays gradually coarsen upward to sands and the sands are replaced by very lenticular, thinly bedded, fine to medium gravels at the top of the section.

PLATE XI

PLATE XII. Muddy Creek Formation

Figure 1. Outcrop photograph taken at locality 11 exhibiting bedding. Bedding disruption of this type seems to be localized in the distal portions of the fan system and may be related to ground water movement.

Figure 2. Typical outcrop of Muddy Creek sediments exhibiting beds of fairly constant thickness good lateral continuity and poor sorting. Hammer is 40 cm. long.

Figure 3. Distal playa sediments of the non-evaporite portion of the Muddy Creek basin. Silts exhibit crude bedding with some ripple laminations. Occasional zones of pebbles and cobbles are present in one pebble thick beds. White bed in the upper center of the photograph is a vitric tuff. Photo is 6 meters high. (locality 47)

PLATE XII

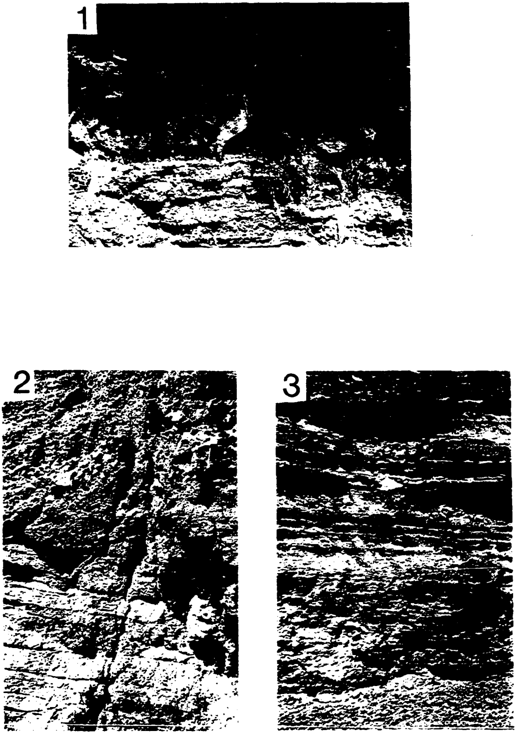

PLATE XIII. Muddy Creek Formation: Angular unconformity
mudflow

Figure 1. Local angular unconformities such as this one are exposed in some of the deeper washes draining the River Mountains. (locality 59). Hammer is 50 cm. long.

Figure 2. The lowermost proximal beds of the Muddy Creek formation appear to have been deposited by mudflows. The beds are flat-bottomed, frequently exhibit grading and are very continuous laterally. Larger particles which are matrix supported often project into overlying beds. At this locality (9c) the mudflow beds are overlain by better sorted fine to medium conglomerates deposited by less viscous flows. Hammer is 50 cm. in length.

PLATE XIII

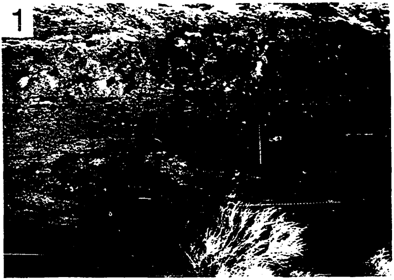

PLATES XIV. Muddy Creek Formation: Sedimentary structures

Figure 1. Flat bottomed continuous mud-flow deposits alternating with very lenticular scour and fill deposits just above and to the left of the scale which is 30 cm. long. (locality 10)

Figure 2. Graded pebbly mudstones are common in the mid-valley playa deposits. These beds are most likely the result of flows entering a standing body of water. (locality 21)

Figure 3. Vitric tuffs are preserved in the playa deposits and in the distal fan sediments of the Muddy Creek Formation. (locality 2). The tuffs frequently contain ripple laminations on their upper surfaces and a very thin dessication cracked porcelain-like material at the base. This basal lamination could either be a baked zone or an accumulation of fine ash.

Figure 4. Cross bedding in small channel at locality 11. Hammer is 40 cm. long.

PLATE XIV

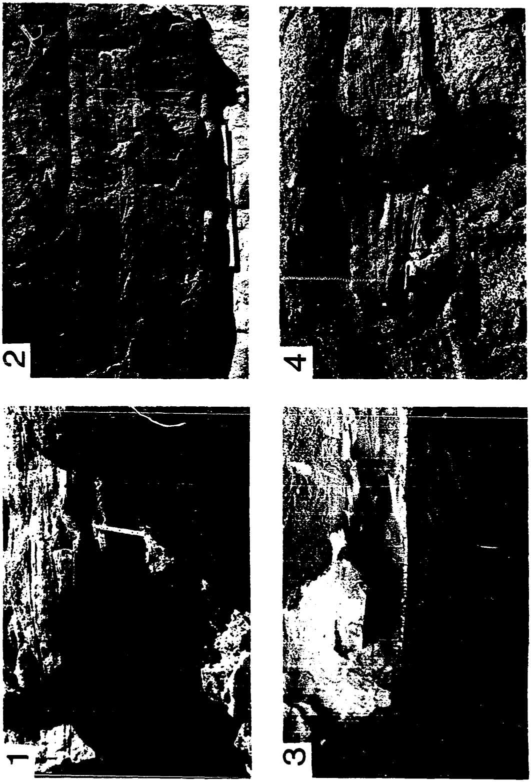

PLATE XV. Muddy Creek Formation

Figure 1. Sandstone dike near the base of section at locality 8, possibly induced by earthquakes which disturbed packing arrangements of saturated sandstones.

Figure 2. Large boulder at locality 8A. Surrounding sediment is very poorly sorted, indistinctly bedded sand and fine gravel.

PLATE XV

1

2

PLATE XVI. Muddy Creek Formation: Evaporites

Figure 1. Bedded gypsum at locality 9B displays parallel and contorted bedding in the lower half of the photograph. Ripple-laminated zone at scale level contains secondary nodular gypsum.

Figure 2. Recent salt playa in Death Valley, California. Dessication polygons are curled creating pan-like structures.

Figure 3. Bedded gypsum at the bottom of the photograph is overlain by ripple-laminated zone shown in Figure 1. Pan-like structure is apparent in upper middle of the photo. Bedding above the laminated zone appears to have been partially destroyed by recrystallization. Dessication cracked silty zone is present just below the hammer and a limestone nodule can be seen in the extreme upper right of the picture. Hammer is 40 cm. long.

PLATE XVI

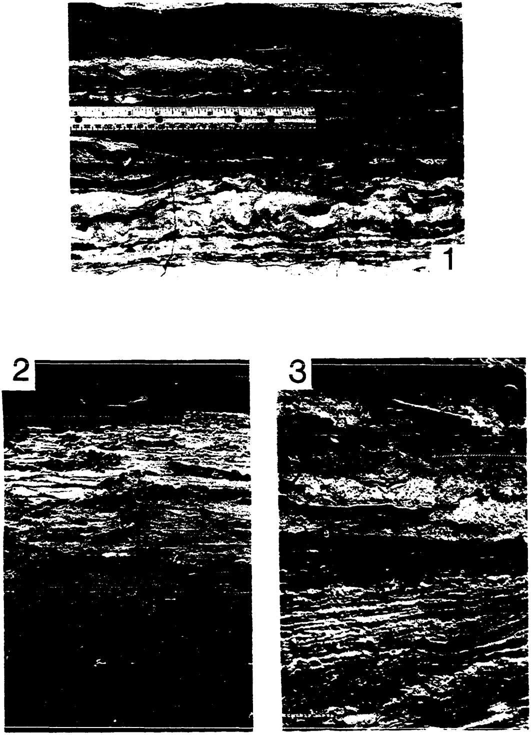

APPENDIX ii

X-Ray Diffraction Patterns -
Muddy Creek Formation Clays.

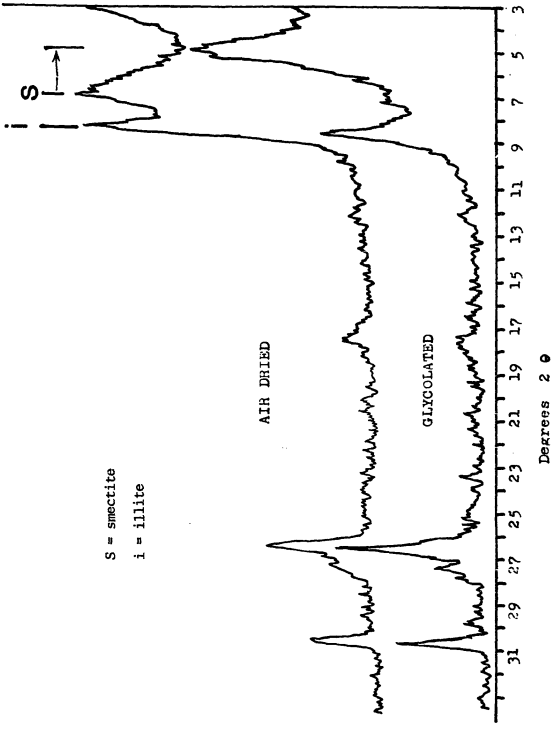
S = smectite
i = illite
S
i
AIR DRIED
GLYCOLATED
Degrees 2 θ
3
5
7
9
11
13
15
17
19
21
23
25
27
29
31

APPENDIX iii

Characteristics of the sepiolite
mineral associated with the
Muddy Creek Formation.

X-Ray Diffraction
Differential Thermal Analysis
Chemical Analyses

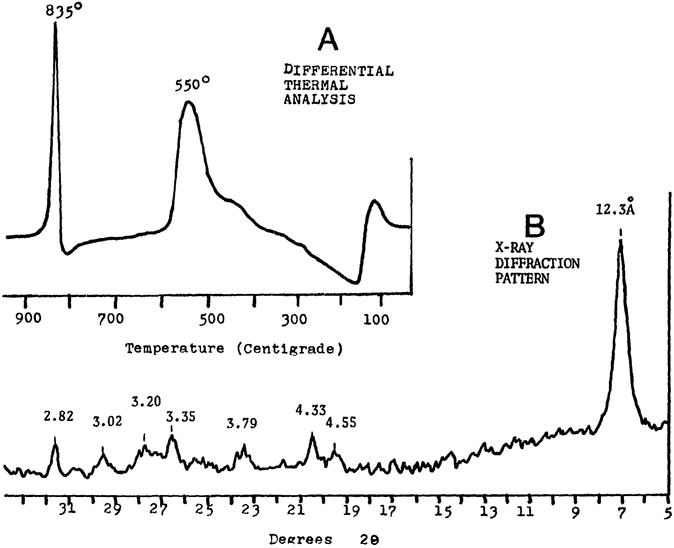
835°
550°
A
DIFFERENTIAL
THERMAL
ANALYSIS
900
700
500
300
100
Temperature (Centigrade)
B
X-RAY
DIFFRACTION
PATTERN
12.3Å
2.82
3.02
3.20
3.35
3.79
4.33
4.55
31
29
27
25
23
21
19
17
15
13
11
9
7
5
Degrees 2θ

Chemical analyses of sepiolites from the Muddy Creek Formation.[1]

	SP-1*	SP-2**
SiO_2	61.20	69.35
Al_2O_3	5.00	0.60
Fe_2O_3	1.15	0.00
MnO	0.01	0.01
MgO	21.60	29.87
CaO	4.55	0.00
Na_2O	4.72	0.07
K_2O	1.42	0.02

[1]Atomic absorbtion analyses made on Perkin-Elmer equipment at the University of Cincinnati.

*Locality 45.
**Locality 8.

APPENDIX iv

Chemical composition of vitric tuffs
associated with the
Muddy Creek Formation.

Chemical composition of tuffs associated with the Muddy Creek formation.

Sample #	SiO_2	Al_2O_3	Fe_{tot}	MgO	CaO	Na_2O	K_2O
2-3	73.06	14.5	2.46	1.14	2.22	3.41	3.21
2-7	67.6	14.6	2.23	2.22	1.48	8.44	3.41
4-5	71.5	15.5	2.11	2.81	1.70	2.95	3.44
9F-2	75.62	12.7	0.97	1.51	2.63	2.69	3.90
33-1	76.50	12.5	0.87	1.13	0.66	2.53	5.79
33-10	69.88	14.3	3.12	4.72	2.30	2.42	3.26
39-2	70.49	12.8	2.16	4.29	1.94	3.50	4.82
47-2	72.62	14.6	2.53	1.38	2.36	3.42	3.09
86-72	76.36	12.6	0.92	0.95	1.11	2.72	5.34

APPENDIX V

Summary table of particle form data

SAMPLE NUMBER	L-AXIS	I-AXIS	S-AXIS	AVERAGE L I S	ST. DEV. OF AV. LIS	I/L RATIO	S/I RATIO	S/L RATIO	L-I/L-S RATIO	$\overline{OP}$ INDEX	ST. DEV. OP	M P S	ST. DEV. M P S	SPHERICITY INDEX	FLATNESS INDEX	MAX. L	MAX. I
KC-2	60.5	40.3	26.5	42.4	26.9	.675	.642	.428	.586	.87	9.71	.637	.16	.647	2.54	170	127
KC-3	65.4	41.7	26.4	44.5	30.9	.682	.628	.427	.543	2.34	8.96	.630	.15	.648	2.31	194	130
KC-4	58.1	37.1	21.0	38.7	29.6	.666	.596	.385	.565	.85	8.70	.599	.16	.621	2.56	320	175
KC-5	62.2	42.9	24.4	43.2	42.6	.694	.588	.399	.508	.29	6.78	.608	.12	.642	2.36	320	270
KC-6	57.5	38.3	23.3	39.7	27.2	.670	.608	.398	.562	1.11	5.77	.616	.12	.636	2.29	168	149
KC-7	49.1	32.3	19.3	33.6	18.1	.667	.618	.404	.570	1.33	5.69	.622	.13	.638	2.29	115	85
KC-8	56.7	39.7	26.4	40.9	31.9	.704	.646	.448	.547	.77	6.35	.654	.13	.672	2.14	200	142
KC-9	60.4	40.8	26.1	42.4	27.4	.688	.652	.438	.561	1.12	6.30	.651	.11	.662	2.13	150	130
KC-10	71.3	49.4	30.8	50.5	35.4	.715	.634	.447	.513	.31	4.89	.651	.10	.678	2.04	218	148
KC-11	63.8	43.5	27.4	44.9	42.1	.653	.632	.405	.586	2.24	6.10	.627	.10	.633	2.25	270	265
KC-12	69.0	47.2	28.2	48.2	45.1	.682	.600	.406	.542	.82	6.11	.615	.14	.641	2.36	350	230
KC-13	59.2	42.8	23.2	41.8	39.8	.709	.548	.382	.486	-1.19	7.58	.583	.14	.636	2.66	330	260
KC-14	34.5	23.7	13.6	23.9	16.9	.689	.583	.397	.526	.23	6.40	.603	.15	.637	2.53	110	68
KC-15	60.5	43.5	28.9	44.3	32.5	.716	.664	.473	.555	.85	4.66	.673	.12	.690	1.99	180	127
KC-16	47.1	32.1	21.3	33.5	28.7	.691	.670	.464	.585	1.75	3.97	.671	.12	.678	1.98	269	197
KC-17	51.5	36.8	24.2	37.5	37.3	.719	.647	.457	.534	.27	5.90	.659	.13	.682	2.05	305	220
KC-21	37.0	25.8	16.9	26.6	21.5	.700	.623	.432	.534	.65	4.97	.639	.12	.664	2.17	136	95
LW-1	148.1	103.1	69.2	106.8	38.6	.712	.675	.478	.550	1.26	5.26	.680	.11	.691	1.93	380	240
LW-2	208.1	137.3	93.6	146.3	58.8	.664	.685	.453	.620	2.72	4.54	.671	.11	.664	1.99	445	380
LW-6	95.9	61.8	41.5	66.4	33.3	.666	.687	.456	.615	2.63	4.75	.671	.12	.664	2.05	222	157

APPENDIX vi

Summary table of
correlation and regression of
mean bed thickness and
mean maximum particle size -
Muddy Creek Formation.

SECTION NUMBER	MEAN Bed THICKNESS (CM)	MEAN LARGEST GRAIN (CM)	CORRELATION COEFFICIENT	$100R^2$	SLOPE OF REGRESSION LINE	INTERCEPT OF REGRESSION LINE (CM)
M4A	26.5	7.3	-0.106	1.12	-0.32	28.8
M4B	50.3	22.3	0.775	60.01	1.32	20.8
M5	30.8	6.5	0.041	0.17	0.15	29.9
M5A	61.9	7.2	0.456	20.83	3.52	36.5
M6	55.3	23.4	0.585	34.26	0.69	39.2
M8	25.3	11.5	-0.042	0.18	-0.05	25.9
M8A	23.7	15.5	0.682	46.6	0.82	10.9
M9	27.9	16.8	0.390	15.20	0.45	20.4
M9C	34.3	24.6	0.889	78.99	0.79	14.8
M9D	40.2	7.1	0.152	2.32	0.24	38.4
M10	37.2	15.3	0.481	23.11	1.23	18.3
M11	26.0	19.6	0.538	28.94	0.41	17.8
M12	52.5	27.5	0.648	42.06	1.40	13.9
M20	34.2	25.9	0.276	7.64	0.44	22.8
M21	14.0	7.5	0.806	65.07	0.82	7.8
M22	23.4	8.1	0.388	15.03	0.55	18.8
M23	34.3	9.7	0.346	11.98	0.99	24.7
M30	81.0	21.4	0.640	40.96	1.82	41.8
M31	26.4	8.9	0.768	59.03	2.18	7.0
M32	46.2	19.5	0.545	29.65	0.74	31.8
M33	30.6	16.2	0.508	25.78	0.99	14.5
M34	23.5	7.6	-0.159	2.53	-0.68	28.7
M35	26.8	16.8	0.428	18.30	0.59	16.9
M40	37.6	18.5	0.763	58.17	1.30	13.6
M42	41.4	8.0	0.149	2.22	0.77	35.3
M43	39.6	11.9	0.638	40.77	1.18	25.5
M44	40.4	17.0	0.437	19.13	0.54	31.1
M45	44.1	20.4	0.589	34.78	1.20	19.6
M46	40.3	16.9	0.080	0.64	0.19	37.0
M48	17.7	6.9	-0.272	7.37	-0.91	24.0
M49	29.4	21.4	0.253	6.41	0.30	22.8
M50	56.3	32.5	0.810	65.63	1.32	13.4
M51	38.8	24.9	0.344	11.82	0.41	28.4
M52	38.8	24.4	0.513	26.31	0.48	27.0
M53	49.2	25.1	0.339	11.49	0.32	41.1
M54	35.5	23.7	0.414	17.51	0.57	21.9
M55	47.3	31.8	0.423	17.90	1.32	5.0
M56	37.4	27.8	0.811	65.78	0.57	21.3
M58	47.7	28.4	0.637	40.61	0.85	23.5
M59	18.9	14.7	0.207	4.29	0.11	17.2

APPENDIX vii

Summary Tables of
particle form data
listed by locality.

KC refers to Kyle Canyon,
LW refers to Lida Wash.

KC-1-2	OBS	A	B	C	MAX.PROJ.SP.	B/A	C/B	SPHER.I.	FLAT.I.	AV.ABC	SL	LILS
	1	150.0	100.0	45.0	0.5133	0.667	0.450	0.5851	2.7778	98.3	0.300	0.476
	2	72.0	42.0	25.0	0.5916	0.583	0.595	0.5876	2.2800	46.3	0.347	0.638
	3	60.0	39.0	30.0	0.7275	0.650	0.769	0.6878	1.6500	43.0	0.500	0.700
	4	20.0	14.0	6.0	0.5051	0.700	0.429	0.5947	2.8333	13.3	0.300	0.429
	5	50.0	42.0	17.0	0.5166	0.840	0.405	0.6588	2.7059	36.3	0.340	0.242
	6	170.0	80.0	54.0	0.5988	0.471	0.675	0.5311	2.3148	101.3	0.318	0.776
	7	95.0	75.0	55.0	0.7518	0.789	0.733	0.7705	1.5455	75.0	0.579	0.500
	8	65.0	34.0	33.0	0.7900	0.523	0.971	0.6431	1.5000	44.0	0.508	0.969
	9	20.0	15.0	10.0	0.6936	0.750	0.667	0.7214	1.7500	15.0	0.500	0.500
	10	34.0	24.0	4.0	0.2700	0.706	0.167	0.4366	7.2500	20.7	0.118	0.333
	11	11.0	10.0	3.0	0.4345	0.909	0.300	0.6285	3.5000	8.0	0.273	0.125
	12	46.0	18.0	14.0	0.6189	0.391	0.778	0.4923	2.2857	26.0	0.304	0.875
	13	17.0	10.0	6.0	0.5964	0.588	0.600	0.5924	2.2500	11.0	0.353	0.636
	14	150.0	127.0	120.0	0.9110	0.847	0.945	0.8783	1.1542	132.3	0.800	0.767
	15	80.0	75.0	32.0	0.5550	0.938	0.427	0.7214	2.4219	62.3	0.400	0.104
	16	124.0	55.0	19.0	0.3758	0.444	0.345	0.4085	4.7105	66.0	0.153	0.657
	17	70.0	48.0	22.0	0.5245	0.686	0.458	0.5999	2.6818	46.7	0.314	0.458
	18	52.0	34.0	18.0	0.5683	0.654	0.529	0.6097	2.3889	34.7	0.346	0.529
	19	57.0	52.0	41.0	0.8279	0.912	0.788	0.8691	1.3293	50.0	0.719	0.313
	20	45.0	28.0	23.0	0.7490	0.622	0.821	0.6828	1.5870	32.0	0.511	0.773
	21	56.0	33.0	20.0	0.6007	0.589	0.606	0.5951	2.2250	36.3	0.357	0.639
	22	71.0	30.0	18.0	0.5341	0.423	0.600	0.4753	2.8056	39.7	0.254	0.774
	23	72.0	50.0	24.0	0.5432	0.694	0.480	0.6143	2.5417	48.7	0.333	0.458
	24	110.0	93.0	84.0	0.8837	0.845	0.903	0.8644	1.2083	95.7	0.764	0.654
	25	60.0	46.0	3.0	0.1486	0.767	0.065	0.3375	17.6667	36.3	0.050	0.246
	26	45.0	30.0	30.0	0.8737	0.667	1.000	0.7633	1.2500	35.0	0.667	1.000
	27	98.0	60.0	54.0	0.7917	0.612	0.900	0.6964	1.4630	70.7	0.551	0.864
	28	116.0	83.0	63.0	0.7445	0.716	0.759	0.7300	1.5794	87.3	0.543	0.623
	29	30.0	15.0	8.0	0.5223	0.500	0.533	0.5112	2.8125	17.7	0.267	0.682
	30	27.0	19.0	12.0	0.6550	0.704	0.632	0.6791	1.9167	19.3	0.444	0.533
	31	49.0	23.0	22.0	0.7547	0.469	0.957	0.5954	1.6364	31.3	0.449	0.963
	32	46.0	20.0	15.0	0.6257	0.435	0.750	0.5218	2.2000	27.0	0.326	0.839
	33	87.0	61.0	21.0	0.4367	0.701	0.344	0.5535	3.5238	56.3	0.241	0.394
	34	40.0	30.0	16.0	0.5978	0.750	0.533	0.6697	2.1875	28.7	0.400	0.417
	35	30.0	20.0	14.0	0.6890	0.667	0.700	0.6779	1.7857	21.3	0.467	0.625
	36	45.0	34.0	32.0	0.8748	0.756	0.941	0.8131	1.2344	37.0	0.711	0.846
	37	38.0	23.0	20.0	0.7708	0.605	0.870	0.6832	1.5250	27.0	0.526	0.833
	38	72.0	67.0	47.0	0.7710	0.931	0.701	0.8470	1.4787	62.0	0.653	0.200
	39	29.0	15.0	5.0	0.3863	0.517	0.333	0.4471	4.4000	16.3	0.172	0.583
	40	70.0	50.0	40.0	0.7705	0.714	0.800	0.7420	1.5000	53.3	0.571	0.667
	41	48.0	20.0	15.0	0.6169	0.417	0.750	0.5072	2.2667	27.7	0.313	0.848
	42	23.0	20.0	15.0	0.7881	0.870	0.750	0.8279	1.4333	19.3	0.652	0.375
	43	37.0	25.0	25.0	0.8776	0.676	1.000	0.7702	1.2400	29.0	0.676	1.000
	44	24.0	20.0	10.0	0.5931	0.833	0.500	0.7031	2.2000	18.0	0.417	0.286
	45	72.0	45.0	30.0	0.6528	0.625	0.667	0.6389	1.9500	49.0	0.417	0.643
	46	20.0	15.0	10.0	0.6936	0.750	0.667	0.7214	1.7500	15.0	0.500	0.500
	47	24.0	20.0	9.0	0.5529	0.833	0.450	[illegible]	2.4444	17.7	0.375	0.267
	48	31.0	20.0	14.0	0.6815	0.645	0.700	0.6632	1.8214	21.7	0.452	0.647
	49	110.0	60.0	50.0	0.7238	0.545	0.833	0.6285	1.7000	73.3	0.455	0.833
	50	56.0	47.0	24.0	0.6029	0.839	0.511	0.7114	2.1458	42.3	0.429	0.281
COLUMN AVERAGE		60.5	40.3	26.5	0.6376	0.675	0.642	0.6474	2.5362	42.4	0.428	0.586
ST.DV.					0.1600			0.1225	2.4223	26.9		

KC-1-3 OBS	A	B	C	MAX.PROJ.SP.	B/A	C/B	SPHER.I.	FLAT.I.	AV.ABC	SL	LILS
1	50.0	43.0	18.0	0.5325	0.860	0.419	0.6768	2.5833	37.0	0.360	0.219
2	29.0	22.0	20.0	0.8560	0.759	0.909	0.8060	1.2750	23.7	0.690	0.778
3	40.0	20.0	13.0	0.5959	0.500	0.650	0.5460	2.3077	24.3	0.325	0.741
4	40.0	20.0	20.0	0.7939	0.500	1.000	0.6303	1.5000	26.7	0.500	1.000
5	17.0	15.0	5.0	0.4615	0.882	0.333	0.6381	3.2000	12.3	0.294	0.167
6	25.0	20.0	20.0	0.9284	0.800	1.000	0.8619	1.1250	21.7	0.800	1.000
7	60.0	27.0	15.0	0.5182	0.450	0.556	0.4831	2.9000	34.0	0.250	0.733
8	55.0	37.0	14.0	0.4587	0.673	0.378	0.5556	3.2857	35.3	0.255	0.439
9	17.0	12.0	5.0	0.4971	0.706	0.417	0.5924	2.9000	11.3	0.294	0.417
10	48.0	45.0	23.0	0.6259	C.938	0.511	0.7661	2.0217	38.7	0.479	0.120
11	23.0	14.0	5.0	0.4270	0.609	0.357	0.5099	3.7000	14.0	0.217	0.500
12	194.0	85.0	53.0	0.5547	0.438	0.624	0.4932	2.6321	110.7	0.273	0.773
13	70.0	20.0	13.0	0.4946	0.286	0.650	0.3761	3.4615	34.3	0.186	0.877
14	48.0	30.0	22.0	0.6955	0.625	0.733	0.6595	1.7727	33.3	0.458	0.692
15	35.0	25.0	22.0	0.8210	0.714	0.880	0.7659	1.3636	27.3	0.629	0.769
16	84.0	68.0	25.0	0.4786	0.810	0.368	0.6225	3.0400	59.0	0.298	0.271
17	26.0	15.0	9.0	0.5925	0.577	0.600	0.5848	2.2778	16.7	0.346	0.647
18	10.0	5.0	3.0	0.5649	0.500	0.600	0.5317	2.5000	6.0	0.300	0.714
19	24.0	14.0	6.0	0.4753	0.583	0.429	0.5267	3.1667	14.7	0.250	0.556
20	25.0	23.0	17.0	0.7953	0.920	0.739	0.8554	1.4118	21.7	0.680	0.250
21	60.0	55.0	42.0	0.8117	0.917	0.764	0.8626	1.3690	52.3	0.700	0.278
22	35.0	35.0	25.0	0.7992	1.000	0.714	0.8940	1.4000	31.7	0.714	0.0
23	161.0	37.0	21.0	0.4203	0.230	0.568	0.3110	4.7143	73.0	0.130	0.886
24	23.0	5.0	5.0	0.6016	0.217	1.000	0.3619	2.8000	11.0	0.217	1.000
25	65.0	58.0	25.0	0.5497	0.892	0.431	0.7004	2.4600	49.3	0.385	0.175
26	58.0	50.0	25.0	0.5999	0.862	0.500	0.7192	2.1600	44.3	0.431	0.242
27	25.0	23.0	16.0	0.7638	0.920	0.696	0.8383	1.5000	21.3	0.640	0.222
28	30.0	23.0	15.0	0.6886	0.767	0.652	0.7267	1.7667	22.7	0.500	0.467
29	17.0	13.0	4.0	0.4171	0.765	0.308	0.5649	3.7500	11.3	0.235	0.308
30	38.0	25.0	17.0	0.6728	0.658	0.680	0.6655	1.8529	26.7	0.447	0.619
31	67.0	65.0	47.0	0.7977	0.970	0.723	0.8797	1.4043	59.7	0.701	0.100
32	82.0	50.0	42.0	0.7551	0.610	0.840	0.6787	1.5714	58.0	0.512	0.800
33	42.0	35.0	25.0	0.7522	0.833	0.714	0.7918	1.5400	34.0	0.595	0.412
34	58.0	28.0	18.0	0.5846	0.483	0.643	0.5315	2.3889	34.7	0.310	0.750
35	51.0	50.0	30.0	0.7069	0.980	0.600	0.8325	1.6833	43.7	0.588	0.048
36	120.0	100.0	100.0	0.9411	0.833	1.000	0.8857	1.1000	106.7	0.833	1.000
37	132.0	100.0	44.0	0.5277	0.758	0.440	0.6324	2.6364	92.0	0.333	0.364
38	93.0	45.0	20.0	0.4576	0.484	0.444	0.4707	3.4500	52.7	0.215	0.658
39	65.0	41.0	21.0	0.5493	0.631	0.512	0.5888	2.5238	42.3	0.323	0.545
40	98.0	50.0	27.0	0.53[illegible]	0.510	0.540	0.5203	2.7407	58.3	0.276	0.676
41	167.0	130.0	110.0	0.8231	0.778	0.846	0.8006	1.3500	135.7	0.659	0.649
42	42.0	40.0	32.0	0.8480	0.952	0.800	0.8987	1.2813	38.0	0.762	0.200
43	74.0	65.0	50.0	0.8042	0.878	0.769	0.8405	1.3900	63.0	0.676	0.375
44	122.0	100.0	40.0	0.5084	0.820	0.400	0.6456	2.7750	87.3	0.328	0.268
45	90.0	35.0	25.0	0.5836	0.389	0.714	0.4766	2.5000	50.0	0.278	0.846
46	163.0	120.0	80.0	0.6893	0.736	0.667	0.7125	1.7687	121.0	0.491	0.518
47	155.0	43.0	22.0	0.4176	0.277	0.512	0.3406	4.5000	73.3	0.142	0.842
48	170.0	70.0	45.0	0.5545	0.412	0.643	0.4780	2.6667	95.0	0.265	0.800
49	30.0	20.0	12.0	0.6217	0.667	0.600	0.6439	2.0833	20.7	0.400	0.556
50	18.0	13.0	7.0	0.5941	0.722	0.538	0.6552	2.2143	12.7	0.389	0.455
COLUMN AVERAGE	65.4	41.7	26.4	0.6308	0.682	0.628	0.6486	2.3153	44.5	0.427	0.534
ST.DV.				0.1458			0.1573	0.8715	30.9		

KC-1-4	OBS	A	B	C	MAX.PROJ.SP.	B/A	C/B	SPHER.I.	FLAT.I.	AV.ABC	SL	LILS
	1	48.0	35.0	33.0	0.8656	0.729	0.943	0.7946	1.2576	38.7	0.688	0.867
	2	68.0	41.0	15.0	0.4325	0.603	0.366	0.5108	3.6333	41.3	0.221	0.500
	3	60.0	53.0	16.0	0.4322	0.883	0.302	0.6179	3.5313	43.0	0.267	0.159
	4	35.0	26.0	23.0	0.8347	0.743	0.885	0.7876	1.3261	28.0	0.657	0.750
	5	72.0	35.0	18.0	0.5051	0.486	0.514	0.4957	2.9722	41.7	0.250	0.685
	6	47.0	20.0	17.0	0.6752	0.426	0.850	0.5362	1.9706	28.0	0.362	0.900
	7	21.0	17.0	13.0	0.7796	0.810	0.765	0.7945	1.4615	17.0	0.619	0.500
	8	24.0	21.0	4.0	0.3170	0.875	0.190	0.5267	5.6250	16.3	0.167	0.150
	9	24.0	14.0	6.0	0.4753	0.583	0.429	0.5267	3.1667	14.7	0.250	0.356
	10	13.0	7.0	5.0	0.6504	0.538	0.714	0.5920	2.0000	8.3	0.385	0.750
	11	60.0	24.0	9.0	0.3835	0.400	0.375	0.3919	4.6667	31.0	0.150	0.706
	12	72.0	34.0	20.0	0.5470	0.472	0.588	0.5084	2.6500	42.0	0.278	0.731
	13	35.0	23.0	22.0	0.8442	0.657	0.957	0.7450	1.3182	26.7	0.629	0.923
	14	53.0	50.0	13.0	0.3999	0.943	0.260	0.6142	3.9615	38.7	0.245	0.075
	15	86.0	64.0	21.0	0.4315	0.744	0.328	0.5667	3.5714	57.0	0.244	0.338
	16	51.0	24.0	22.0	0.7342	0.471	0.917	0.5880	1.7045	32.3	0.431	0.331
	17	194.0	80.0	57.0	0.5941	0.412	0.712	0.4952	2.4035	110.3	0.294	0.332
	18	320.0	175.0	125.0	0.6537	0.547	0.714	0.5981	1.9800	206.7	0.381	0.744
	19	42.0	32.0	30.0	0.8750	0.762	0.938	0.8166	1.2333	34.7	0.714	0.833
	20	65.0	47.0	34.0	0.7235	0.723	0.723	0.7234	1.6471	48.7	0.523	0.561
	21	45.0	28.0	17.0	0.6124	0.622	0.607	0.6175	2.1471	30.0	0.378	0.607
	22	61.0	53.0	32.0	0.6819	0.869	0.604	0.7699	1.7813	48.7	0.525	0.276
	23	56.0	56.0	15.0	0.4159	1.000	0.268	0.6449	3.7333	42.3	0.268	0.0
	24	73.0	44.0	14.0	0.3941	0.603	0.318	0.4875	4.1786	43.7	0.192	0.492
	25	30.0	22.0	15.0	0.6988	0.733	0.682	0.7160	1.7333	22.3	0.500	0.333
	26	40.0	30.0	14.0	0.5470	0.750	0.467	0.6406	2.5000	28.0	0.350	0.385
	27	57.0	40.0	28.0	0.7008	0.702	0.700	0.7014	1.7321	41.7	0.491	0.386
	28	40.0	22.0	22.0	0.8195	0.550	1.000	0.6716	1.4091	28.0	0.550	1.000
	29	60.0	31.0	23.0	0.6579	0.517	0.742	0.5832	1.9783	38.0	0.353	0.744
	30	23.0	22.0	18.0	0.8620	0.957	0.818	0.9081	1.2500	21.0	0.783	0.200
	31	48.0	44.0	15.0	0.4744	0.917	0.341	0.6595	3.0667	35.7	0.313	0.121
	32	35.0	24.0	24.0	0.8819	0.686	1.000	0.7778	1.2292	27.7	0.656	1.000
	33	115.0	57.0	43.0	0.6561	0.496	0.754	0.5705	2.0000	71.7	0.374	0.806
	34	13.0	8.0	7.0	0.7783	0.615	0.875	0.6922	1.5000	9.3	0.538	0.833
	35	39.0	28.0	14.0	0.5644	0.718	0.500	0.6367	2.3929	27.0	0.359	0.440
	36	50.0	37.0	7.0	0.2984	0.740	0.189	0.4700	6.2143	31.3	0.140	0.302
	37	55.0	31.0	17.0	0.5538	0.564	0.548	0.5588	2.5294	34.3	0.309	0.632
	38	25.0	17.0	11.0	0.6581	0.680	0.647	0.6691	1.9091	17.7	0.440	0.571
	39	53.0	49.0	24.0	0.6056	0.925	0.490	0.7483	2.1250	42.0	0.453	0.134
	40	77.0	41.0	20.0	0.5026	0.532	0.488	0.5175	2.9500	46.0	0.260	0.632
	41	46.0	26.0	14.0	0.5476	0.565	0.538	0.5565	2.5714	28.7	0.304	0.625
	42	60.0	27.0	13.0	0.4711	0.450	0.481	0.4606	3.3462	33.3	0.217	0.702
	43	37.0	20.0	16.0	0.7022	0.541	0.800	0.6163	1.7813	24.3	0.432	0.310
	44	53.0	42.0	20.0	0.5646	0.792	0.476	0.6690	2.3750	38.3	0.377	0.333
	45	28.0	16.0	9.0	0.5658	0.571	0.563	0.5688	2.4444	17.7	0.321	0.632
	46	43.0	35.0	15.0	0.5311	0.814	0.429	0.6575	2.6000	31.0	0.349	0.286
	47	47.0	21.0	13.0	0.5556	0.447	0.619	0.4985	2.6154	27.0	0.277	0.765
	48	35.0	15.0	8.0	0.4962	0.429	0.533	0.4613	3.1250	19.3	0.229	0.741
	49	80.0	65.0	40.0	0.6754	0.813	0.615	0.7408	1.8125	61.7	0.509	0.375
	50	89.0	80.0	18.0	0.3574	0.899	0.225	0.5668	4.6944	62.3	0.202	0.127
COLUMN AVERAGE		58.1	37.1	21.0	0.5997	0.666	0.596	0.6213	2.5561	38.7	0.385	0.565
ST.DV.					0.1561			0.1123	1.1395	29.6		

KC-1-5 OBS	A	B	C	MAX.PROJ.SP.	B/A	C/B	SPHER.I.	FLAT.I.	AV.ABC	SL	LILS
1	26.0	20.0	9.0	0.5384	0.769	0.450	0.6436	2.5556	18.3	0.346	0.353
2	91.0	70.0	32.0	0.5441	0.769	0.457	0.6470	2.5156	64.3	0.352	0.356
3	15.0	12.0	9.0	0.7665	0.800	0.750	0.7832	1.5000	12.0	0.600	0.500
4	70.0	21.0	14.0	0.5112	0.300	0.667	0.3919	3.2500	35.0	0.200	0.875
5	93.0	55.0	20.0	0.4280	0.591	0.364	0.5032	3.7000	56.0	0.215	0.521
6	85.0	73.0	40.0	0.6368	0.859	0.548	0.7396	1.9750	66.0	0.471	0.267
7	33.0	20.0	8.0	0.4598	0.606	0.400	0.5280	3.3125	20.3	0.242	0.520
8	38.0	27.0	11.0	0.4907	0.711	0.407	0.5906	2.9545	25.3	0.289	0.407
9	24.0	13.0	5.0	0.4315	0.542	0.385	0.4836	3.7000	14.0	0.208	0.579
10	71.0	34.0	19.0	0.5311	0.479	0.559	0.5045	2.7632	41.3	0.258	0.712
11	84.0	37.0	20.0	0.5052	0.440	0.541	0.4719	3.0250	47.0	0.238	0.734
12	158.0	104.0	62.0	0.6165	0.658	0.596	0.6371	2.1129	108.0	0.392	0.563
13	78.0	75.0	58.0	0.8317	0.962	0.773	0.8943	1.3190	70.3	0.744	0.150
14	74.0	38.0	31.0	0.6994	0.514	0.816	0.5995	1.8065	47.7	0.419	0.837
15	17.0	10.0	3.0	0.3759	0.588	0.300	0.4703	4.5000	10.0	0.176	0.500
16	41.0	25.0	10.0	0.4607	0.610	0.400	0.5302	3.3000	25.3	0.244	0.516
17	116.0	76.0	55.0	0.7003	0.655	0.724	0.6775	1.7455	82.3	0.474	0.656
18	60.0	37.0	22.0	0.6022	0.617	0.595	0.6095	2.2045	39.7	0.367	0.605
19	72.0	44.0	32.0	0.6865	0.611	0.727	0.6479	1.8125	49.3	0.444	0.700
20	108.0	47.0	35.0	0.6229	0.435	0.745	0.5209	2.2143	63.3	0.324	0.836
21	34.0	21.0	18.0	0.7687	0.618	0.857	0.6892	1.5278	24.3	0.529	0.813
22	79.0	60.0	34.0	0.6251	0.759	0.567	0.6891	2.0441	57.7	0.430	0.422
23	31.0	20.0	10.0	0.5447	0.645	0.500	0.5929	2.5500	20.3	0.323	0.524
24	45.0	23.0	23.0	0.7997	0.511	1.000	0.6395	1.4783	30.3	0.511	1.000
25	31.0	17.0	10.0	0.5750	0.548	0.588	0.5617	2.4000	19.3	0.323	0.667
26	26.0	24.0	8.0	0.4684	0.923	0.333	0.6576	3.1250	19.3	0.308	0.111
27	320.0	270.0	140.0	0.6102	0.844	0.519	0.7176	2.1071	243.3	0.438	0.278
28	30.0	22.0	5.0	0.3362	0.733	0.227	0.4966	5.2000	19.0	0.167	0.320
29	44.0	34.0	20.0	0.6445	0.773	0.588	0.7058	1.9500	32.7	0.455	0.417
30	40.0	37.0	19.0	0.6251	0.925	0.514	0.7604	2.0263	32.0	0.475	0.143
31	41.0	37.0	17.0	0.5757	0.902	0.459	0.7208	2.2941	31.7	0.415	0.167
32	136.0	72.0	55.0	0.6763	0.529	0.764	0.5985	1.8909	87.7	0.404	0.790
33	10.0	9.0	5.0	0.6528	0.900	0.556	0.7665	1.9000	8.0	0.500	0.200
34	15.0	9.0	6.0	0.6439	0.600	0.667	0.6217	2.0000	10.0	0.400	0.667
35	19.0	17.0	7.0	0.5337	0.895	0.412	0.6910	2.5714	14.3	0.368	0.167
36	40.0	23.0	12.0	0.5393	0.575	0.522	0.5570	2.6250	25.0	0.300	0.607
37	18.0	17.0	7.0	0.5434	0.944	0.412	0.7164	2.5000	14.0	0.389	0.091
38	26.0	20.0	17.0	0.8223	0.769	0.850	0.7954	1.3529	21.0	0.654	0.667
39	89.0	44.0	37.0	0.7047	0.494	0.841	0.5905	1.7973	56.7	0.416	0.865
40	122.0	96.0	45.0	0.5574	0.787	0.469	0.6624	2.4222	87.7	0.369	0.338
41	10.0	10.0	5.0	0.6303	1.000	0.500	0.7939	2.0000	8.3	0.500	0.0
42	48.0	26.0	25.0	0.7943	0.542	0.962	0.6561	1.4800	33.0	0.521	0.957
43	40.0	28.0	15.0	0.5860	0.700	0.536	0.6406	2.2667	27.7	0.375	0.480
44	33.0	20.0	12.0	0.6023	0.606	0.600	0.6043	2.2083	21.7	0.364	0.619
45	40.0	32.0	21.0	0.7013	0.800	0.656	0.7491	1.7143	31.0	0.525	0.421
46	20.0	17.0	14.0	0.8324	0.850	0.824	0.8412	1.3214	17.0	0.700	0.500
47	40.0	32.0	11.0	0.4559	0.800	0.344	0.6040	3.2727	27.7	0.275	0.276
48	250.0	220.0	85.0	0.5087	0.880	0.386	0.6691	2.7647	185.0	0.340	0.182
49	45.0	25.0	25.0	0.8222	0.556	1.000	0.6761	1.4000	31.7	0.556	1.000
50	32.0	25.0	19.0	0.7672	0.781	0.760	0.7743	1.5000	25.3	0.594	0.538
COLUMN AVERAGE	62.2	42.9	24.4	0.6077	0.694	0.588	0.6423	2.3591	43.2	0.399	0.508
ST.DV.				0.1239			0.1055	0.8152	42.6		

KC-1-6 OBS	A	B	C	MAX.PROJ.SP.	B/A	C/B	SPHER.I.	FLAT.I.	AV.ABC	SL	LILS
1	64.0	42.0	24.0	0.5987	0.656	0.571	0.6270	2.2083	43.3	0.375	0.550
2	141.0	67.0	51.0	0.6508	0.475	0.761	0.5563	2.0392	86.3	0.362	0.822
3	25.0	15.0	15.0	0.8436	0.600	1.000	0.7116	1.3333	18.3	0.600	[illegible]
4	26.0	14.0	12.0	0.7343	0.538	0.857	0.6290	1.6667	17.3	0.462	[illegible]
5	14.0	8.0	4.0	0.5231	0.571	0.500	0.5469	2.7500	8.7	0.286	0.600
6	72.0	37.0	33.0	0.7424	0.514	0.892	0.6179	1.6515	47.3	0.458	0.847
7	40.0	30.0	16.0	0.5978	0.750	0.533	0.6697	2.1875	28.7	0.400	0.417
8	160.0	70.0	60.0	0.6853	0.438	0.857	0.5478	1.9167	96.7	0.375	[illegible]
9	60.0	47.0	30.0	0.6836	0.783	0.638	0.7319	1.7833	45.7	0.500	0.433
10	78.0	60.0	43.0	0.7340	0.769	0.717	0.7515	1.6047	60.3	0.551	0.514
11	10.0	9.0	5.0	0.6528	0.900	0.556	0.7665	1.9000	8.0	0.500	[illegible]
12	12.0	7.0	4.0	0.5757	0.583	0.571	0.5797	2.3750	7.7	0.333	0.625
13	27.0	20.0	10.0	0.5703	0.741	0.500	0.6501	2.3500	19.0	0.370	0.412
14	53.0	40.0	12.0	0.4084	0.755	0.300	0.5552	3.8750	35.0	0.226	0.317
15	40.0	25.0	18.0	0.6871	0.625	0.720	0.6555	1.8056	27.7	0.450	0.682
16	168.0	149.0	78.0	0.6244	0.887	0.523	0.7442	2.0321	131.7	0.464	0.211
17	15.0	8.0	3.0	0.4221	0.533	0.375	0.4746	3.8333	8.7	0.200	0.583
18	37.0	20.0	12.0	0.5798	0.541	0.600	0.5600	2.3750	23.0	0.324	0.680
19	43.0	25.0	17.0	0.6457	0.581	0.680	0.6129	2.0000	28.3	0.395	0.692
20	42.0	33.0	13.0	0.4962	0.786	0.394	0.6245	2.8846	29.3	0.310	0.310
21	50.0	38.0	28.0	0.7447	0.760	0.737	0.7524	1.5714	38.7	0.560	0.545
22	38.0	32.0	18.0	0.6438	0.842	0.563	0.7364	1.9444	29.3	0.474	0.300
23	82.0	46.0	42.0	0.7764	0.561	0.913	0.6601	1.5238	56.7	0.512	0.700
24	29.0	20.0	11.0	0.5934	0.690	0.550	0.6398	2.2273	20.0	0.379	0.500
25	89.0	60.0	33.0	0.5889	0.674	0.550	0.6302	2.2576	60.7	0.371	0.518
26	40.0	20.0	14.0	0.6260	0.500	0.700	0.5597	2.1429	24.7	0.350	0.769
27	135.0	80.0	41.0	0.5383	0.593	0.512	0.5649	2.6220	85.3	0.304	0.585
28	98.0	82.0	72.0	0.8642	0.837	0.878	0.8504	1.2500	84.0	0.735	0.615
29	42.0	25.0	23.0	0.7959	0.595	0.920	0.6885	1.4565	30.0	0.548	0.895
30	40.0	24.0	21.0	0.7718	0.600	0.875	0.6807	1.5238	28.3	0.525	0.842
31	31.0	26.0	12.0	0.5635	0.839	0.462	0.6876	2.3750	23.0	0.387	0.263
32	126.0	81.0	38.0	0.5214	0.643	0.469	0.5791	2.7237	81.7	0.302	0.511
33	17.0	10.0	4.0	0.4552	0.588	0.400	0.5176	3.3750	10.3	0.235	0.538
34	26.0	17.0	7.0	0.4807	0.654	0.412	0.5608	3.0714	16.7	0.269	0.474
35	52.0	40.0	27.0	0.7053	0.769	0.675	0.7367	1.7037	39.7	0.519	0.480
36	7.0	6.0	3.0	0.5987	0.857	0.500	0.7164	2.1667	5.3	0.429	0.250
37	25.0	17.0	10.0	0.6177	0.680	0.588	0.6482	2.1000	17.3	0.400	0.533
38	50.0	23.0	12.0	0.5006	0.460	0.522	0.4801	3.0417	28.3	0.240	0.711
39	32.0	23.0	20.0	0.8162	0.719	0.870	0.7661	1.3750	25.0	0.625	0.750
40	20.0	10.0	6.0	0.5649	0.500	0.600	0.5317	2.5000	12.0	0.300	0.714
41	102.0	75.0	20.0	0.3743	0.735	0.267	0.5247	4.4250	65.7	0.196	0.329
42	72.0	65.0	20.0	0.4409	0.903	0.308	0.6309	3.4250	52.3	0.278	0.135
43	50.0	38.0	12.0	0.4236	0.760	0.316	0.5674	3.6667	33.3	0.240	0.316
44	50.0	35.0	16.0	0.5272	0.700	0.457	0.6076	2.6563	33.7	0.320	0.441
45	106.0	72.0	60.0	0.7786	0.679	0.833	0.7274	1.4833	79.3	0.566	0.739
46	46.0	39.0	17.0	0.5444	0.848	0.436	0.6795	2.5000	34.0	0.370	0.241
47	58.0	43.0	15.0	0.4489	0.741	0.349	0.5770	3.3667	38.7	0.259	0.349
48	67.0	40.0	25.0	0.6158	0.597	0.625	0.6065	2.1400	44.0	0.373	0.643
49	68.0	32.0	27.0	0.6948	0.471	0.844	0.5720	1.8519	42.3	0.397	0.878
50	100.0	70.0	52.0	0.7285	0.700	0.743	0.7142	1.6346	74.0	0.520	0.625
COLUMN AVERAGE	57.5	38.3	23.3	0.6160	0.670	0.608	0.6361	2.2935	39.7	0.348	0.562
ST.DV.				0.1216			0.0841	0.7367	27.2		

	OBS	A	B	C	MAX.PROJ.SP.	B/A	C/B	SPHER.I.	FLAT.I.	AV.ABC	SL	LILS
KC-1-7	1	18.0	13.0	9.0	0.7024	0.722	0.692	0.7124	1.7222	13.3	0.500	0.556
	2	75.0	46.0	31.0	0.6534	0.613	0.674	0.6332	1.9516	50.7	0.413	0.659
	3	24.0	13.0	7.0	0.5399	0.542	0.538	0.5409	2.6429	14.7	0.292	0.647
	4	16.0	14.0	12.0	0.8632	0.875	0.857	0.8691	1.2500	14.0	0.750	0.500
	5	38.0	31.0	15.0	0.5762	0.816	0.484	0.6857	2.3000	28.0	0.395	0.304
	6	19.0	15.0	3.0	0.3164	0.789	0.200	0.4999	5.6667	12.3	0.158	0.250
	7	27.0	22.0	17.0	0.7867	0.815	0.773	0.8007	1.4412	22.0	0.630	0.500
	8	27.0	16.0	15.0	0.8047	0.593	0.938	0.6908	1.4333	19.3	0.556	0.917
	9	37.0	28.0	16.0	0.6278	0.757	0.571	0.6894	2.0313	27.0	0.432	0.429
	10	107.0	78.0	42.0	0.5960	0.729	0.538	0.6592	2.2024	75.7	0.393	0.446
	11	45.0	25.0	20.0	0.7087	0.556	0.800	0.6276	1.7500	30.0	0.444	0.800
	12	30.0	20.0	7.0	0.4342	0.667	0.350	0.5381	3.5714	19.0	0.233	0.435
	13	30.0	19.0	17.0	0.7976	0.633	0.895	0.7109	1.4412	22.0	0.567	0.846
	14	30.0	14.0	10.0	0.6201	0.467	0.714	0.5381	2.2000	18.0	0.333	0.800
	15	50.0	30.0	22.0	0.6861	0.600	0.733	0.6418	1.8182	34.0	0.440	0.714
	16	94.0	60.0	50.0	0.7627	0.638	0.833	0.6979	1.5400	68.0	0.532	0.773
	17	86.0	40.0	15.0	0.4033	0.465	0.375	0.4333	4.2000	47.0	0.174	0.648
	18	42.0	30.0	14.0	0.5381	0.714	0.467	0.6201	2.5714	28.7	0.333	0.429
	19	36.0	24.0	12.0	0.5507	0.667	0.500	0.6060	2.5000	24.0	0.333	0.500
	20	43.0	33.0	10.0	0.4134	0.767	0.303	0.5633	3.8000	28.7	0.233	0.303
	21	50.0	35.0	17.0	0.5490	0.700	0.486	0.6200	2.5000	34.0	0.340	0.455
	22	42.0	34.0	16.0	0.5642	0.810	0.471	0.6759	2.3750	30.7	0.381	0.308
	23	38.0	25.0	10.0	0.4725	0.658	0.400	0.5577	3.1500	24.3	0.263	0.464
	24	47.0	35.0	18.0	0.5821	0.745	0.514	0.6585	2.2778	33.3	0.383	0.414
	25	74.0	38.0	19.0	0.5048	0.514	0.500	0.5093	2.9474	43.7	0.257	0.655
	26	42.0	34.0	23.0	0.7184	0.810	0.676	0.7627	1.6522	33.0	0.548	0.421
	27	73.0	45.0	24.0	0.5600	0.616	0.533	0.5877	2.4583	47.3	0.329	0.571
	28	90.0	63.0	20.0	0.4136	0.700	0.317	0.5381	3.8250	57.7	0.222	0.386
	29	15.0	13.0	6.0	0.5697	0.867	0.462	0.7027	2.3333	11.3	0.400	0.222
	30	18.0	13.0	7.0	0.5941	0.722	0.538	0.6552	2.2143	12.7	0.389	0.455
	31	55.0	23.0	20.0	0.6815	0.418	0.870	0.5341	1.9500	32.7	0.364	0.914
	32	12.0	9.0	5.0	0.6143	0.750	0.556	0.6789	2.1000	8.7	0.417	0.429
	33	31.0	19.0	17.0	0.7889	0.613	0.895	0.6955	1.4706	22.3	0.548	0.857
	34	36.0	13.0	13.0	0.7124	0.361	1.000	0.5074	1.8846	20.7	0.361	1.000
	35	105.0	84.0	43.0	0.5944	0.800	0.512	0.6896	2.1977	77.3	0.410	0.339
	36	43.0	33.0	22.0	0.6989	0.767	0.667	0.7325	1.7273	32.7	0.512	0.476
	37	65.0	53.0	43.0	0.8128	0.815	0.811	0.8142	1.3721	53.7	0.662	0.545
	38	74.0	44.0	21.0	0.5139	0.595	0.477	0.5529	2.8095	46.3	0.284	0.566
	39	85.0	35.0	32.0	0.7011	0.412	0.914	0.5375	1.8750	50.7	0.376	0.943
	40	42.0	30.0	20.0	0.6824	0.714	0.667	0.6983	1.8000	30.7	0.476	0.545
	41	60.0	40.0	21.0	0.5688	0.667	0.525	0.6159	2.3810	40.3	0.350	0.513
	42	58.0	50.0	30.0	0.6773	0.862	0.600	0.7642	1.8000	46.0	0.517	0.286
	43	115.0	85.0	27.0	0.4213	0.739	0.318	0.5581	3.7037	75.7	0.235	0.341
	44	66.0	42.0	37.0	0.7906	0.636	0.881	0.7095	1.4595	48.3	0.561	0.828
	45	50.0	33.0	28.0	0.7805	0.660	0.848	0.7179	1.4821	37.0	0.560	0.773
	46	23.0	15.0	12.0	0.7476	0.652	0.800	0.6984	1.5833	16.7	0.522	0.727
	47	23.0	12.0	7.0	0.5624	0.522	0.583	0.5418	2.5000	14.0	0.304	0.688
	48	33.0	17.0	12.0	0.6358	0.515	0.706	0.5725	2.0833	20.7	0.364	0.762
	49	92.0	58.0	42.0	0.6917	0.630	0.724	0.6605	1.7857	64.0	0.457	0.680
	50	24.0	16.0	7.0	0.5038	0.667	0.438	0.5797	2.8571	15.7	0.292	0.471
COLUMN AVERAGE		49.1	32.3	19.3	0.6218	0.667	0.618	0.6377	2.2918	33.6	0.404	0.570
ST.DV.					0.1261			0.0914	0.8534	18.1		

KC-1-8	OBS	A	B	C	MAX.PROJ.SP.	B/A	C/B	SPHER.I.	FLAT.I.	AV.ABC	SL	LILS
	1	23.0	23.0	14.0	0.7185	1.000	0.609	0.8476	1.6429	20.0	0.609	0.0
	2	144.0	105.0	67.0	0.6674	0.729	0.638	0.6977	1.8582	105.3	0.465	0.506
	3	73.0	45.0	38.0	0.7606	0.616	0.844	0.6869	1.5526	52.0	0.521	0.800
	4	23.0	15.0	11.0	0.7055	0.652	0.733	0.6784	1.7273	16.3	0.478	0.667
	5	46.0	36.0	19.0	0.6021	0.783	0.528	0.6866	2.1579	33.7	0.413	0.370
	6	147.0	85.0	66.0	0.7040	0.578	0.776	0.6382	1.7576	99.3	0.449	0.765
	7	80.0	42.0	24.0	0.5558	0.525	0.571	0.5404	2.5417	48.7	0.300	0.679
	8	35.0	15.0	5.0	0.3628	0.429	0.333	0.3945	5.0000	18.3	0.143	0.667
	9	60.0	46.0	44.0	0.8886	0.767	0.957	0.8255	1.2045	50.0	0.733	0.875
	10	130.0	110.0	80.0	0.7651	0.846	0.727	0.8047	1.5000	106.7	0.615	0.400
	11	76.0	65.0	55.0	0.8493	0.855	0.846	0.8524	1.2818	65.3	0.724	0.524
	12	7.0	4.0	2.0	0.5231	0.571	0.500	0.5469	2.7500	4.3	0.286	0.600
	13	52.0	37.0	30.0	0.7765	0.712	0.811	0.7434	1.4833	39.7	0.577	0.682
	14	60.0	40.0	26.0	0.6558	0.667	0.650	0.6613	1.9231	42.0	0.433	0.588
	15	70.0	49.0	40.0	0.7757	0.700	0.816	0.7370	1.4875	53.0	0.571	0.700
	16	23.0	12.0	7.0	0.5624	0.522	0.583	0.5418	2.5000	14.0	0.304	0.688
	17	15.0	10.0	6.0	0.6217	0.667	0.600	0.6439	2.0833	10.3	0.400	0.556
	18	22.0	13.0	11.0	0.7509	0.591	0.846	0.6663	1.5909	15.3	0.500	0.818
	19	22.0	14.0	3.0	0.3084	0.636	0.214	0.4431	6.0000	13.0	0.136	0.421
	20	22.0	16.0	15.0	0.8615	0.727	0.938	0.7917	1.2667	17.7	0.682	0.857
	21	32.0	18.0	17.0	0.7948	0.563	0.944	0.6688	1.4706	22.3	0.531	0.933
	22	72.0	60.0	37.0	0.6820	0.833	0.617	0.7540	1.7838	56.3	0.514	0.343
	23	41.0	28.0	15.0	0.5812	0.683	0.536	0.6301	2.3000	28.0	0.366	0.500
	24	69.0	42.0	37.0	0.7790	0.609	0.881	0.6888	1.5000	49.3	0.536	0.844
	25	120.0	65.0	42.0	0.6096	0.542	0.646	0.5748	2.2024	75.7	0.350	0.705
	26	25.0	23.0	10.0	0.5535	0.920	0.435	0.7168	2.4000	19.3	0.400	0.133
	27	22.0	20.0	10.0	0.6106	0.909	0.500	0.7451	2.1000	17.3	0.455	0.167
	28	56.0	25.0	16.0	0.5679	0.446	0.640	0.5037	2.5313	32.3	0.286	0.775
	29	34.0	28.0	19.0	0.7240	0.824	0.679	0.7723	1.6316	27.0	0.559	0.400
	30	70.0	43.0	28.0	0.6389	0.614	0.651	0.6266	2.0179	47.0	0.400	0.643
	31	22.0	19.0	7.0	0.4898	0.864	0.368	0.6504	2.9286	16.0	0.318	0.200
	32	63.0	40.0	36.0	0.8014	0.635	0.900	0.7135	1.4306	46.3	0.571	0.852
	33	72.0	40.0	20.0	0.5182	0.556	0.500	0.5367	2.8000	44.0	0.278	0.615
	34	20.0	18.0	10.0	0.6528	0.900	0.556	0.7665	1.9000	16.0	0.500	0.200
	35	12.0	8.0	6.0	0.7214	0.667	0.750	0.6936	1.6667	8.7	0.500	0.667
	36	36.0	29.0	21.0	0.7505	0.806	0.724	0.7776	1.5476	28.7	0.583	0.467
	37	85.0	73.0	23.0	0.4405	0.859	0.315	0.6151	3.4348	60.3	0.271	0.194
	38	8.0	5.0	3.0	0.6085	0.625	0.600	0.6169	2.1667	5.3	0.375	0.600
	39	67.0	48.0	34.0	0.7113	0.716	0.708	0.7140	1.6912	49.7	0.507	0.576
	40	68.0	52.0	29.0	0.6199	0.765	0.558	0.6886	2.0690	49.7	0.426	0.410
	41	39.0	32.0	20.0	0.6846	0.821	0.625	0.7496	1.7750	30.3	0.513	0.368
	42	27.0	24.0	5.0	0.3383	0.889	0.208	0.5484	5.1000	18.7	0.185	0.136
	43	177.0	142.0	76.0	0.6128	0.802	0.535	0.7012	2.0987	131.7	0.429	0.347
	44	24.0	13.0	10.0	0.6846	0.542	0.769	0.6091	1.8500	15.7	0.417	0.786
	45	200.0	131.0	112.0	0.7825	0.655	0.855	0.7161	1.4777	147.7	0.560	0.784
	46	76.0	62.0	44.0	0.7436	0.816	0.710	0.7790	1.5682	60.7	0.579	0.438
	47	56.0	53.0	21.0	0.5300	0.946	0.396	0.7083	2.5952	43.3	0.375	0.086
	48	21.0	17.0	10.0	0.6546	0.810	0.588	0.7280	1.9000	16.0	0.476	0.364
	49	73.0	36.0	32.0	0.7306	0.493	0.889	0.6005	1.7031	47.0	0.438	0.902
	50	19.0	10.0	7.0	0.6368	0.526	0.700	0.5791	2.0714	12.0	0.368	0.750
COLUMN AVERAGE		56.7	39.7	26.4	0.6535	0.704	0.646	0.6720	2.1404	40.9	0.448	0.547
ST.DV.					0.1279			0.0994	0.9532	31.9		

KC-1-9	OBS	A	B	C	MAX.PROJ.SP.	B/A	C/B	SPHER.I.	FLAT.I.	AV.ABC	SL	LILS
	1	92.0	50.0	20.0	0.4434	0.543	0.400	0.4910	3.5500	54.0	0.217	0.583
	2	43.0	29.0	20.0	0.6848	0.674	0.690	0.6797	1.8000	30.7	0.465	0.609
	3	21.0	16.0	8.0	0.5757	0.762	0.500	0.6624	2.3125	15.0	0.381	0.385
	4	50.0	49.0	17.0	0.4908	0.980	0.347	0.6935	2.9118	38.7	0.340	0.030
	5	84.0	65.0	38.0	0.6422	0.774	0.585	0.7050	1.9605	62.3	0.452	0.413
	6	24.0	19.0	14.0	0.7549	0.792	0.737	0.7732	1.5357	19.0	0.583	0.500
	7	150.0	65.0	60.0	0.7176	0.433	0.923	0.5579	1.7917	91.7	0.400	0.944
	8	42.0	33.0	18.0	0.6163	0.786	0.545	0.6960	2.0833	31.0	0.429	0.375
	9	106.0	82.0	70.0	0.8262	0.774	0.854	0.7996	1.3429	86.0	0.660	0.667
	10	25.0	20.0	20.0	0.9284	0.800	1.000	0.8619	1.1250	21.7	0.800	1.000
	11	30.0	15.0	9.0	0.5649	0.500	0.600	0.5317	2.5000	18.0	0.300	0.714
	12	61.0	35.0	24.0	0.6464	0.574	0.686	0.6092	2.0000	40.0	0.393	0.703
	13	41.0	35.0	19.0	0.6316	0.854	0.543	0.7343	2.0000	31.7	0.463	0.273
	14	41.0	29.0	20.0	0.6957	0.707	0.690	0.7016	1.7500	30.0	0.488	0.571
	15	47.0	37.0	27.0	0.7486	0.787	0.730	0.7678	1.5556	37.0	0.574	0.500
	16	27.0	16.0	11.0	0.6546	0.593	0.688	0.6230	1.9545	18.0	0.407	0.688
	17	55.0	33.0	25.0	0.7012	0.600	0.758	0.6488	1.7600	37.7	0.455	0.733
	18	123.0	72.0	46.0	0.6208	0.585	0.639	0.6030	2.1196	80.3	0.374	0.662
	19	150.0	107.0	55.0	0.5737	0.713	0.514	0.6398	2.3364	104.0	0.367	0.453
	20	97.0	38.0	37.0	0.7191	0.392	0.974	0.5310	1.8243	57.3	0.381	0.983
	21	37.0	32.0	24.0	0.7867	0.865	0.750	0.8249	1.4375	31.0	0.649	0.385
	22	95.0	68.0	10.0	0.2496	0.716	0.147	0.4227	8.1500	57.7	0.105	0.318
	23	72.0	40.0	31.0	0.6939	0.556	0.775	0.6210	1.8065	47.7	0.431	0.780
	24	75.0	55.0	32.0	0.6288	0.733	0.582	0.6791	2.0313	54.0	0.427	0.465
	25	50.0	25.0	20.0	0.6843	0.500	0.800	0.5851	1.8750	31.7	0.400	0.833
	26	24.0	19.0	6.0	0.4294	0.792	0.316	0.5831	3.5833	16.3	0.250	0.278
	27	34.0	18.0	10.0	0.5470	0.529	0.556	0.5383	2.6000	20.7	0.294	0.667
	28	20.0	20.0	10.0	0.6303	1.000	0.500	0.7939	2.0000	16.7	0.500	0.0
	29	88.0	48.0	43.0	0.7595	0.545	0.896	0.6438	1.5814	59.7	0.489	0.889
	30	66.0	47.0	37.0	0.7616	0.712	0.787	0.7366	1.5270	50.0	0.561	0.655
	31	103.0	67.0	56.0	0.7690	0.650	0.836	0.7074	1.5179	75.3	0.544	0.766
	32	140.0	130.0	85.0	0.7352	0.929	0.654	0.8263	1.5882	118.3	0.607	0.182
	33	23.0	19.0	11.0	0.6521	0.826	0.579	0.7340	1.9091	17.7	0.478	0.333
	34	50.0	41.0	20.0	0.5803	0.820	0.488	0.6899	2.2750	37.0	0.400	0.300
	35	131.0	80.0	56.0	0.6691	0.611	0.700	0.6394	1.8839	89.0	0.427	0.680
	36	140.0	115.0	57.0	0.5869	0.821	0.496	0.6944	2.2368	104.0	0.407	0.301
	37	18.0	10.0	5.0	0.5182	0.556	0.500	0.5367	2.8000	11.0	0.278	0.615
	38	24.0	13.0	10.0	0.6846	0.542	0.769	0.6091	1.8500	15.7	0.417	0.786
	39	27.0	10.0	10.0	0.7184	0.370	1.000	0.5161	1.8500	15.7	0.370	1.000
	40	20.0	12.0	12.0	0.8436	0.600	1.000	0.7116	1.3333	14.7	0.600	1.000
	41	31.0	20.0	10.0	0.5447	0.645	0.500	0.5929	2.5500	20.3	0.323	0.524
	42	40.0	31.0	18.0	0.6396	0.775	0.581	0.7041	1.9722	29.7	0.450	0.409
	43	20.0	16.0	12.0	0.7665	0.800	0.750	0.7832	1.5000	16.0	0.600	0.500
	44	32.0	23.0	15.0	0.6739	0.719	0.652	0.6961	1.8333	23.3	0.469	0.529
	45	90.0	64.0	45.0	0.7060	0.711	0.703	0.7087	1.7111	66.3	0.500	0.578
	46	40.0	21.0	13.0	0.5863	0.525	0.619	0.5550	2.3462	24.7	0.325	0.704
	47	55.0	42.0	19.0	0.5390	0.764	0.452	0.6416	2.5526	38.7	0.345	0.361
	48	26.0	21.0	10.0	0.5682	0.808	0.476	0.6775	2.3500	19.0	0.385	0.313
	49	91.0	50.0	35.0	0.6460	0.549	0.700	0.5960	2.0143	58.7	0.385	0.732
	50	47.0	39.0	25.0	0.6989	0.830	0.641	0.7616	1.7200	37.0	0.532	0.364
COLUMN AVERAGE		60.4	40.8	26.1	0.6507	0.688	0.652	0.6624	2.1320	42.4	0.438	0.561
ST.DV.					0.1148			0.0950	1.0013	27.4		

KC-1-10	OBS	A	B	C	MAX.PROJ.SP.	B/A	C/B	SPHER.I.	FLAT.I.	AV.ABC	SL	LILS
	1	110.0	65.0	50.0	0.7047	0.591	0.769	0.6455	1.7500	75.0	0.455	0.750
	2	60.0	44.0	23.0	0.5855	0.733	0.523	0.6554	2.2609	42.3	0.383	0.432
	3	15.0	12.0	8.0	0.7087	0.800	0.667	0.7530	1.6875	11.7	0.533	0.429
	4	72.0	60.0	44.0	0.7655	0.833	0.733	0.7987	1.5000	58.7	0.611	0.429
	5	16.0	13.0	11.0	0.8349	0.813	0.846	0.8237	1.3182	13.3	0.688	0.600
	6	26.0	22.0	11.0	0.5961	0.846	0.500	0.7103	2.1818	19.7	0.423	0.267
	7	20.0	20.0	12.0	0.7116	1.000	0.600	0.8436	1.6667	17.3	0.600	0.0
	8	170.0	145.0	72.0	0.5950	0.853	0.497	0.7124	2.1875	129.0	0.424	0.255
	9	123.0	90.0	26.0	0.3942	0.732	0.289	0.5371	4.0962	79.7	0.211	0.340
	10	32.0	20.0	15.0	0.7060	0.625	0.750	0.6644	1.7333	22.3	0.469	0.706
	11	90.0	67.0	42.0	0.6641	0.744	0.627	0.7032	1.8690	66.3	0.467	0.479
	12	111.0	75.0	37.0	0.5482	0.676	0.493	0.6087	2.5135	74.3	0.333	0.486
	13	100.0	78.0	55.0	0.7295	0.780	0.705	0.7544	1.6182	77.7	0.550	0.489
	14	50.0	35.0	34.0	0.8710	0.700	0.971	0.7810	1.2500	39.7	0.680	0.938
	15	35.0	31.0	21.0	0.7410	0.886	0.677	0.8102	1.5714	29.0	0.600	0.286
	16	30.0	28.0	15.0	0.6449	0.933	0.536	0.7759	1.9333	24.3	0.500	0.133
	17	89.0	74.0	38.0	0.6033	0.831	0.514	0.7083	2.1447	67.0	0.427	0.294
	18	44.0	40.0	32.0	0.8350	0.909	0.800	0.8713	1.3125	38.7	0.727	0.333
	19	17.0	15.0	8.0	0.6311	0.882	0.533	0.7463	2.0000	13.3	0.471	0.222
	20	110.0	65.0	45.0	0.6570	0.591	0.692	0.6232	1.9444	73.3	0.409	0.692
	21	22.0	10.0	8.0	0.6629	0.455	0.800	0.5491	2.0000	13.3	0.364	0.857
	22	82.0	55.0	25.0	0.5178	0.671	0.455	0.5895	2.7400	54.0	0.305	0.474
	23	27.0	20.0	13.0	0.6792	0.741	0.650	0.7094	1.8077	20.0	0.481	0.500
	24	65.0	45.0	35.0	0.7484	0.692	0.778	0.7199	1.5714	48.3	0.538	0.667
	25	67.0	33.0	25.0	0.6566	0.493	0.758	0.5689	2.0000	41.7	0.373	0.810
	26	57.0	47.0	29.0	0.6799	0.825	0.617	0.7488	1.7931	44.3	0.509	0.357
	27	12.0	9.0	4.0	0.5295	0.750	0.444	0.6303	2.6250	8.3	0.333	0.375
	28	22.0	15.0	11.0	0.7160	0.682	0.733	0.6988	1.6818	16.0	0.500	0.636
	29	54.0	41.0	18.0	0.5273	0.759	0.439	0.6328	2.6389	37.7	0.333	0.361
	30	56.0	30.0	20.0	0.6201	0.536	0.667	0.5765	2.1500	35.3	0.357	0.722
	31	38.0	25.0	8.0	0.4073	0.658	0.320	0.5177	3.9375	23.7	0.211	0.433
	32	72.0	43.0	29.0	0.6479	0.597	0.674	0.6222	1.9828	48.0	0.403	0.674
	33	45.0	25.0	13.0	0.5319	0.556	0.520	0.5438	2.6923	27.7	0.289	0.625
	34	76.0	44.0	23.0	0.5412	0.579	0.523	0.5599	2.6087	47.7	0.303	0.604
	35	76.0	54.0	32.0	0.6298	0.711	0.593	0.6691	2.0313	54.0	0.421	0.500
	36	190.0	98.0	77.0	0.6831	0.516	0.786	0.5938	1.8701	121.7	0.405	0.814
	37	19.0	13.0	10.0	0.7400	0.684	0.769	0.7117	1.6000	14.0	0.526	0.667
	38	81.0	70.0	36.0	0.6117	0.864	0.514	0.7271	2.0972	62.3	0.444	0.244
	39	210.0	120.0	85.0	0.6597	0.571	0.708	0.6141	1.9412	138.3	0.405	0.720
	40	52.0	40.0	20.0	0.5775	0.769	0.500	0.6666	2.3000	37.3	0.385	0.375
	41	83.0	80.0	55.0	0.7697	0.964	0.688	0.8613	1.4818	72.7	0.663	0.107
	42	53.0	42.0	18.0	0.5264	0.792	0.429	0.6459	2.6389	37.7	0.340	0.314
	43	218.0	148.0	115.0	0.7431	0.679	0.777	0.7104	1.5913	160.3	0.528	0.680
	44	94.0	69.0	35.0	0.5741	0.734	0.507	0.6492	2.3286	66.0	0.372	0.424
	45	38.0	26.0	15.0	0.6110	0.684	0.577	0.6467	2.1333	26.3	0.395	0.522
	46	63.0	40.0	36.0	0.8014	0.635	0.900	0.7135	1.4306	46.3	0.571	0.852
	47	56.0	28.0	24.0	0.7164	0.500	0.857	0.5987	1.7500	36.0	0.429	0.875
	48	195.0	120.0	75.0	0.6221	0.615	0.625	0.6189	2.1000	130.0	0.385	0.625
	49	92.0	67.0	34.0	0.5727	0.728	0.507	0.6459	2.3382	64.3	0.370	0.431
	50	28.0	15.0	13.0	0.7385	0.536	0.867	0.6292	1.6538	18.7	0.464	0.867
COLUMN AVERAGE		71.3	49.4	30.8	0.6514	0.715	0.634	0.6779	2.0411	50.5	0.447	0.513
ST.DV.					0.1010			0.0874	0.5605	35.4		

KC-1-11	OBS	A	B	C	MAX.PROJ.SP.	B/A	C/B	SPHER.I.	FLAT.I.	AV.ABC	SL	LILS
	1	23.0	11.0	5.0	0.4627	0.478	0.455	0.4706	3.4000	13.0	0.217	0.667
	2	59.0	44.0	40.0	0.8512	0.746	0.909	0.7968	1.2875	47.7	0.678	0.789
	3	20.0	15.0	10.0	0.6936	0.750	0.667	0.7214	1.7500	15.0	0.500	0.500
	4	110.0	90.0	42.0	0.5630	0.818	0.467	0.6788	2.3810	80.7	0.382	0.294
	5	32.0	25.0	21.0	0.8201	0.781	0.840	0.8005	1.3571	26.0	0.656	0.636
	6	42.0	26.0	15.0	0.5909	0.619	0.577	0.6050	2.2667	27.7	0.357	0.593
	7	75.0	56.0	45.0	0.7843	0.747	0.804	0.7654	1.4556	58.7	0.600	0.633
	8	80.0	54.0	24.0	0.5112	0.675	0.444	0.5875	2.7917	52.7	0.300	0.464
	9	26.0	14.0	12.0	0.7343	0.538	0.857	0.6290	1.6667	17.3	0.462	0.857
	10	50.0	37.0	28.0	0.7513	0.740	0.757	0.7458	1.5536	38.3	0.560	0.591
	11	37.0	25.0	20.0	0.7564	0.676	0.800	0.7150	1.5500	27.3	0.541	0.706
	12	97.0	43.0	40.0	0.7268	0.443	0.930	0.5679	1.7500	60.0	0.412	0.947
	13	43.0	23.0	12.0	0.5264	0.535	0.522	0.5308	2.7500	26.0	0.279	0.645
	14	12.0	7.0	6.0	0.7542	0.583	0.857	0.6634	1.5833	8.3	0.500	0.833
	15	137.0	101.0	47.0	0.5428	0.737	0.465	0.6327	2.5319	95.0	0.343	0.400
	16	93.0	56.0	25.0	0.4936	0.602	0.446	0.5453	2.9800	58.0	0.269	0.544
	17	41.0	13.0	10.0	0.5728	0.317	0.769	0.4264	2.7000	21.3	0.244	0.903
	18	30.0	22.0	13.0	0.6353	0.733	0.591	0.6827	2.0000	21.7	0.433	0.471
	19	34.0	24.0	15.0	0.6512	0.706	0.625	0.6781	1.9333	24.3	0.441	0.526
	20	37.0	24.0	6.0	0.3439	0.649	0.250	0.4724	5.0833	22.3	0.162	0.419
	21	34.0	27.0	17.0	0.6805	0.794	0.630	0.7352	1.7941	26.0	0.500	0.412
	22	25.0	14.0	12.0	0.7440	0.560	0.857	0.6457	1.6250	17.0	0.480	0.846
	23	23.0	22.0	10.0	0.5828	0.957	0.455	0.7466	2.2500	18.3	0.435	0.077
	24	38.0	26.0	16.0	0.6378	0.684	0.615	0.6607	2.0000	26.7	0.421	0.545
	25	43.0	20.0	20.0	0.7750	0.465	1.000	0.6006	1.5750	27.7	0.465	1.000
	26	170.0	78.0	75.0	0.7516	0.459	0.962	0.5875	1.6533	107.7	0.441	0.968
	27	21.0	12.0	8.0	0.6336	0.571	0.667	0.6019	2.0625	13.7	0.381	0.692
	28	50.0	32.0	24.0	0.7116	0.640	0.750	0.6750	1.7083	35.3	0.480	0.692
	29	91.0	80.0	72.0	0.8931	0.879	0.900	0.8861	1.1875	81.0	0.791	0.579
	30	107.0	83.0	35.0	0.5170	0.776	0.422	0.6334	2.7143	75.0	0.327	0.333
	31	270.0	265.0	200.0	0.9240	0.981	0.755	0.8993	1.3375	245.0	0.741	0.071
	32	45.0	20.0	12.0	0.5432	0.444	0.600	0.4916	2.7083	25.7	0.267	0.758
	33	15.0	13.0	5.0	0.5046	0.867	0.385	0.6613	2.8000	11.0	0.333	0.200
	34	26.0	20.0	5.0	0.3640	0.769	0.250	0.5292	4.6000	17.0	0.192	0.286
	35	42.0	21.0	12.0	0.5469	0.500	0.571	0.5231	2.6250	25.0	0.286	0.700
	36	94.0	63.0	33.0	0.5690	0.670	0.524	0.6177	2.3788	63.3	0.351	0.508
	37	36.0	22.0	15.0	0.6577	0.611	0.682	0.6341	1.9333	24.3	0.417	0.667
	38	26.0	20.0	9.0	0.5384	0.769	0.450	0.6436	2.5556	18.3	0.346	0.353
	39	160.0	107.0	56.0	0.5682	0.669	0.523	0.6166	2.3839	107.7	0.350	0.510
	40	120.0	72.0	42.0	0.5891	0.600	0.583	0.5947	2.2857	78.0	0.350	0.615
	41	24.0	11.0	6.0	0.5151	0.458	0.545	0.4861	2.9167	13.7	0.250	0.722
	42	20.0	14.0	7.0	0.5597	0.700	0.500	0.6260	2.4286	13.7	0.350	0.462
	43	32.0	16.0	9.0	0.5412	0.500	0.563	0.5204	2.6667	19.0	0.281	0.696
	44	60.0	42.0	20.0	0.5418	0.700	0.476	0.6159	2.5500	40.7	0.333	0.450
	45	55.0	44.0	23.0	0.6027	0.800	0.523	0.6945	2.1522	40.7	0.418	0.344
	46	137.0	88.0	63.0	0.6907	0.642	0.716	0.6663	1.7857	96.0	0.460	0.662
	47	20.0	10.0	10.0	0.7939	0.500	1.000	0.6303	1.5000	13.3	0.500	1.000
	48	60.0	21.0	13.0	0.5122	0.350	0.619	0.4236	3.1154	31.3	0.217	0.830
	49	195.0	152.0	82.0	0.6102	0.779	0.539	0.6897	2.1159	143.0	0.421	0.381
	50	73.0	48.0	25.0	0.5632	0.658	0.521	0.6087	2.4200	48.7	0.342	0.521
COLUMN AVERAGE		63.8	43.5	27.4	0.6266	0.653	0.632	0.6332	2.2520	44.9	0.405	0.586
ST.DV.					0.1223			0.1036	0.7588	42.1		

KC-1-12	OBS	A	B	C	MAX.PROJ.SP.	B/A	C/B	SPHER.I.	FLAT.I.	AV.ABC	SL	LILS
	1	36.0	35.0	25.0	0.7918	0.972	0.714	0.8774	1.4200	32.0	0.694	0.091
	2	94.0	56.0	27.0	0.5177	0.596	0.482	0.5555	2.7778	59.0	0.287	0.567
	3	88.0	49.0	32.0	0.6196	0.557	0.653	0.5875	2.1406	56.3	0.364	0.696
	4	70.0	61.0	30.0	0.5954	0.871	0.492	0.7204	2.1833	53.7	0.429	0.225
	5	40.0	30.0	12.0	0.4936	0.750	0.400	0.6085	2.9167	27.3	0.300	0.357
	6	143.0	78.0	50.0	0.6077	0.545	0.641	0.5759	2.2100	90.3	0.350	0.699
	7	208.0	148.0	98.0	0.6785	0.712	0.662	0.6949	1.8163	151.3	0.471	0.545
	8	22.0	11.0	7.0	0.5875	0.500	0.636	0.5422	2.3571	13.3	0.318	0.733
	9	83.0	56.0	40.0	0.7011	0.675	0.714	0.6879	1.7375	59.7	0.482	0.628
	10	45.0	33.0	26.0	0.7695	0.733	0.788	0.7513	1.5000	34.7	0.578	0.632
	11	45.0	31.0	24.0	0.7449	0.689	0.774	0.7165	1.5833	33.3	0.533	0.667
	12	350.0	230.0	110.0	0.5320	0.657	0.478	0.5914	2.6364	230.0	0.314	0.500
	13	62.0	62.0	55.0	0.9233	1.000	0.887	0.9609	1.1273	59.7	0.887	0.0
	14	201.0	159.0	150.0	0.8897	0.791	0.943	0.8390	1.2000	170.0	0.746	0.824
	15	57.0	40.0	33.0	0.7819	0.702	0.825	0.7409	1.4697	43.3	0.579	0.708
	16	22.0	13.0	6.0	0.5015	0.591	0.462	0.5445	2.9167	13.7	0.273	0.563
	17	48.0	28.0	24.0	0.7542	0.583	0.857	0.6634	1.5833	33.3	0.500	0.833
	18	20.0	10.0	8.0	0.6843	0.500	0.800	0.5851	1.8750	12.7	0.400	0.833
	19	20.0	15.0	5.0	0.4372	0.750	0.333	0.5727	3.5000	13.3	0.250	0.333
	20	32.0	17.0	11.0	0.6062	0.531	0.647	0.5677	2.2273	20.0	0.344	0.714
	21	33.0	17.0	10.0	0.5631	0.515	0.588	0.5388	2.5000	20.0	0.303	0.696
	22	139.0	103.0	37.0	0.4576	0.741	0.359	0.5824	3.2703	93.0	0.266	0.353
	23	30.0	15.0	7.0	0.4779	0.500	0.467	0.4890	3.2143	17.3	0.233	0.652
	24	50.0	30.0	23.0	0.7068	0.600	0.767	0.6514	1.7391	34.3	0.460	0.741
	25	23.0	16.0	10.0	0.6480	0.696	0.625	0.6715	1.9500	16.3	0.435	0.538
	26	19.0	13.0	4.0	0.4020	0.684	0.308	0.5245	4.0000	12.0	0.211	0.400
	27	27.0	16.0	9.0	0.5727	0.593	0.563	0.5827	2.3889	17.3	0.333	0.611
	28	10.0	10.0	4.0	0.5432	1.000	0.400	0.7370	2.5000	8.0	0.400	0.0
	29	83.0	47.0	22.0	0.4991	0.566	0.468	0.5318	2.9545	50.7	0.265	0.590
	30	20.0	16.0	8.0	0.5851	0.800	0.500	0.6843	2.2500	14.7	0.400	0.333
	31	61.0	43.0	40.0	0.8482	0.705	0.930	0.7734	1.3000	48.0	0.656	0.857
	32	155.0	105.0	82.0	0.7450	0.677	0.781	0.7106	1.5854	114.0	0.529	0.685
	33	90.0	80.0	35.0	0.5544	0.889	0.438	0.7021	2.4286	68.3	0.399	0.182
	34	30.0	16.0	10.0	0.5931	0.533	0.625	0.5626	2.3000	18.7	0.333	0.700
	35	60.0	49.0	33.0	0.7184	0.817	0.673	0.7660	1.6515	47.3	0.550	0.407
	36	72.0	50.0	15.0	0.3972	0.694	0.300	0.5253	4.0667	45.7	0.208	0.386
	37	54.0	40.0	35.0	0.8279	0.741	0.875	0.7832	1.3429	43.0	0.648	0.737
	38	60.0	32.0	30.0	0.7770	0.533	0.938	0.6439	1.5333	40.7	0.500	0.933
	39	47.0	22.0	12.0	0.5187	0.468	0.545	0.4929	2.8750	27.0	0.255	0.714
	40	88.0	69.0	20.0	0.4042	0.784	0.290	0.5631	3.9250	59.0	0.227	0.279
	41	38.0	27.0	25.0	0.8478	0.711	0.926	0.7763	1.3000	30.0	0.658	0.846
	42	236.0	165.0	48.0	0.3900	0.699	0.291	0.5223	4.1771	149.7	0.203	0.378
	43	78.0	56.0	35.0	0.6548	0.718	0.625	0.6858	1.9143	56.3	0.449	0.512
	44	25.0	20.0	7.0	0.4614	0.800	0.350	0.6076	3.2143	17.3	0.280	0.278
	45	74.0	46.0	41.0	0.7906	0.622	0.891	0.7012	1.4634	53.7	0.554	0.848
	46	27.0	11.0	6.0	0.4952	0.407	0.545	0.4494	3.1667	14.7	0.222	0.762
	47	16.0	15.0	6.0	0.5317	0.938	0.400	0.7060	2.5833	12.3	0.375	0.100
	48	42.0	28.0	9.0	0.4103	0.667	0.321	0.5231	3.8889	26.3	0.214	0.424
	49	25.0	21.0	10.0	0.5757	0.840	0.476	0.6955	2.3000	18.7	0.400	0.267
	50	50.0	22.0	12.0	0.5081	0.440	0.545	0.4730	3.0000	28.0	0.240	0.737
COLUMN AVERAGE		69.0	47.2	28.4	0.6145	0.682	0.600	0.6408	2.3592	48.2	0.406	0.542
ST.DV.					0.1429			0.1107	0.8341	45.1		

KC-1-13	OBS	A	B	C	MAX.PROJ.SP.	B/A	C/B	SPHER.I.	FLAT.I.	AV.ABC	SL	LILS
	1	52.0	32.0	25.0	0.7217	0.615	0.781	0.6666	1.6800	36.3	0.481	0.741
	2	155.0	135.0	105.0	0.8078	0.871	0.778	0.8389	1.3810	131.7	0.677	0.400
	3	18.0	13.0	9.0	0.7024	0.722	0.692	0.7124	1.7222	13.3	0.500	0.556
	4	17.0	13.0	4.0	0.4171	0.765	0.308	0.5649	3.7500	11.3	0.235	0.308
	5	112.0	82.0	39.0	0.5495	0.732	0.476	0.6344	2.4872	77.7	0.348	0.411
	6	28.0	22.0	10.0	0.5458	0.786	0.455	0.6550	2.5000	20.0	0.357	0.333
	7	42.0	25.0	14.0	0.5718	0.595	0.560	0.5836	2.3929	27.0	0.333	0.607
	8	330.0	260.0	150.0	0.6404	0.788	0.577	0.7104	1.9667	246.7	0.455	0.389
	9	67.0	54.0	11.0	0.3226	0.806	0.204	0.5099	5.5000	44.0	0.164	0.232
	10	56.0	45.0	15.0	0.4473	0.804	0.333	0.5996	3.3667	38.7	0.268	0.268
	11	71.0	35.0	18.0	0.5074	0.493	0.514	0.5003	2.9444	41.3	0.254	0.679
	12	95.0	65.0	25.0	0.4664	0.684	0.385	0.5650	3.2000	61.7	0.263	0.429
	13	101.0	61.0	35.0	0.5840	0.604	0.574	0.5940	2.3143	65.7	0.347	0.606
	14	90.0	78.0	24.0	0.4349	0.867	0.308	0.6140	3.5000	64.0	0.267	C.182
	15	51.0	47.0	27.0	0.6728	0.922	0.574	0.7874	1.8148	41.7	0.529	0.167
	16	40.0	30.0	12.0	0.4936	0.750	0.400	0.6085	2.9167	27.3	0.300	0.357
	17	64.0	60.0	16.0	0.4058	0.938	0.267	0.6169	3.8750	46.7	0.250	0.083
	18	22.0	17.0	11.0	0.6868	0.773	0.647	0.7286	1.7727	16.7	0.500	0.455
	19	50.0	30.0	27.0	0.7864	0.600	0.900	0.6871	1.4815	35.7	0.540	0.870
	20	67.0	31.0	28.0	0.7229	0.463	0.903	0.5786	1.7500	42.0	0.418	0.923
	21	74.0	41.0	33.0	0.7109	0.554	0.805	0.6278	1.7424	49.3	0.446	0.805
	22	29.0	20.0	11.0	0.5934	0.690	0.550	0.6398	2.2273	20.0	0.379	0.500
	23	33.0	22.0	17.0	0.7358	0.667	0.773	0.7005	1.6176	24.0	0.515	0.688
	24	26.0	17.0	7.0	0.4807	0.654	0.412	0.5608	3.0714	16.7	0.269	0.474
	25	31.0	20.0	11.0	0.5804	0.645	0.550	0.6120	2.3182	20.7	0.355	0.550
	26	27.0	20.0	7.0	0.4497	0.741	0.350	0.5773	3.3571	18.0	0.259	0.350
	27	43.0	30.0	22.0	0.7215	0.695	0.733	0.7096	1.6591	31.7	0.512	0.619
	28	34.0	28.0	16.0	0.6457	0.824	0.571	0.7293	1.9375	26.0	0.471	0.333
	29	16.0	13.0	5.0	0.4939	0.813	0.385	0.6335	2.9000	11.3	0.313	0.273
	30	20.0	13.0	10.0	0.7275	0.650	0.769	0.6878	1.6500	14.3	0.500	0.700
	31	53.0	40.0	5.0	0.2280	0.755	0.125	0.4148	9.3000	32.7	0.094	0.271
	32	42.0	21.0	14.0	0.6060	0.500	0.667	0.5507	2.2500	25.7	0.333	0.750
	33	37.0	32.0	18.0	0.6495	0.865	0.563	0.7495	1.9167	29.0	0.486	0.263
	34	137.0	104.0	55.0	0.5969	0.759	0.529	0.6732	2.1909	98.7	0.401	0.402
	35	95.0	75.0	61.0	0.8055	0.789	0.813	0.7975	1.3934	77.0	0.642	0.588
	36	160.0	138.0	67.0	0.5883	0.862	0.486	0.7124	2.2239	121.7	0.419	0.237
	37	19.0	14.0	10.0	0.7220	0.737	0.714	0.7295	1.6500	14.3	0.526	0.556
	38	20.0	11.0	7.0	0.6065	0.550	0.636	0.5777	2.2143	12.7	0.350	0.692
	39	55.0	30.0	14.0	0.4919	0.545	0.467	0.5182	3.0357	33.0	0.255	0.610
	40	15.0	10.0	10.0	0.8737	0.667	1.000	0.7633	1.2500	11.7	0.667	1.000
	41	46.0	38.0	29.0	0.7838	0.826	0.763	0.8047	1.4483	37.7	0.630	0.471
	42	37.0	27.0	21.0	0.7616	0.730	0.778	0.7456	1.5238	28.3	0.568	0.625
	43	28.0	21.0	7.0	0.4372	0.750	0.333	0.5727	3.5000	18.7	0.250	0.333
	44	15.0	14.0	5.0	0.4923	0.933	0.357	0.6779	2.9000	11.3	0.333	0.100
	45	53.0	43.0	19.0	0.5414	0.811	0.442	0.6628	2.5263	38.3	0.358	0.294
	46	43.0	27.0	9.0	0.4120	0.628	0.333	0.5088	3.8889	26.3	0.209	0.471
	47	102.0	37.0	10.0	0.2985	0.363	0.270	0.3292	6.9500	49.7	0.098	0.707
	48	23.0	14.0	5.0	0.4270	'0.609	0.357	0.5099	3.7000	14.0	0.217	0.500
	49	50.0	36.0	20.0	0.6060	0.720	0.556	0.6607	2.1500	35.3	0.400	0.467
	50	84.0	47.0	31.0	0.6247	0.560	0.660	0.5914	2.1129	54.0	0.369	0.698
COLUMN AVERAGE		59.5	42.8	23.2	0.5836	0.709	0.548	0.6357	2.6584	41.8	0.382	0.486
ST.DV.					0.1441			0.1004	1.4361	39.8		

KC-14 OBS	A	B	C	MAX.PROJ.SP.	B/A	C/B	SPHER.I.	FLAT.I.	AV.ABC	SL	LILS
1	48.0	30.0	12.0	0.4645	0.625	0.400	0.5389	3.2500	30.0	0.250	0.500
2	40.0	31.0	17.0	0.6157	0.775	0.548	0.6909	2.0882	29.3	0.425	0.391
3	27.0	16.0	7.0	0.4844	0.593	0.438	0.5359	3.0714	16.7	0.259	0.550
4	110.0	68.0	51.0	0.7034	0.618	0.750	0.6596	1.7451	76.3	0.464	0.712
5	7.0	5.0	2.0	0.4856	0.714	0.400	0.5891	3.0000	4.7	0.286	0.400
6	41.0	23.0	12.0	0.5348	0.561	0.522	0.5479	2.6667	25.3	0.293	0.621
7	20.0	9.0	3.0	0.3688	0.450	0.333	0.4075	4.8333	10.7	0.150	0.647
8	47.0	30.0	24.0	0.7422	0.638	0.800	0.6885	1.6042	33.7	0.511	0.739
9	60.0	36.0	27.0	0.6965	0.600	0.750	0.6466	1.7778	41.0	0.450	0.727
10	70.0	64.0	27.0	0.5463	0.914	0.422	0.7068	2.4815	53.7	0.386	0.140
11	55.0	41.0	22.0	0.5990	0.745	0.537	0.6683	2.1818	39.3	0.400	0.424
12	33.0	21.0	20.0	0.8328	0.636	0.952	0.7281	1.3500	24.7	0.606	0.923
13	9.0	8.0	5.0	0.7031	0.889	0.625	0.7906	1.7000	7.3	0.556	0.250
14	13.0	10.0	8.0	0.7898	0.769	0.800	0.7795	1.4375	10.3	0.615	0.600
15	15.0	12.0	6.0	0.5851	0.800	0.500	0.6843	2.2500	11.0	0.400	0.333
16	14.0	11.0	5.0	0.5458	0.786	0.455	0.6550	2.5000	10.0	0.357	0.333
17	17.0	13.0	10.0	0.7679	0.765	0.769	0.7664	1.5000	13.3	0.588	0.571
18	10.0	10.0	5.0	0.6303	1.000	0.500	0.7939	2.0000	8.3	0.500	0.0
19	45.0	32.0	8.0	0.3546	0.711	0.250	0.5022	4.8125	28.3	0.178	0.351
20	24.0	22.0	12.0	0.6488	0.917	0.545	0.7712	1.9167	19.3	0.500	0.167
21	6.0	4.0	2.0	0.5507	0.667	0.500	0.6060	2.5000	4.0	0.333	0.500
22	5.0	3.0	3.0	0.8436	0.600	1.000	0.7116	1.3333	3.7	0.600	1.000
23	12.0	6.0	5.0	0.7031	0.500	0.833	0.5931	1.8000	7.7	0.417	0.857
24	66.0	46.0	20.0	0.5092	0.697	0.435	0.5958	2.8000	44.0	0.303	0.435
25	27.0	13.0	13.0	[illegible]	0.481	1.000	0.6146	1.5385	17.7	0.481	1.000
26	23.0	17.0	3.0	0.2848	0.739	0.176	0.4589	6.6667	14.3	0.130	0.300
27	27.0	22.0	12.0	0.6238	0.815	0.545	0.7130	2.0417	20.3	0.444	0.333
28	63.0	52.0	30.0	0.6504	0.825	0.577	0.7327	1.9167	48.3	0.476	0.333
29	14.0	7.0	5.0	0.6345	0.500	0.714	0.5634	2.1000	8.7	0.357	0.778
30	37.0	33.0	14.0	0.5438	0.892	0.424	0.6965	2.5000	28.0	0.378	0.174
31	13.0	7.0	6.0	0.7343	0.538	0.857	0.6290	1.6667	8.7	0.462	0.857
32	62.0	47.0	16.0	0.4449	0.758	0.340	0.5808	3.4063	41.7	0.258	0.326
33	26.0	23.0	21.0	[illegible]	0.885	0.913	0.8941	1.1667	23.3	0.808	0.600
34	16.0	15.0	9.0	0.6965	0.938	0.600	0.8081	1.7222	13.3	0.563	0.143
35	22.0	16.0	3.0	0.2950	0.727	0.188	0.4632	6.3333	13.7	0.136	0.316
36	63.0	41.0	13.0	0.4033	0.651	0.317	0.5124	4.0000	39.0	0.206	0.440
37	17.0	15.0	13.0	0.8720	0.882	0.867	0.8772	1.2308	15.0	0.765	0.500
38	86.0	58.0	49.0	0.7839	0.674	0.845	0.7272	1.4694	64.3	0.570	0.757
39	34.0	21.0	14.0	0.6502	0.618	0.667	0.6339	1.9643	23.0	0.412	0.650
40	91.0	66.0	44.0	0.6859	0.725	0.667	0.7054	1.7841	67.0	0.484	0.532
41	20.0	16.0	7.0	0.5353	0.800	0.438	0.6545	2.5714	14.3	0.350	0.308
42	22.0	10.0	9.0	0.7170	0.455	0.900	0.5711	1.7778	13.7	0.409	[illegible]
43	34.0	20.0	10.0	0.5282	0.588	0.500	0.5575	2.7000	21.3	0.294	0.583
44	17.0	9.0	3.0	0.3893	0.529	0.333	0.4541	4.3333	9.7	0.176	0.571
45	17.0	10.0	5.0	0.5282	0.588	0.500	0.5575	2.7000	10.7	0.294	0.583
46	40.0	29.0	13.0	0.5265	0.725	0.448	0.6179	2.6538	27.3	0.325	0.407
47	58.0	28.0	13.0	0.4707	0.483	0.464	0.4769	3.3077	33.0	0.224	0.667
48	49.0	28.0	24.0	0.7490	0.571	0.857	0.6544	1.6042	33.7	0.490	0.840
49	31.0	20.0	12.0	0.6150	0.645	0.600	0.6300	2.1250	21.0	0.387	0.579
50	24.0	11.0	4.0	0.3932	0.458	0.364	0.4247	4.3750	13.0	0.167	0.650
COLUMN AVERAGE	34.5	23.7	13.6	0.6030	0.689	0.583	0.6373	2.5251	23.9	0.337	0.526
ST.DV.				0.1509			0.1134	1.2222	16.9		

KC-15	OBS	A	B	C	MAX.PROJ.SP.	B/A	C/B	SPHER.I.	FLAT.I.	AV.ABC	SL	ILS
	1	104.0	65.0	51.0	0.7276	0.625	0.785	0.6745	1.6569	73.3	0.490	0.736
	2	11.0	9.0	7.0	0.7912	0.818	0.778	0.8047	1.4286	9.0	0.636	0.500
	3	131.0	85.0	61.0	0.6942	0.649	0.718	0.6713	1.7705	92.3	0.466	0.657
	4	20.0	11.0	7.0	0.6085	0.550	0.636	0.5777	2.2148	12.7	0.350	0.692
	5	11.0	6.0	4.0	0.6238	0.545	0.667	0.5835	2.1250	7.0	0.364	0.714
	6	90.0	58.0	55.0	0.8339	0.644	0.948	0.7332	1.3455	67.7	0.611	0.914
	7	48.0	41.0	36.0	0.8701	0.854	0.878	0.8622	1.2361	41.7	0.750	0.583
	8	106.0	87.0	75.0	0.8482	0.821	0.862	0.8345	1.2867	89.3	0.708	0.613
	9	86.0	74.0	33.0	0.5555	0.860	0.446	0.6014	2.4242	64.3	0.384	0.226
	10	52.0	31.0	25.0	0.7294	0.596	0.806	0.6596	1.6600	36.0	0.481	0.778
	11	48.0	39.0	19.0	0.5781	0.813	0.487	0.6854	2.2895	35.3	0.396	0.310
	12	163.0	127.0	91.0	0.7370	0.779	0.717	0.7579	1.5934	127.0	0.558	0.500
	13	14.0	13.0	6.0	0.5830	0.929	0.462	0.7358	2.2500	11.0	0.429	0.125
	14	23.0	17.0	10.0	0.6350	0.739	0.588	0.6852	2.0000	16.7	0.435	0.462
	15	32.0	20.0	20.0	0.8551	0.625	1.000	0.7312	1.3000	24.0	0.625	1.000
	16	45.0	25.0	17.0	0.6360	0.556	0.680	0.5946	2.0588	29.0	0.378	0.714
	17	17.0	10.0	3.0	0.3759	0.588	0.300	0.4703	4.5000	10.0	0.176	0.500
	18	55.0	31.0	21.0	0.6374	0.564	0.677	0.5996	2.0476	35.7	0.382	0.706
	19	37.0	26.0	20.0	0.7466	0.703	0.769	0.7244	1.5750	27.7	0.541	0.647
	20	28.0	20.0	8.0	0.4856	0.714	0.400	0.5891	3.0000	18.7	0.286	0.400
	21	61.0	58.0	37.0	0.7289	0.951	0.638	0.8325	1.6081	52.0	0.607	0.125
	22	21.0	15.0	6.0	0.4856	0.714	0.400	0.5891	3.0000	14.0	0.286	0.400
	23	112.0	84.0	24.0	0.3945	0.750	0.286	0.5440	4.0833	73.3	0.214	0.318
	24	31.0	25.0	13.0	0.6022	0.806	0.520	0.6970	2.1538	23.0	0.419	0.333
	25	44.0	30.0	27.0	0.8206	0.682	0.900	0.7481	1.3704	33.7	0.614	0.824
	26	100.0	62.0	44.0	0.6787	0.620	0.710	0.6488	1.8409	68.7	0.440	0.679
	27	40.0	37.0	20.0	0.6468	0.925	0.541	0.7735	1.9250	32.3	0.500	0.150
	28	126.0	82.0	55.0	0.6443	0.651	0.671	0.6576	1.8909	87.7	0.437	0.620
	29	120.0	82.0	73.0	0.8153	0.683	0.890	0.7465	1.3836	91.7	0.608	0.809
	30	17.0	12.0	10.0	0.7887	0.706	0.833	0.7463	1.4500	13.0	0.588	0.714
	31	36.0	23.0	16.0	0.6765	0.639	0.696	0.6576	1.8438	25.0	0.444	0.650
	32	6.0	5.0	3.0	0.4497	0.833	0.600	0.7471	1.8333	4.7	0.500	0.333
	33	28.0	20.0	20.0	0.8960	0.714	1.000	0.7992	1.2000	22.7	0.714	1.000
	34	12.0	7.0	5.0	0.6679	0.583	0.714	0.6244	1.9000	8.0	0.417	0.714
	35	47.0	34.0	20.0	0.6305	0.723	0.588	0.6755	2.0250	33.7	0.426	0.481
	36	36.0	32.0	28.0	0.8797	0.889	0.875	0.8843	1.2143	32.0	0.778	0.500
	37	16.0	10.0	6.0	0.6085	0.625	0.600	0.6169	2.1667	10.7	0.375	0.600
	38	125.0	115.0	57.0	0.6094	0.920	0.496	0.7488	2.1053	99.0	0.456	0.147
	39	180.0	86.0	43.0	0.4928	0.478	0.500	0.4854	3.0930	103.0	0.239	0.686
	40	34.0	24.0	18.0	0.7352	0.706	0.750	0.7205	1.6111	25.3	0.529	0.625
	41	100.0	84.0	45.0	0.6227	0.840	0.536	0.7233	2.0444	76.3	0.450	0.291
	42	8.0	5.0	3.0	0.6085	0.625	0.600	0.6169	2.1667	5.3	0.375	0.600
	43	55.0	38.0	23.0	0.6329	0.691	0.605	0.6614	2.0217	38.7	0.418	0.531
	44	135.0	103.0	59.0	0.6305	0.763	0.573	0.6937	2.0169	99.0	0.437	0.421
	45	93.0	79.0	73.0	0.8986	0.849	0.924	0.8737	1.1781	81.7	0.785	0.700
	46	60.0	43.0	26.0	0.6402	0.717	0.605	0.6775	1.9808	43.0	0.433	0.500
	47	113.0	77.0	57.0	0.7203	0.681	0.740	0.7007	1.6667	82.3	0.504	0.643
	48	36.0	21.0	18.0	0.7542	0.583	0.857	0.6634	1.5833	25.0	0.500	0.833
	49	25.0	17.0	6.0	0.4395	0.680	0.353	0.5468	3.5000	16.0	0.240	0.421
	50	85.0	70.0	41.0	0.6564	0.824	0.586	0.7353	1.8902	65.3	0.482	0.341
COLUMN AVERAGE		60.5	43.5	28.9	0.6729	0.716	0.664	0.6900	1.9902	44.3	0.473	0.555
ST.DV.					0.1249			0.0929	0.6882	32.5		

KC-16	OBS	A	B	C	MAX.PROJ.SP.	B/A	C/B	SPHER.I.	FLAT.I.	AV.ABC	SL	LILS
	1	42.0	25.0	14.0	0.5718	0.595	0.560	0.5836	2.3929	27.0	0.333	0.607
	2	46.0	31.0	25.0	0.7598	0.674	0.806	0.7157	1.5400	34.0	0.543	0.714
	3	12.0	10.0	4.0	0.5112	0.833	0.400	0.6528	2.7500	8.7	0.333	0.250
	4	5.0	3.0	2.0	0.6439	0.600	0.667	0.6217	2.0000	3.3	0.400	0.667
	5	28.0	17.0	13.0	0.7083	0.607	0.765	0.6560	1.7308	19.3	0.464	0.733
	6	10.0	8.0	5.0	0.6789	0.800	0.625	0.7370	1.8000	7.7	0.500	0.400
	7	30.0	17.0	12.0	0.6563	0.567	0.706	0.6100	1.9583	19.7	0.400	0.722
	8	26.0	15.0	10.0	0.6356	0.577	0.667	0.6057	2.0500	17.0	0.385	0.688
	9	53.0	32.0	13.0	0.4640	0.604	0.406	0.5294	3.2692	32.7	0.245	0.525
	10	61.0	30.0	18.0	0.5618	0.492	0.600	0.5258	2.5278	36.3	0.295	0.721
	11	34.0	32.0	19.0	0.6926	0.941	0.594	0.8074	1.7368	28.3	0.559	0.133
	12	95.0	75.0	62.0	0.8142	0.789	0.827	0.8019	1.3710	77.3	0.653	0.606
	13	269.0	197.0	115.0	0.6299	0.732	0.584	0.6793	2.0261	193.7	0.428	0.468
	14	49.0	35.0	20.0	0.6159	0.714	0.571	0.6634	2.1000	34.7	0.408	0.483
	15	26.0	20.0	13.0	0.6878	0.769	0.650	0.7275	1.7692	19.7	0.500	0.462
	16	121.0	59.0	53.0	0.7330	0.488	0.898	0.5981	1.6981	77.7	0.438	0.912
	17	69.0	50.0	30.0	0.6392	0.725	0.600	0.6807	1.9833	49.7	0.435	0.487
	18	19.0	12.0	7.0	0.5993	0.632	0.583	0.6154	2.2143	12.7	0.368	0.583
	19	76.0	37.0	20.0	0.5224	0.487	0.541	0.5045	2.8250	44.3	0.263	0.696
	20	21.0	14.0	5.0	0.4401	0.667	0.357	0.5418	3.5000	13.3	0.238	0.438
	21	67.0	37.0	26.0	0.6488	0.552	0.703	0.5987	2.0000	43.3	0.388	0.732
	22	67.0	48.0	32.0	0.6831	0.716	0.667	0.6997	1.7969	49.0	0.478	0.543
	23	53.0	37.0	20.0	0.5890	0.698	0.541	0.6413	2.2500	36.7	0.377	0.485
	24	43.0	32.0	20.0	0.6627	0.744	0.625	0.7024	1.8750	31.7	0.465	0.478
	25	17.0	12.0	8.0	0.6798	0.706	0.667	0.6928	1.8125	12.3	0.471	0.556
	26	73.0	39.0	21.0	0.5374	0.534	0.538	0.5360	2.6667	44.3	0.288	0.654
	27	46.0	34.0	17.0	0.5699	0.739	0.500	0.6491	2.3529	32.3	0.370	0.414
	28	61.0	49.0	42.0	0.8389	0.803	0.857	0.8210	1.3095	50.7	0.689	0.632
	29	46.0	28.0	25.0	0.7860	0.609	0.893	0.6919	1.4800	33.0	0.543	0.857
	30	14.0	10.0	7.0	0.7050	0.714	0.700	0.7097	1.7143	10.3	0.500	0.571
	31	93.0	52.0	42.0	0.7147	0.559	0.808	0.6324	1.7262	62.3	0.452	0.804
	32	61.0	43.0	21.0	0.5523	0.705	0.488	0.6240	2.4762	41.7	0.344	0.450
	33	35.0	31.0	30.0	0.9396	0.886	0.968	0.9123	1.1000	32.0	0.857	0.800
	34	19.0	13.0	10.0	0.7400	0.684	0.769	0.7117	1.6000	14.0	0.526	0.667
	35	36.0	25.0	20.0	0.7633	0.694	0.800	0.7282	1.5250	27.0	0.556	0.688
	36	16.0	8.0	7.0	0.7263	0.500	0.875	0.6028	1.7143	10.3	0.438	0.889
	37	17.0	10.0	4.0	0.4552	0.588	0.400	0.5176	3.3750	10.3	0.235	0.538
	38	45.0	42.0	25.0	0.6918	0.933	0.595	0.8036	1.7400	37.3	0.556	0.150
	39	50.0	36.0	25.0	0.7031	0.720	0.694	0.7116	1.7200	37.0	0.500	0.560
	40	53.0	38.0	33.0	0.8149	0.717	0.868	0.7645	1.3788	41.3	0.623	0.750
	41	30.0	21.0	16.0	0.7409	0.700	0.762	0.7203	1.5938	22.3	0.533	0.643
	42	45.0	35.0	11.0	0.4255	0.778	0.314	0.5753	3.6364	30.3	0.244	0.294
	43	56.0	38.0	24.0	0.6472	0.679	0.632	0.6628	1.9583	39.3	0.429	0.563
	44	15.0	11.0	10.0	0.8464	0.733	0.909	0.7880	1.3000	12.0	0.667	0.800
	45	21.0	16.0	14.0	0.8357	0.762	0.875	0.7981	1.3214	17.0	0.667	0.714
	46	66.0	56.0	36.0	0.7054	0.848	0.643	0.7737	1.6944	52.7	0.545	0.333
	47	17.0	15.0	13.0	0.8720	0.882	0.867	0.8772	1.2308	15.0	0.765	0.500
	48	30.0	22.0	19.0	0.8180	0.733	0.864	0.7746	1.3684	23.7	0.633	0.727
	49	57.0	36.0	21.0	0.5993	0.632	0.583	0.6154	2.2143	38.0	0.368	0.583
	50	14.0	10.0	7.0	0.7050	0.714	0.700	0.7097	1.7143	10.3	0.500	0.571
COLUMN AVERAGE		47.1	32.1	21.3	0.6713	0.691	0.670	0.6781	1.9778	33.5	0.464	0.585
ST.DV.					0.1159			0.0948	0.5902	28.7		

KC-17	OBS	A	B	C	MAX.PROJ.SP.	B/A	C/B	SPHER.I.	FLAT.I.	AV.ABC	SL	LILS
	1	24.0	15.0	6.0	0.4645	0.625	0.400	0.5389	3.2500	15.0	0.250	0.500
	2	66.0	42.0	34.0	0.7473	0.636	0.810	0.6898	1.5882	47.3	0.515	0.750
	3	92.0	77.0	53.0	0.7349	0.837	0.688	0.7843	1.5943	74.0	0.576	0.385
	4	82.0	45.0	44.0	0.8067	0.549	0.978	0.6656	1.443[illegible]	57.0	0.537	0.974
	5	7.0	5.0	2.0	0.4856	0.714	0.400	0.5891	3.0000	4.7	0.286	0.400
	6	21.0	19.0	8.0	0.5437	0.905	0.421	0.7014	2.5000	16.0	0.381	0.154
	7	8.0	5.0	3.0	0.6085	0.625	0.600	0.6169	2.1667	5.3	0.375	0.600
	8	12.0	10.0	7.0	0.7421	0.833	0.700	0.7865	1.5714	9.7	0.583	0.400
	9	20.0	15.0	10.0	0.6936	0.750	0.667	0.7214	1.7500	15.0	0.500	0.500
	10	92.0	74.0	47.0	0.6874	0.804	0.635	0.7437	1.7660	71.0	0.511	0.400
	11	24.0	14.0	13.0	0.7955	0.583	0.929	0.6814	1.4615	17.0	0.542	0.909
	12	42.0	38.0	12.0	0.4489	0.905	0.316	0.6373	3.3333	30.7	0.286	0.133
	13	305.0	220.0	180.0	0.7847	0.721	0.818	0.7525	1.4583	235.0	0.590	0.680
	14	30.0	20.0	14.0	0.6890	0.667	0.700	0.6779	1.7857	21.3	0.467	0.625
	15	57.0	39.0	38.0	0.8662	0.684	0.974	0.7700	1.2632	44.7	0.667	0.947
	16	141.0	131.0	64.0	0.6056	0.929	0.489	0.7501	2.1250	112.0	0.454	0.130
	17	20.0	15.0	8.0	0.5978	0.750	0.533	0.6497	2.1875	14.3	0.400	0.417
	18	85.0	65.0	42.0	0.6837	0.765	0.646	0.7232	1.7857	64.0	0.494	0.465
	19	30.0	25.0	22.0	0.8643	0.833	0.880	0.8487	1.2500	25.7	0.733	0.625
	20	128.0	53.0	40.0	0.6181	0.414	0.755	0.5061	2.2625	73.7	0.313	0.852
	21	38.0	33.0	21.0	0.7041	0.868	0.636	0.7831	1.6905	30.7	0.553	0.294
	22	24.0	21.0	6.0	0.4153	0.875	0.286	0.6028	3.7500	17.0	0.250	0.167
	23	65.0	34.0	26.0	0.6740	0.523	0.765	0.5940	1.9038	41.7	0.400	0.795
	24	102.0	84.0	47.0	0.6367	0.824	0.560	0.7242	1.9787	77.7	0.461	0.327
	25	33.0	29.0	16.0	0.6446	0.879	0.552	0.7527	1.9375	26.0	0.485	0.235
	26	24.0	14.0	9.0	0.6227	0.583	0.643	0.6028	2.1111	15.7	0.375	0.667
	27	47.0	35.0	30.0	0.8180	0.745	0.857	0.7806	1.3667	37.3	0.638	0.706
	28	37.0	24.0	21.0	0.7921	0.649	0.875	0.7169	1.4524	27.3	0.568	0.813
	29	41.0	21.0	11.0	0.5202	0.512	0.524	0.5164	2.8182	24.3	0.268	0.667
	30	12.0	9.0	8.0	0.8401	0.750	0.889	0.7939	1.3125	9.7	0.667	0.750
	31	10.0	10.0	6.0	0.7116	1.000	0.600	0.8436	1.6667	8.7	0.600	0.0
	32	24.0	18.0	9.0	0.5727	0.750	0.500	0.6555	2.3333	17.0	0.375	0.400
	33	29.0	22.0	9.0	0.5029	0.759	0.409	0.6178	2.8333	20.0	0.310	0.350
	34	50.0	30.0	16.0	0.5550	0.600	0.533	0.5772	2.5000	32.0	0.320	0.588
	35	141.0	93.0	62.0	0.6646	0.660	0.667	0.6622	1.8871	98.7	0.440	0.608
	36	35.0	30.0	11.0	0.4870	0.857	0.367	0.6461	2.9545	25.3	0.314	0.208
	37	19.0	12.0	8.0	0.6550	0.632	0.667	0.6433	1.9375	13.0	0.421	0.636
	38	46.0	40.0	12.0	0.4281	0.870	0.300	0.6102	3.5833	32.7	0.261	0.176
	39	33.0	26.0	24.0	0.8757	0.788	0.923	0.8307	1.2292	27.7	0.727	0.778
	40	23.0	12.0	7.0	0.5424	0.522	0.583	0.5418	2.5000	14.0	0.304	0.688
	41	15.0	11.0	8.0	0.7295	0.733	0.727	0.7315	1.6250	11.3	0.533	0.571
	42	43.0	28.0	11.0	0.4853	0.651	0.393	0.5506	3.2273	27.3	0.256	0.469
	43	58.0	40.0	25.0	0.6461	0.690	0.625	0.6677	1.9600	41.0	0.431	0.545
	44	55.0	52.0	37.0	0.7824	0.945	0.712	0.8601	1.4459	48.0	0.673	0.167
	45	61.0	39.0	28.0	0.6910	0.639	0.718	0.6648	1.7857	42.7	0.459	0.667
	46	65.0	45.0	23.0	0.5658	0.692	0.511	0.6260	2.3913	44.3	0.354	0.476
	47	8.0	5.0	4.0	0.7370	0.625	0.800	0.6769	1.6250	5.7	0.500	0.750
	48	73.0	44.0	23.0	0.5485	0.603	0.523	0.5751	2.5435	46.7	0.315	0.580
	49	28.0	14.0	14.0	0.7939	0.500	1.000	0.6303	1.5000	18.7	0.500	1.000
	50	50.0	36.0	32.0	0.8286	0.720	0.889	0.7726	1.3438	39.3	0.640	0.778
COLUMN AVERAGE		51.5	36.8	24.2	0.6588	0.719	0.647	0.6822	2.0547	37.5	0.457	0.534
ST.DV.					0.1260			0.0902	0.6556	37.3		

LW-1	OBS	A	B	C	MAX.PROJ.SP.	B/A	C/B	SPHER.I.	FLAT.I.	AV.ABC	SL	LILS
	1	127.0	60.0	56.0	0.7441	0.472	0.933	0.5931	1.6696	81.0	0.441	0.944
	2	107.0	100.0	70.0	0.7710	0.935	0.700	0.8489	1.4786	92.3	0.654	0.189
	3	100.0	80.0	35.0	0.5353	0.800	0.438	0.6545	2.5714	71.7	0.350	0.308
	4	160.0	132.0	90.0	0.7268	0.825	0.682	0.7744	1.6222	127.3	0.563	0.400
	5	151.0	120.0	103.0	0.8367	0.795	0.858	0.8155	1.3155	124.7	0.682	0.646
	6	50.0	50.0	33.0	0.7583	1.000	0.660	0.8708	1.5152	44.3	0.660	0.0
	7	120.0	100.0	40.0	0.5112	0.833	0.400	0.6528	2.7500	86.7	0.333	0.250
	8	125.0	103.0	40.0	0.4994	0.824	0.388	0.6415	2.8500	89.3	0.320	0.259
	9	111.0	76.0	48.0	0.6491	0.685	0.632	0.6668	1.9479	78.3	0.432	0.556
	10	58.0	45.0	37.0	0.8066	0.776	0.822	0.7912	1.3919	46.7	0.638	0.619
	11	123.0	115.0	94.0	0.8550	0.935	0.817	0.8941	1.2660	110.7	0.764	0.276
	12	146.0	107.0	69.0	0.6732	0.733	0.645	0.7025	1.8333	107.3	0.473	0.506
	13	212.0	121.0	118.0	0.8159	0.571	0.975	0.6826	1.4110	150.3	0.557	0.968
	14	160.0	76.0	34.0	0.4568	0.475	0.447	0.4660	3.4706	90.0	0.212	0.667
	15	107.0	71.0	48.0	0.6721	0.664	0.676	0.6680	1.8542	75.3	0.449	0.610
	16	77.0	50.0	38.0	0.7214	0.649	0.760	0.6846	1.6711	55.0	0.494	0.692
	17	194.0	110.0	74.0	0.6358	0.567	0.673	0.6006	2.0541	126.0	0.381	0.700
	18	120.0	90.0	62.0	0.7089	0.750	0.689	0.7293	1.6935	90.7	0.517	0.517
	19	154.0	102.0	95.0	0.8315	0.662	0.931	0.7423	1.3474	117.0	0.617	0.881
	20	140.0	131.0	51.0	0.5218	0.936	0.389	0.6988	2.6569	107.3	0.364	0.101
	21	380.0	240.0	150.0	0.6275	0.632	0.625	0.6297	2.0667	256.7	0.395	0.609
	22	185.0	116.0	100.0	0.7755	0.627	0.862	0.6975	1.5050	133.7	0.541	0.812
	23	86.0	71.0	52.0	0.7624	0.826	0.732	0.7935	1.5096	69.7	0.605	0.441
	24	105.0	88.0	50.0	0.6471	0.838	0.568	0.7365	1.9300	81.0	0.476	0.309
	25	282.0	158.0	100.0	0.6080	0.560	0.633	0.5838	2.2000	180.0	0.355	0.681
	26	164.0	130.0	91.0	0.7299	0.793	0.700	0.7607	1.6154	128.3	0.555	0.466
	27	131.0	100.0	58.0	0.6359	0.763	0.580	0.6968	1.9914	96.3	0.443	0.425
	28	118.0	68.0	61.0	0.7742	0.576	0.897	0.6681	1.5246	82.3	0.517	0.877
	29	194.0	148.0	94.0	0.6754	0.763	0.635	0.7177	1.8191	145.3	0.485	0.460
	30	121.0	84.0	64.0	0.7389	0.694	0.762	0.7163	1.6016	89.7	0.529	0.649
	31	214.0	123.0	68.0	0.5604	0.575	0.553	0.5677	2.4779	135.0	0.318	0.623
	32	108.0	94.0	86.0	0.8999	0.870	0.915	0.8851	1.1744	96.0	0.796	0.636
	33	174.0	120.0	68.0	0.6053	0.690	0.567	0.6462	2.1618	120.7	0.391	0.509
	34	174.0	150.0	93.0	0.6923	0.862	0.620	0.7726	1.7419	139.0	0.534	0.296
	35	120.0	70.0	43.0	0.6041	0.583	0.614	0.5938	2.2093	77.7	0.358	0.649
	36	71.0	47.0	23.0	0.5415	0.662	0.489	0.5989	2.5652	47.0	0.324	0.500
	37	124.0	85.0	60.0	0.6993	0.685	0.706	0.6925	1.7417	89.7	0.484	0.609
	38	81.0	57.0	40.0	0.7027	0.704	0.702	0.7033	1.7250	59.3	0.494	0.585
	39	151.0	84.0	79.0	0.7897	0.556	0.940	0.6630	1.4873	104.7	0.523	0.931
	40	177.0	134.0	77.0	0.6302	0.757	0.575	0.6908	2.0195	129.3	0.435	0.430
	41	148.0	94.0	90.0	0.8352	0.635	0.957	0.7285	1.3444	110.7	0.608	0.931
	42	135.0	84.0	68.0	0.7418	0.622	0.810	0.6795	1.6103	95.7	0.504	0.761
	43	140.0	50.0	21.0	0.3983	0.357	0.420	0.3773	4.5238	70.3	0.150	0.756
	44	154.0	136.0	74.0	0.6397	0.883	0.544	0.7517	1.9595	121.3	0.481	0.225
	45	202.0	134.0	72.0	0.5767	0.663	0.537	0.6187	2.3333	136.0	0.356	0.523
	46	137.0	94.0	50.0	0.5793	0.686	0.532	0.6306	2.3100	93.7	0.365	0.494
	47	185.0	108.0	64.0	0.5900	0.584	0.593	0.5870	2.2891	119.0	0.346	0.636
	48	260.0	164.0	144.0	0.7866	0.631	0.878	0.7045	1.4722	189.3	0.554	0.828
	49	182.0	140.0	93.0	0.6978	0.769	0.664	0.7328	1.7312	138.3	0.511	0.472
	50	162.0	143.0	91.0	0.7099	0.883	0.636	0.7917	1.6758	132.0	0.562	0.268
COLUMN AVERAGE		148.1	103.1	69.2	0.6797	0.712	0.675	0.6919	1.9337	106.8	0.478	0.550
ST.DV.					0.1104			0.0970	0.6014	38.6		

LW-2	OBS	A	B	C	MAX.PROJ.SP.	B/A	C/B	SPHER.I.	FLAT.I.	AV.ABC	SL	LILS
	1	150.0	90.0	50.0	0.5703	0.600	0.556	0.5851	2.4000	96.7	0.333	0.600
	2	90.0	70.0	25.0	0.4633	0.778	0.357	0.6004	3.2000	61.7	0.278	0.308
	3	85.0	64.0	35.0	0.6087	0.753	0.547	0.6771	2.1286	61.3	0.412	0.420
	4	95.0	45.0	30.0	0.5952	0.474	0.667	0.5312	2.3333	56.7	0.316	0.769
	5	130.0	85.0	70.0	0.7628	0.654	0.824	0.7064	1.5357	95.0	0.538	0.750
	6	240.0	200.0	150.0	0.7770	0.833	0.750	0.8047	1.4667	196.7	0.625	0.444
	7	190.0	120.0	75.0	0.6275	0.632	0.625	0.6297	2.0667	128.3	0.395	0.609
	8	110.0	85.0	55.0	0.6868	0.773	0.647	0.7286	1.7727	83.3	0.500	0.455
	9	100.0	37.0	30.0	0.6245	0.370	0.811	0.4809	2.2833	55.7	0.300	0.900
	10	271.0	200.0	160.0	0.7790	0.738	0.800	0.7583	1.4719	210.3	0.590	0.640
	11	145.0	120.0	85.0	0.7463	0.828	0.708	0.7859	1.5588	116.7	0.586	0.417
	12	150.0	100.0	72.0	0.7020	0.667	0.720	0.6843	1.7361	107.3	0.480	0.641
	13	115.0	70.0	50.0	0.6775	0.609	0.714	0.6423	1.8500	78.3	0.435	0.692
	14	130.0	100.0	80.0	0.7898	0.769	0.800	0.7795	1.4375	103.3	0.615	0.600
	15	250.0	180.0	105.0	0.6260	0.720	0.583	0.6715	2.0476	178.3	0.420	0.483
	16	145.0	110.0	80.0	0.7378	0.759	0.727	0.7482	1.5938	111.7	0.552	0.538
	17	200.0	100.0	60.0	0.5649	0.500	0.600	0.5317	2.5000	120.0	0.300	0.714
	18	125.0	90.0	50.0	0.6060	0.720	0.556	0.6607	2.1500	88.3	0.400	0.467
	19	240.0	125.0	80.0	0.5978	0.521	0.640	0.5582	2.2813	148.3	0.333	0.719
	20	445.0	380.0	250.0	0.7179	0.854	0.658	0.7830	1.6500	358.3	0.562	0.333
	21	120.0	80.0	60.0	0.7214	0.667	0.750	0.6936	1.6667	86.7	0.500	0.667
	22	230.0	150.0	140.0	0.8284	0.652	0.933	0.7352	1.3571	173.3	0.609	0.889
	23	390.0	210.0	150.0	0.6504	0.538	0.714	0.5920	2.0000	250.0	0.385	0.750
	24	175 0	140.0	100.0	0.7420	0.800	0.714	0.7705	1.5750	138.3	0.571	0.467
	25	420.0	280.0	170.0	0.6267	0.667	0.607	0.6465	2.0588	290.0	0.405	0.560
	26	250.0	170.0	120.0	0.6974	0.680	0.706	0.6888	1.7500	180.0	0.480	0.615
	27	205.0	130.0	85.0	0.6475	0.634	0.654	0.6409	1.9706	140.0	0.415	0.625
	28	160.0	130.0	80.0	0.6754	0.813	0.615	0.7408	1.8125	123.3	0.500	0.375
	29	230.0	175.0	115.0	0.6903	0.761	0.657	0.7248	1.7609	173.3	0.500	0.478
	30	215.0	130.0	125.0	0.8239	0.605	0.962	0.7060	1.3800	156.7	0.581	0.944
	31	285.0	140.0	80.0	0.5437	0.491	0.571	0.5170	2.6563	168.3	0.281	0.707
	32	250.0	185.0	125.0	0.6967	0.740	0.676	0.7181	1.7400	186.7	0.500	0.520
	33	160.0	130.0	80.0	0.6754	0.813	0.615	0.7408	1.8125	123.3	0.500	0.375
	34	240.0	150.0	35.0	0.3244	0.625	0.233	0.4504	5.5714	141.7	0.146	0.439
	35	175.0	100.0	80.0	0.7154	0.571	0.800	0.6395	1.7188	118.3	0.457	0.789
	36	140.0	92.0	75.0	0.7589	0.657	0.815	0.7063	1.5467	102.3	0.536	0.738
	37	245.0	130.0	110.0	0.7245	0.531	0.846	0.6202	1.7045	161.7	0.449	0.852
	38	220.0	110.0	60.0	0.5302	0.500	0.545	0.5151	2.7500	130.0	0.273	0.688
	39	205.0	150.0	150.0	0.9012	0.732	1.000	0.8122	1.1833	168.3	0.732	1.000
	40	275.0	190.0	150.0	0.7554	0.691	0.789	0.7225	1.5500	205.0	0.545	0.680
	41	215.0	155.0	80.0	0.5773	0.721	0.516	0.6452	2.3125	150.0	0.372	0.444
	42	240.0	130.0	100.0	0.6846	0.542	0.769	0.6091	1.8500	156.7	0.417	0.786
	43	260.0	180.0	85.0	0.5368	0.692	0.472	0.6097	2.5882	175.0	0.327	0.457
	44	345.0	150.0	85.0	0.5191	0.435	0.567	0.4753	2.9118	193.3	0.246	0.750
	45	250.0	230.0	120.0	0.6306	0.920	0.522	0.7617	2.0000	200.0	0.480	0.154
	46	270.0	130.0	100.0	0.6583	0.481	0.769	0.5632	2.0000	166.7	0.370	0.824
	47	160.0	115.0	50.0	0.5144	0.719	0.435	0.6082	2.7500	108.3	0.313	0.409
	48	140.0	90.0	90.0	0.8632	0.643	1.000	0.7451	1.2778	106.7	0.643	1.000
	49	320.0	170.0	140.0	0.7118	0.531	0.824	0.6151	1.7500	210.0	0.438	0.833
	50	210.0	170.0	150.0	0.8575	0.810	0.882	0.8333	1.2667	176.7	0.714	0.667
COLUMN AVERAGE		208.1	137.3	93.6	0.6709	0.664	0.685	0.6639	1.9947	146.3	0.453	0.620
ST.DV.					0.1095			0.0950	0.6882	58.8		

LW-6 OBS	A	B	C	MAX.PROJ.SP.	B/A	C/B	SPHER.I.	FLAT.I.	AV.ABC	SL	LILS
1	148.0	102.0	41.0	0.4815	0.689	0.402	0.5761	3.0488	97.0	0.277	0.430
2	130.0	70.0	45.0	0.6063	0.538	0.643	0.5715	2.2222	81.7	0.346	0.706
3	222.0	157.0	68.0	0.5104	0.707	0.433	0.6009	2.7868	149.0	0.306	0.422
4	127.0	80.0	32.0	0.4657	0.630	0.400	0.5428	3.2344	79.7	0.252	0.495
5	147.0	61.0	37.0	0.5348	0.415	0.607	0.4713	2.8108	81.7	0.252	0.782
6	94.0	70.0	30.0	0.5156	0.745	0.429	0.6197	2.7333	64.7	0.319	0.375
7	53.0	28.0	27.0	0.7892	0.528	0.964	0.6459	1.5000	36.0	0.509	0.962
8	49.0	31.0	25.0	0.7440	0.633	0.806	0.6862	1.6000	35.0	0.510	0.750
9	62.0	45.0	27.0	0.6396	0.726	0.600	0.6814	1.9815	44.7	0.635	0.486
10	71.0	41.0	40.0	0.8193	0.577	0.976	0.6880	1.4000	50.7	0.563	0.968
11	62.0	41.0	30.0	0.7077	0.661	0.732	0.6842	1.7167	44.3	0.484	0.656
12	121.0	98.0	60.0	0.6724	0.810	0.612	0.7380	1.8250	93.0	0.496	0.377
13	68.0	53.0	42.0	0.7883	0.779	0.792	0.7839	1.4405	54.3	0.618	0.577
14	97.0	70.0	51.0	0.7265	0.722	0.729	0.7242	1.6373	72.7	0.526	0.587
15	184.0	155.0	69.0	0.5509	0.842	0.445	0.6813	2.4565	136.0	0.375	0.252
16	143.0	115.0	72.0	0.6808	0.804	0.626	0.7400	1.7917	110.0	0.503	0.394
17	111.0	83.0	74.0	0.8409	0.748	0.892	0.7931	1.3108	89.3	0.667	0.757
18	141.0	76.0	57.0	0.6721	0.539	0.750	0.6021	1.9035	91.3	0.404	0.774
19	194.0	140.0	100.0	0.7170	0.722	0.714	0.7194	1.6700	144.7	0.515	0.574
20	92.0	61.0	50.0	0.7639	0.663	0.820	0.7119	1.5300	67.7	0.543	0.738
21	116.0	70.0	50.0	0.6755	0.603	0.714	0.6386	1.8600	78.7	0.431	0.697
22	61.0	46.0	26.0	0.6225	0.754	0.565	0.6853	2.0577	44.3	0.426	0.429
23	105.0	73.0	68.0	0.8451	0.695	0.932	0.7667	1.3088	82.0	0.648	0.865
24	108.0	50.0	30.0	0.5507	0.463	0.600	0.5051	2.6333	62.7	0.278	0.744
25	152.0	84.0	70.0	0.7269	0.553	0.833	0.6340	1.6857	102.0	0.461	0.829
26	160.0	78.0	62.0	0.6756	0.487	0.795	0.5741	1.9194	100.0	0.387	0.937
27	156.0	82.0	50.0	0.5806	0.526	0.610	0.5526	2.3800	96.0	0.321	0.698
28	106.0	65.0	48.0	0.6944	0.613	0.738	0.6527	1.7813	73.0	0.453	0.707
29	135.0	64.0	46.0	0.6259	0.474	0.719	0.5449	2.1630	81.7	0.341	0.798
30	78.0	65.0	60.0	0.8922	0.833	0.923	0.8624	1.1917	67.7	0.769	0.722
31	180.0	92.0	55.0	0.5677	0.511	0.598	0.5389	2.4727	109.0	0.306	0.704
32	122.0	90.0	50.0	0.6109	0.738	0.556	0.6714	2.1200	87.3	0.410	0.444
33	130.0	57.0	48.0	0.6777	0.438	0.842	0.5453	1.9479	78.3	0.369	0.890
34	47.0	27.0	19.0	0.6580	0.574	0.704	0.6150	1.9474	31.0	0.404	0.714
35	35.0	20.0	15.0	0.6853	0.571	0.750	0.6259	1.8333	23.3	0.429	0.750
36	77.0	61.0	56.0	0.8741	0.792	0.918	0.8323	1.2321	64.7	0.727	0.762
37	23.0	20.0	9.0	0.5608	0.870	0.450	0.6984	2.3889	17.3	0.391	0.214
38	20.0	12.0	7.0	0.5891	0.600	0.583	0.5947	2.2857	13.0	0.350	0.615
39	30.0	25.0	13.0	0.6088	0.833	0.520	0.7124	2.1154	22.7	0.433	0.294
40	80.0	46.0	34.0	0.6800	0.575	0.739	0.6255	1.8529	53.3	0.425	0.739
41	52.0	29.0	5.0	0.2953	0.558	0.172	0.3775	8.1000	28.7	0.096	0.489
42	42.0	34.0	25.0	0.7595	0.810	0.735	0.7842	1.5200	33.7	0.595	0.471
43	124.0	67.0	66.0	0.8065	0.540	0.985	0.6603	1.4470	85.7	0.532	0.983
44	65.0	41.0	27.0	0.6494	0.631	0.659	0.6402	1.9630	44.3	0.415	0.632
45	51.0	50.0	36.0	0.7982	0.980	0.720	0.8846	1.4028	45.7	0.706	0.067
46	67.0	44.0	25.0	0.5966	0.657	0.568	0.6261	2.2200	45.3	0.373	0.548
47	20.0	16.0	10.0	0.6789	0.800	0.625	0.7370	1.8000	15.3	0.500	0.400
48	39.0	26.0	17.0	0.6584	0.667	0.654	0.6626	1.9118	27.3	0.436	0.591
49	23.0	22.0	18.0	0.8620	0.957	0.818	0.9081	1.2500	21.0	0.783	0.200
50	75.0	55.0	52.0	0.8688	0.733	0.945	0.7983	1.2500	60.7	0.693	0.870
COLUMN AVERAGE	95.9	61.8	41.5	0.6712	0.646	0.687	0.6643	2.0528	66.4	0.456	0.615
ST.DV.				0.1238			0.1056	1.0008	33.3		

APPENDIX viii

Textural parameters of
Alluvial-Fan sediments.

KC refers to Kyle Canyon localities,
LW refers to Lida Wash localities.

SAMPLE NUMBER	STANDARD DEVIATION	SKEWNESS	KURTOSIS	GRAPHIC MEAN
KC-14-1	1.953	-0.357	1.096	3.227
KC-14-2	0.832	-0.243	1.168	4.350
KC-14-3	1.898	-0.559	0.767	2.383
KC-14-4	2.867	-0.574	0.572	2.783
KC-14-5	0.618	-0.113	1.195	4.517
KC-15-1	0.867	-0.178	1.033	4.173
KC-15-2	1.769	-0.113	0.836	2.537
KC-15-3	1.517	-0.479	1.529	3.587
KC-15-4	2.265	0.242	0.602	1.667
KC-15-5	2.230	0.283	0.721	1.563
KC-16-1	2.108	0.563	0.765	0.983
KC-16-2	2.350	-0.634	0.535	2.510
KC-16-4	2.088	-0.533	0.697	2.507
KC-16-5	1.554	-0.123	1.277	3.923
KC-17-1	1.928	0.284	0.907	1.330
KC-17-2	0.878	0.197	1.187	-0.050
KC-17-3	2.054	0.263	0.670	1.653
KC-17-4	2.004	0.456	0.961	1.070
KC-17-5	1.638	0.522	1.337	0.370
KC-18-1	2.154	-0.065	0.572	1.943
KC-18-2	2.020	0.091	0.605	1.533
KC-18-3	2.196	-0.232	0.540	1.907
KC-18-4	1.553	0.177	0.929	0.880
KC-18-5	1.959	-0.049	0.623	2.310

SAMPLE NUMBER	STANDARD DEVIATION	SKEWNESS	KURTOSIS	GRAPHIC MEAN
KC-19-1	1.925	-0.579	1.082	3.000
KC-19-2	0.938	-0.385	1.373	3.927
KC-19-3	2.055	0.531	1.049	0.933
KC-19-5	1.601	0.412	1.236	0.740
KC-20-1	0.793	0.002	1.007	4.560
KC-20-2	2.191	-0.416	0.731	2.423
KC-20-3	2.024	0.079	0.747	1.507
KC-20-4	1.530	-0.146	0.951	3.110
KC-20-5	2.129	-0.076	0.683	2.043
KC-21-1	1.703	0.502	1.213	0.523
KC-21-2	2.094	0.607	1.949	0.883
KC-21-3	2.244	0.459	0.759	1.267
KC-21-4	1.639	0.656	1.168	0.417
KC-21-5	2.132	-0.537	1.149	3.493
KC-22-1	1.799	0.598	1.142	0.523
KC-22-2	2.252	0.285	0.612	1.467
KC-22-3	2.154	-0.104	0.622	2.163
KC-22-4	1.896	0.636	1.744	0.510
KC-23-1	0.677	-0.094	0.937	3.803
KC-23-2	2.344	-0.129	0.572	2.057
KC-23-3	1.948	0.518	0.992	0.873
KC-23-4	1.670	-0.566	0.881	3.323
KC-23-5	2.199	0.179	0.688	1.810
KC-27-2	1.753	-0.193	0.917	2.483

SAMPLE NUMBER	STANDARD DEVIATION	SKEWNESS	KURTOSIS	GRAPHIC MEAN
KC-27-3	2.128	0.459	0.860	1.147
KC-27-4	1.003	-0.067	1.113	4.960
LW-1-1	1.349	0.226	1.008	0.583
LW-1-2	2.264	0.533	0.907	1.240
LW-1-3	2.366	0.398	0.636	1.473
LW-1-4	2.454	-0.048	0.550	2.007
LW-1-5	2.042	0.501	0.793	1.107
LW-1-6	1.798	0.429	0.991	0.933
LW-1-7	0.912	-0.200	1.050	4.310
LW-1-8	1.884	0.418	0.956	0.940
LW-1-9	1.151	-0.027	0.986	0.363
LW-1-10	1.669	0.664	1.562	0.213
LW-2-1	1.397	0.195	1.276	0.890
LW-2-2	1.813	0.599	1.500	0.620
LW-2-3	1.771	0.539	1.236	0.507
LW-2-4	1.583	0.189	0.852	2.570
LW-2-5	1.769	0.406	1.109	0.823
LW-2-6	1.245	0.401	1.224	0.130
LW-2-7	2.325	0.394	0.632	1.510
LW-2-8	1.929	0.422	0.909	1.157
LW-2-9	1.804	0.476	0.977	0.827
LW-6-1	1.489	0.334	1.246	0.540
LW-6-2	2.215	0.212	0.669	1.840
LW-6-3	2.287	0.046	0.625	2.050

SAMPLE NUMBER	STANDARD DEVIATION	SKEWNESS	KURTOSIS	GRAPHIC MEAN
LW-6-4	2.133	0.082	0.656	2.117
LW-6-5	1.322	0.287	1.329	0.343
LW-1-6I	2.193	0.221	1.243	0.243
LW-1-5I	2.278	0.382	1.092	0.327

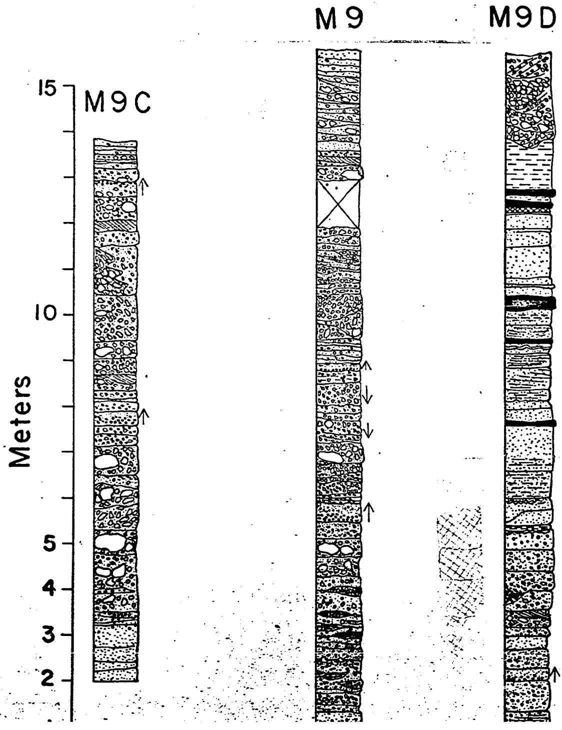
M9
M9D
15
M9C
10
Meters
5
4
3
2

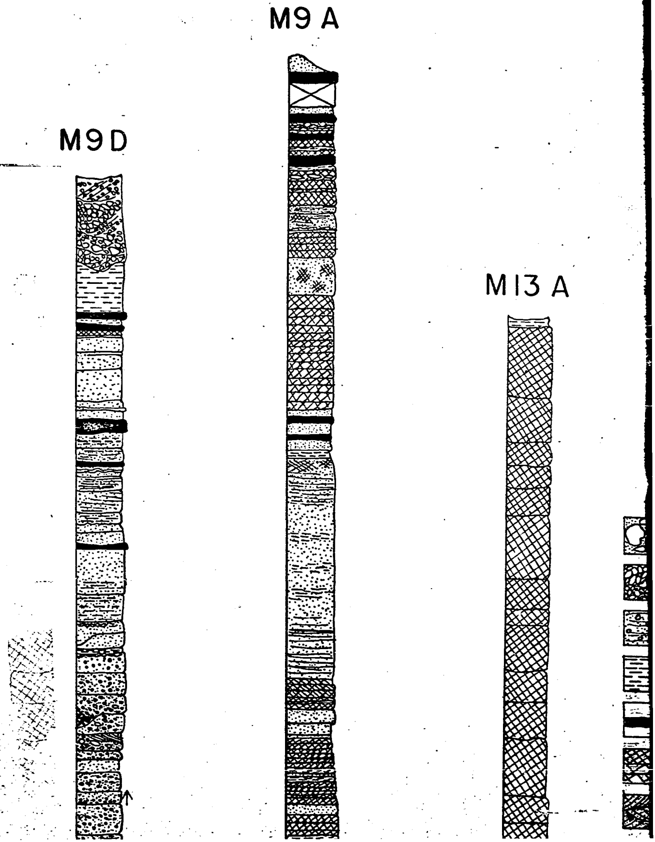
M9D
M9A
M13A

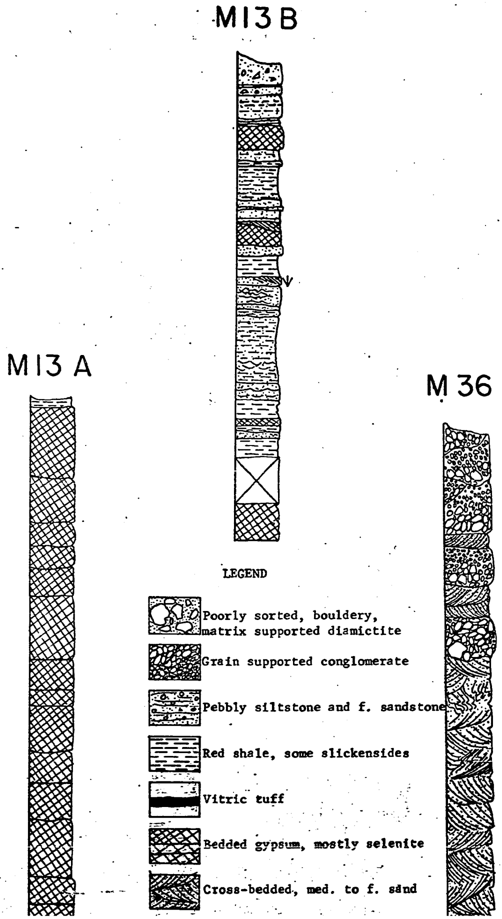
M13 B
M13 A
M 36
LEGEND
Poorly sorted, bouldery, matrix supported diamictite
Grain supported conglomerate
Pebbly siltstone and f. sandstone
Red shale, some slickensides
Vitric tuff
Bedded gypsum, mostly selenite
Cross-bedded, med. to f. sand

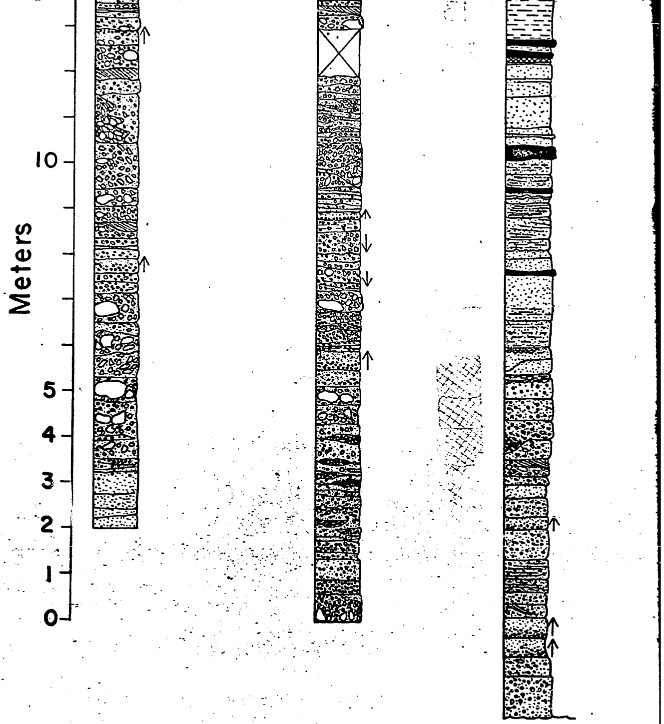
Meters
10
5
4
3
2
1
0

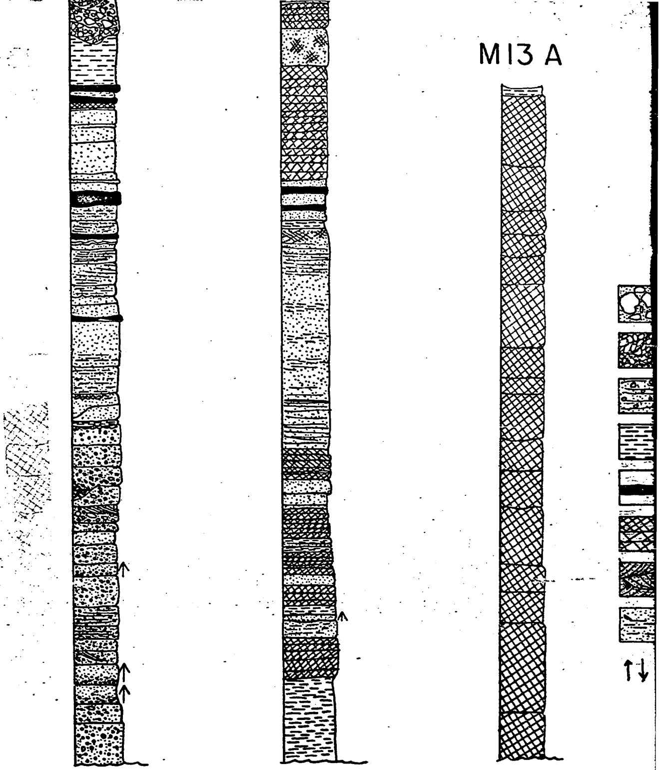
M13 A

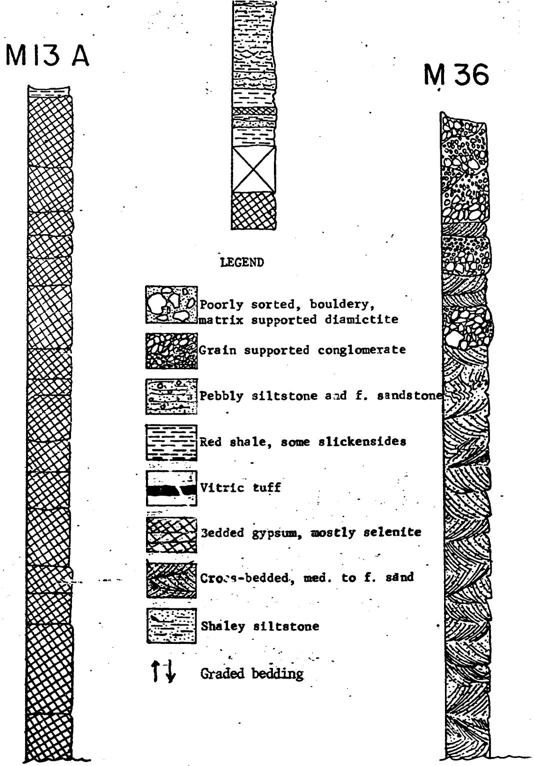
M13 A
M 36
LEGEND
Poorly sorted, bouldery, matrix supported diamictite
Grain supported conglomerate
Pebbly siltstone and f. sandstone
Red shale, some slickensides
Vitric tuff
Bedded gypsum, mostly selenite
Cross-bedded, med. to f. sand
Shaley siltstone
Graded bedding